

A model study for Eu-rich EuO

DISSERTATION

zur Erlangung des akademischen Grades
doctor rerum naturalium
(Dr. rer. nat.)
im Fach Physik

eingereicht an der
Mathematisch-Naturwissenschaftlichen Fakultät I
Humboldt-Universität zu Berlin

von

Herrn Dipl.-Phys. Peter Sinjukow
geboren am 04.08.1974 in Karl-Marx-Stadt

Präsident der Humboldt-Universität zu Berlin:

Prof. Dr. Jürgen Mlynek

Dekan der Mathematisch-Naturwissenschaftlichen Fakultät I:

Prof. Thomas Buckhout, PhD

Gutachter:

1. Prof. Dr. Wolfgang Nolting
2. Prof. Dr. Robert Keiper
3. Prof. Dr. Wladyslaw Borgiel

eingereicht am: 20. August 2004

Tag der mündlichen Prüfung: 7. Dezember 2004

Abstract

In this thesis a model is formulated for Eu-rich EuO. It consists in an extension of the Kondo lattice model (KLM). For the KLM only a few exact statements exist. To those we add a new one, namely the exact mapping of the periodic Anderson model on the antiferromagnetic KLM for arbitrary coupling constant J .

Pure EuO is a ferromagnetic semiconductor. Eu-rich EuO exhibits a huge metal-insulator transition near the Curie temperature with a jump in resistivity of up to 13 orders of magnitude. It is the biggest jump in resistivity ever observed in nature. We theoretically reproduce this jump with the Kubo formula. We achieve very good fits already within a not fully self-consistent theory where the magnetization of the Eu spins is taken from a Brillouin function. In a fully self-consistent theory we determine the magnetization, the Curie temperature, the resistivity and other transport properties.

We calculate quantities like the electronic thermal conductivity and the thermopower, for which there are less experimental data to compare with. Nevertheless, e.g. the calculations for the thermal conductivity seem reliable since the Wiedemann-Franz ratio with the electrical conductivity gives a reasonable result.

The conduction-electron number of Eu-rich EuO comes out of the theory independently of the conductivity. So we can calculate from the conductivity and the conduction-electron number the average Drude mobility (or scattering time). This quantity has a jump near the Curie temperature of up to two orders of magnitude for higher impurity (oxygen vacancy) concentrations in agreement with the experiment.

Keywords:

EuO, metal-insulator transition, Kubo formula, Kondo lattice model

Zusammenfassung

In dieser Arbeit wird ein Modell für das Eu-reiche EuO formuliert. Es besteht in einer Erweiterung des Kondo-Gitter-Modells (KGM). Für das KGM existieren nur einige exakte Aussagen. In dieser Arbeit kommt eine neue hinzu, nämlich die exakte Abbildung des periodischen Anderson-Modells auf das antiferromagnetische KGM für beliebige Kopplungsstärke J .

Reines EuO ist ein ferromagnetischer Halbleiter. Eu-reiches EuO zeigt einen gewaltigen Metall-Isolator-Übergang in der Nähe der Curie-Temperatur mit einem Sprung im Widerstand von bis zu 13 Größenordnungen. Das ist der größte Sprung im Widerstand, der jemals in der Natur beobachtet wurde. Wir reproduzieren diesen Sprung theoretisch mit der Kubo-Formel. Wir erzielen sehr gute Fits bereits in einer nicht vollständig selbstkonsistenten Theorie, bei der die Magnetisierung der Eu-Spins einer Brillouin-Funktion entnommen ist. In einer vollständig selbstkonsistenten Theorie bestimmen wir die Magnetisierung, die Curie-Temperatur, den spezifischen Widerstand und andere Transporteigenschaften.

Wir berechnen Größen wie die elektronische Wärmeleitfähigkeit und die Thermokraft, für die weniger experimentelle Daten zum Vergleich vorhanden sind. Nichtsdestoweniger erscheinen z.B. die Rechnungen für die thermische Leitfähigkeit vertrauenswürdig, da das Wiedemann-Franz-Verhältnis mit der elektrischen Leitfähigkeit einen vernünftigen Wert liefert.

Die Leitungselektronenzahl des Eu-reichen EuO kommt aus der Theorie unabhängig von der Leitfähigkeit heraus. Daher können wir aus der Leitfähigkeit und der Leitungselektronenzahl die durchschnittliche Drude-Mobilität (oder Streuzzeit) berechnen. Diese Größe hat für höhere Impurity-(Sauerstoff-Leerstellen)-Konzentrationen einen Sprung in der Nähe der Curie-Temperatur von bis zu zwei Größenordnungen in Übereinstimmung mit dem Experiment.

Schlagwörter:

EuO, Metall-Isolator-Übergang, Kubo-Formel, Kondo-Gitter-Modell

Contents

| | | |
|----------|---|-----------|
| 1 | Introduction | 1 |
| 2 | Motivation and applications of the Kondo lattice model | 7 |
| 3 | Exact results on the Kondo lattice model | 11 |
| 3.1 | Known exact results on the Kondo lattice model | 11 |
| 3.2 | Exact mapping of the periodic Anderson model on the Kondo lattice model | 15 |
| 3.2.1 | Introductory remarks | 15 |
| 3.2.2 | Proof of exact mapping of the PAM in the extended Kondo limit on the KLM for $\mathbf{S} = \frac{1}{2}$ | 18 |
| 3.2.3 | Proof of exact mapping of a degenerate PAM with spin constraint on the KLM for $\mathbf{S} \geq \mathbf{1}$ | 23 |
| 3.2.4 | Proof of the large Fermi volume in the $\mathbf{S} = \frac{1}{2}$ KLM for a nonmagnetic Fermi-liquid state | 28 |
| 4 | Extension of the KLM to a realistic model describing Eu-rich EuO | 33 |
| 4.1 | Realistic model parameters | 35 |
| 5 | Current density operator and transport formulae of the model for Eu-rich EuO | 39 |
| 6 | Solution and results of the model with external parameter $\langle \mathbf{S}^z \rangle$ | 49 |
| 6.1 | Solution of the model with external parameter $\langle \mathbf{S}^z \rangle$ | 49 |
| 6.1.1 | Self-energies | 49 |
| 6.1.2 | Coherent-potential approximation | 51 |
| 6.1.3 | Green's functions | 52 |
| 6.2 | Technical details of the calculations | 54 |
| 6.3 | Results and discussion | 56 |

| | | |
|----------|--|------------|
| 6.3.1 | Fit of resistivity | 56 |
| 6.3.2 | Densities of states and mechanism of the metal-insulator transition | 58 |
| 6.3.3 | Low-temperature minimum in the resistivity of high-resistivity samples | 59 |
| 6.3.4 | Resistivity in a magnetic field and magnetoresistance | 61 |
| 7 | Fully self-consistent solution and results of the model | 63 |
| 7.1 | Fully self-consistent solution of the model | 63 |
| 7.2 | Results and discussion | 66 |
| 7.2.1 | Magnetization and Curie temperature | 66 |
| 7.2.2 | Comparison of theoretical and experimental resistivity | 71 |
| 7.2.3 | Electrical resistivity and chemical potential | 72 |
| 7.2.4 | Electronic thermal conductivity | 74 |
| 7.2.5 | Wiedemann-Franz ratio | 75 |
| 7.2.6 | Seebeck coefficient and figure of merit | 76 |
| 7.2.7 | Conduction electron number and scattering time | 79 |
| 7.2.8 | Impurity electron number | 82 |
| 8 | Summary and outlook | 85 |
| A | Calculations for the proof of the large Fermi volume | 89 |
| B | Calculation of the commutators for the current density operator | 93 |
| C | Vanishing of the u-v term in the partial integration of Eq. (5.46) | 95 |
| D | Atomic limit self-energies | 99 |
| E | Modified RKKY treatment | 101 |

Chapter 1

Introduction

It was in 1953 when Brauer [Brauer, 1953] discovered EuO in solid solution with SrO [Mauger and Godart, 1986]. In 1961 Matthias *et al.* [Matthias et al., 1961] identified EuO as a ferromagnetic semiconductor. From the paramagnetic inverse susceptibility they extrapolated a Curie temperature of 77 K. This was 8 K too high but the exciting point experimentally and theoretically was the identification of EuO as the second truly ferromagnetic semiconductor one year after the discovery of CrBr₃ by Tsubokawa [Tsubokawa, 1960, Wachter, 1979]. In the mid-fifties the possible existence of a ferromagnetic semiconductor or insulator was seriously disputed by the theoreticians. Later one recognized that only the Bloembergen-Rowland exchange [Bloembergen and Rowland, 1955] via the polarization of the valence electrons [Wachter, 1979] could account for the ferromagnetism in insulators or semiconductors. In 1975 and 1976 the nearest and next-nearest neighbor exchange constants J_1 and J_2 for EuO were measured with neutron scattering by Dietrich *et al.* [Dietrich et al., 1975] and Passell *et al.* [Passell et al., 1976], respectively. The values are $J_1 = (0.606 \pm 0.008)k_B$ K and $J_2 = (0.119 \pm 0.015)k_B$ K [Wachter, 1979]. All the europium monochalcogenides, of which EuO is one member amongst EuS, EuSe and EuTe, crystallize in the rock salt structure where the magnetic europium ions occupy the sites of an fcc lattice. Later it was tried to calculate J_1 and J_2 theoretically [Liu, 1980, Liu, 1983, Lee and Liu, 1983, Lee and Liu, 1984] using e.g. the linear combination of atomic orbitals (LCAO) method and perturbation theory [Lee and Liu, 1983, Lee and Liu, 1984]. At least up to that time EuO and EuS were the only known “realizations” of Heisenberg ferromagnets in nature [Lee and Liu, 1984], with a Hamiltonian given by the Heisenberg

model

$$\mathcal{H}_{ff} = - \sum_{ii'} J_{ii'} \vec{S}_i \cdot \vec{S}_{i'} \quad (1.1)$$

where \vec{S}_i is the Eu spin at site \vec{R}_i , which is of magnitude $S = \frac{7}{2}$ stemming from the $4f^7$ electrons, and $J_{ii'}$ is the exchange integral between the spins at sites \vec{R}_i and $\vec{R}_{i'}$. Only recently Kuneš *et al.* [Kuneš *et al.*, 2004] calculated the indirect exchange integrals within density-functional theory using LDA+U. For EuO with the lattice parameter $a = 5.1 \text{ \AA}$ they get their best agreement with the above cited exchange constants and with the Curie temperature of $T_C = 69.3 \text{ K}$ [Wachter, 1979] for the biggest chosen value of $U (= 9 \text{ eV})$.

If one is interested in the physics of the unoccupied conduction band of EuO, one should use the so-called *s-f* (or *d-f*) exchange model or Kondo lattice model (KLM) [Nolting *et al.*, 1987b, Nolting *et al.*, 1987a]. For the consideration of just one conduction band it is given by

$$\mathcal{H} = \sum_{\vec{k}\sigma} \epsilon_{\vec{k}} n_{\vec{k}\sigma}^c - J \sum_i \vec{S}_i \cdot \vec{\sigma}_i^c \quad (1.2)$$

where $\epsilon_{\vec{k}}$ describes the conduction band, $n_{\vec{k}\sigma}^c$ is the number operator for a conduction Bloch electron with wave vector \vec{k} and spin σ , $\vec{\sigma}_i^c$ is the spin operator of the conduction electron at site \vec{R}_i , and J is the constant of exchange between the conduction electron spin and the Eu spin at each site¹. Nolting *et al.* [Nolting *et al.*, 1987b, Nolting *et al.*, 1987a] used a five-band model to describe the five $5d$ conduction bands in EuO and for the first time combined a density-functional theory (DFT) calculation with a many-body evaluation. Schiller in his PhD thesis [Schiller, 2000] attended to the task to account for the correct symmetries of the $5d$ bands.

The most striking effect of the *d-f* exchange is the redshift of the optical absorption edge below the Curie temperature T_C . It was first observed by Busch, Junod and Wachter [Busch *et al.*, 1964, Wachter, 1979]. The corresponding transition is $4f^7 5d^0 \rightarrow 4f^6 5d^1$. Since the $4f$ electrons are very localized within the Eu atoms, the $4f$ levels are almost temperature independent. Hence, the redshift of the absorption edge is due to a redshift of the $5d$ conduction band. Theoretically, this is already reproduced by a simple mean-field picture of the Hamiltonian (1.2). Below the Curie temperature the conduction band is split into a spin-up and a spin-down part. With decreasing temperature the spin-up part is shifted towards lower energies

¹Throughout this thesis we will use J in energy units and all the spin operator eigenvalues without the \hbar .

(redshift) by $-\frac{J}{2}\langle S^z \rangle$ whereas the spin-down-part is moved towards higher energies (blueshift) by $+\frac{J}{2}\langle S^z \rangle$. $\langle S^z \rangle$ is the magnetization of the Eu spins. Both shifts reach their maximum of $\frac{J}{2}S$ at $T = 0$, where $S = \frac{7}{2}$ is the spin quantum number of the localized Eu spins.

As an experimental matter of fact pure EuO single crystals are difficult to be fabricated. The usual method (at least in the 1970's) was to melt Eu and Eu_2O_3 in a (tungsten) crucible and then to cool the crucible slowly down [Oliver et al., 1972, Schoenes and Wachter, 1974]. Depending on the ratio of Eu and Eu_2O_3 used, non-stoichiometric O-rich or Eu-rich EuO samples can be produced. Of exclusive interest for this dissertation is the *Eu-rich EuO*. Interestingly, it has exactly the same Curie temperature T_C as the pure (stoichiometric) EuO [Schoenes and Wachter, 1974]. This has been used as an argument for the fact that the “lattice” of the Eu atoms is still intact in the Eu-rich samples, and that the Eu richness manifests itself in an oxygen deficiency, i.e. in oxygen vacancy sites. (Since in this thesis we are not interested in additional doping with e.g. Gd or La [Wachter, 1979], we will call the oxygen vacancies simply *impurities*.²) However, the explanation of the constancy of T_C is not sufficient since each oxygen vacancy site contributes two electrons, which are otherwise bound in the chemical bonding with the oxygen ions. These impurity electrons, as we will show, can mediate an effective interaction between the Eu $4f$ spins. They should, therefore, in principle be responsible for a change in the Curie temperature (see also [Leroux-Hugon, 1972]). It is one of our results presented in this thesis that the effect on T_C is less than 1 mK.

One of the most important physical properties of the Eu-rich EuO is a metal-insulator transition, which manifests itself in a jump in resistivity near T_C of up to 13 orders of magnitude under certain conditions [Torrance et al., 1972]. Over a temperature range of only several degrees Kelvin, this is the biggest jump in resistivity ever observed in nature. However, the height of the jump is strongly dependent on the growing parameters (see Oliver *et al.* in Ref. [Oliver et al., 1972]). Starting in the 1970's there were several theoretical attempts to describe the metal-insulator transition, some of which we will highlight in the following.

Oliver *et al.* were the first to propose a model for the metal-insulator transition in Eu-rich EuO [Oliver et al., 1970]. According to their first model there is a temperature-independent trap level, which stems from the oxygen vacancy sites and which crosses the redshifted conduction band at a temperature below the Curie temperature. The crossing means that electrons

²Eu-rich EuO will be sometimes written as EuO_{1-d} , where d is the “impurity” concentration.

from the trap level can empty into the conduction band, transforming the system into a metal. Above the crossing temperature the system behaves like a doped semiconductor. The main idea of this model will also be realized within the microscopic model we will present in this thesis.

In a later paper (Ref. [Oliver et al., 1972]) Oliver *et al.* refer to a quantitative fit, which was possible with a total relative band-edge-to-trap-level shift of 0.45 eV (instead of 0.26 eV in their first model). To realize such a big relative shift they assume in their second, refined model (“magnetic double donor”) two effective trap levels. The impurity electron in the first trap level has its spin more or less aligned with the spins of the Eu lattice. The second electron has the opposite spin. Therefore, there is an energy separation which becomes larger with decreasing temperature due to an increasing magnetization. Below T_C when the magnetic exchange increases, the upper trap level is shifted upwards to cross the lower conduction band edge and the lower trap level is shifted downwards. We will show that in our model such a temperature dependent shift of the trap levels is unphysical. Instead there will be a shift of spectral weights. Oliver *et al.*’s model is sometimes called He model because in the ground state each impurity (oxygen vacancy) can absorb two electrons with opposite spin [Shapira et al., 1973, Steeneken, 2002]. Oliver *et al.* in Refs. [Oliver et al., 1970, Oliver et al., 1972] lead with the help of their model a more or less qualitative discussion.

Torrance *et al.* [Torrance et al., 1972] introduced the concept of the so-called “bound magnetic polaron”. With this they describe an electron at an oxygen vacancy which strongly interacts with the neighboring Eu spins and which is able to polarize its immediate surroundings. Therefore, in the paramagnetic phase it is rather localized giving rise to an insulating phase. In the ferromagnetic phase due to the polarization of the Eu spins the oxygen-vacancy (impurity) electron is fairly delocalized causing a metallic phase. Also Torrance *et al.* in Ref. [Torrance et al., 1972] just lead a qualitative discussion.

Leroux-Hugon in Ref. [Leroux-Hugon, 1972] calculates — within the linear response of the dielectric constant and the magnetic susceptibility and by the use of a variational ansatz — the transition temperature of the metal-insulator transition for impurity concentrations of 3.5×10^{19} to $8.3 \times 10^{19} \text{ cm}^{-3}$, which corresponds to 0.12 % to 0.27 %. However, it is unclear why below an impurity concentration of 0.12 % there should be no metallic phase. This contradicts our theory which in principle does not have a lower bound for metallic behavior.

The first calculations of the *resistivity* in dependence on temperature we came across are the calculations by Laks and da Silva [Laks and da Silva, 1976]. They made ansatzes for the internal energy and

the entropy to get the free energy. Moreover they used the simple Drude formula for the conductivity, which is given by $\sigma = n_c e \mu$, where n_c is the conduction electron concentration, e the elementary charge and $\mu = e\tau/m_e^*$ the mobility with m_e^* the effective electron mass and τ the scattering time. For the quasiparticle density of states they used the mean-field expression. The result is a good fit to the conductivity curve of Ref. [Torrance et al., 1972] for temperatures below the Curie temperature but a rather bad agreement for temperatures above.

Spalek *et al.* [Spalek et al., 1977] calculated the carrier concentration and the magnetic susceptibility in dependence on the temperature within a one-electron donor level model and a two-electron donor level model. However, they used mean-field for the conduction band and a magnetization-dependent shift of the one-electron donor level, which contradicts the result of the atomic limit. There is no comparison of their calculated carrier concentration with carrier concentrations from the experiment. Their inverse susceptibility becomes zero at a temperature that is higher than the experimental Curie temperature.

Mauger [Mauger, 1983] tried to quantify the theory of the bound magnetic polaron set out by Torrance *et al.* [Torrance et al., 1972]. He also used the mean-field theory for the conduction band and the simple Drude formula for the conductivity. He made special ansatzes for the free energies of the subsystems. For his fairly good fits to experimental curves he used the concept of compensating impurities for the conduction electrons. The fits were made to measurements of Gd doped EuO and not Eu-rich EuO. Mauger shows in Fig. 1 of his paper a phase diagram of the critical carrier density versus temperature for (Eu-rich?) EuO. It also contains a critical value of the carrier density of $0.6 \times 10^{19} \text{ cm}^{-3}$, which corresponds to 0.02 % electron concentration per lattice site, below which there is no metallic phase. Again, this contradicts our theory, which does not have a lower bound for metallic behaviour.

Most recently Steeneken in his PhD thesis [Steeneken, 2002] calculated the resistivity in dependence on temperature for Eu-rich EuO. His concept of a temperature dependent exchange splitting of the impurity level is, however, questionable since it contradicts the atomic limit result. He used the Drude formula to calculate the resistivity. He developed a theory of the dependence of the distribution of the impurity electron binding energies on the impurity concentration. His resistivity curves fit fairly well to the medium-resistivity samples in Ref. [Oliver et al., 1972] but rather bad to the high-resistivity samples. The inclusion of a very small concentration of acceptor sites or compensating impurities (0.001 %) changes the picture drastically. Now with an oxygen vacancy concentration of 0.025 % he is able to repro-

duce the low-temperature minimum of the high-resistivity samples of Ref. [Oliver et al., 1972] but the high-temperature values of the resistivity are all much too high.

After all these attempts in the past to describe the behaviour of Eu-rich EuO we decided first to develop a *model Hamiltonian* for the system and then to solve it with the help of a Green's function technique. We consider our model Hamiltonian a better starting point than e.g. the usage of special ansatzes for the free energy, which is always connected with some crude approximations. Furthermore we will use the *Kubo formula* for the case of local selfenergies to calculate the conductivity (or equivalently the resistivity). The Kubo formula, which is the correct linear response approach to the many-body problem, is supposed to be much more accurate than the simple Drude formula, where one has to make special assumptions on the mobility (or scattering time) and the effective mass of the electrons. Moreover we will present in this thesis fully self-consistent calculations, which include the self-consistent calculation of the magnetization of the Eu spins and the Curie temperature. We will also calculate other interesting transport quantities, like the thermal conductivity of the electrons and the Seebeck coefficient.

The core of our model Hamiltonian is the famous *Kondo lattice model* [Eq.(1.2)], which we use to mimic the interplay between the Eu spins and the conduction band. In chapter 2 we will give a general overview of the applications of the Kondo lattice model. In chapter 3 we will first collect the exact results known so far for this model. Then we will add a new exact result for the antiferromagnetic Kondo lattice model, namely the exact mapping of the periodic Anderson model (PAM) on the Kondo lattice model and the consequences on the Fermi volume which follow from that. In chapter 4 we will extend the KLM to a realistic model describing Eu-rich EuO with parameters as close as possible to the experiment. In the next chapter the current-density operator and therewith the transport formulae for the extended KLM will be derived. A not fully self-consistent solution with external parameter $\langle S^z \rangle$ and results thereof will be discussed in chapter 6. The fully self-consistent solution and the results following from this will be presented in chapter 7. In the last chapter a summary and conclusions will be given. In the appendices we will include some calculations which are excluded from the main text for better readability.

Chapter 2

Motivation and applications of the Kondo lattice model

The Kondo lattice model (or s - f or s - d model) is one of the most widely used many body models in solid state physics. One of the reasons certainly is its conceptual simplicity, describing an interband exchange interaction between rather localized electrons and itinerant conduction electrons. The ferromagnetic KLM is applied for the empty conduction electron bands of the europium chalcogenides EuX (with $X = \text{O}, \text{S}, \text{Se}, \text{Te}$). EuO and EuS are ferromagnetic, EuSe is an antiferromagnetic/ferrimagnetic, and EuTe is an antiferromagnetic semiconductor [Wachter, 1979]. The most prominent feature of the ferromagnetic semiconductors is the redshift of their optical absorption edge below the Curie temperature [Schoenes and Wachter, 1974]. The absorption is accompanied by the transition $4f^7 5d^0 \rightarrow 4f^6 5d^1$. Since the $4f$ states are rather localized their energies are temperature independent. Hence, the redshift results from a down-shift of the spin-up $5d$ conduction band. This shift can be well understood in a mean-field picture where the conduction band is rigidly shifted proportionally to the Eu-spin magnetization $\langle S^z \rangle$ by an amount of $J\langle S^z \rangle/2$.

A second application of the KLM are the so-called local-moment metals, like Gd, Tb, Dy and $\text{Eu}_{1-x}\text{Gd}_x\text{S}$. In contrast to the (anti)ferromagnetic semiconductors, where the magnetic order of the localized spins is due to some special kind of superexchange (Bloembergen-Rowland interaction [Bloembergen and Rowland, 1955, Liu, 1980, Liu, 1983, Lee and Liu, 1983, Lee and Liu, 1984]), in the local-moment metals an indirect coupling between the localized spins is mediated by the conduction electrons in an RKKY manner [Rudermann and Kittel, 1954, Kasuya, 1956, Yosida, 1957]. In the case of Gd there is at low temperatures a magnetic moment of $7.63\mu_B$. $7\mu_B$ belong to the spin $\frac{7}{2}$ of the $4f$ electrons and $0.63\mu_B$ originate from the conduction

band polarization. Hence the exchange constant J is positive (ferromagnetic).

A third group of materials for which the Kondo lattice model is appropriate are the diluted magnetic semiconductors, e.g. $\text{Ga}_{1-x}\text{Mn}_x\text{As}$ [Matsukura et al., 1998, Dietl et al., 2001b], a group of materials which is especially promising for spintronics applications if it becomes possible to reach T_C 's at or above room temperature. The diluted magnetic semiconductors represent dilute disordered magnetic systems with a small number of magnetic impurities and charge carriers. In the case of $\text{Ga}_{1-x}\text{Mn}_x\text{As}$ at least the majority of Mn ions [Sanvito et al., 2001] is in the $2+$ state contributing a spin of $S = 5/2$ and a hole in the valence band. This hole is antiferromagnetically coupled to the Mn spin [Dietl et al., 2001b, Sanvito et al., 2001, Dietl et al., 2001a, König et al., 2001]. Therefore the antiferromagnetic Kondo lattice model is appropriate here. In contrast, the conduction band is ferromagnetically coupled to the impurity spins [Sanvito et al., 2001].

The manganites (manganese oxides with perovskite structure) $\text{T}_{1-x}\text{D}_x\text{MnO}_3$ ($T =$ trivalent La, Pr, Nd; $D =$ divalent Ca, Sr, Ba, Pb) show the colossal magnetoresistance [Jin et al., 1994, Ramirez, 1997]. The double-exchange mechanism, which leads to ferromagnetism above a certain critical x , was first described by Zener [Zener, 1951, Nolting, 1986]. He used the ferromagnetic Kondo lattice model, which for this reason was for some time also called Zener model. Due to the replacement of the trivalent by divalent ions there appears a mixture of $1 - x$ Mn^{3+} and x Mn^{4+} in the manganite, where the Mn^{4+} ions supply more or less localized spins $S = 3/2$ from their $3d-t_{2g}$ electrons. The Mn^{3+} has an additional $3d-e_g$ electron which is thought to be itinerant. However, the manganites are bad electrical conductors, because the hopping matrix element t is very small compared with the intraatomic spin-spin coupling constant J . The bandwidth W (in the simple cubic case in tight-binding approximation one has $W = 12t$) is estimated $1 - 2$ eV [Satpathy et al., 1996, Pickett and Singh, 1996, Singh and Pickett, 1998], whereas J is at least 1 eV [Satpathy et al., 1996, Okimoto et al., 1995, Millis et al., 1996]. The ferromagnetic Kondo lattice model is certainly not able to describe all details of the rich phases (including phase separation [Ramirez, 1997]) of the manganites but it is looked at as a reasonable framework for gross effects in their physical behavior [Dagotto et al., 1998, Furukawa, 1994].

The so-called heavy-fermion systems form a further class of materials for which the antiferromagnetic Kondo lattice model is commonly applied apart from the periodic Anderson model. It is well known that the spin- $1/2$ antiferromagnetic KLM for small J can be obtained from the PAM in

the so-called Kondo limit by the famous Schrieffer-Wolff transformation. In section 3.2 we will show that the antiferromagnetic KLM for *any* finite J is the exact effective model of the PAM in a special “extended Kondo limit”. Heavy fermions are mainly Ce compounds. The term “heavy fermion system” comes from the fact that the effective masses of the charge carriers are enhanced by up to a factor of 1000 [Hewson, 1997]. This can be seen, for instance, by a respective enhancement of the specific heat. $\text{CeCu}_{6-x}\text{Au}_x$ is a substance where there is a change from a Kondo screened nonmagnetic state at $x = 0$ to a RKKY dominated state with antiferromagnetic ordering for $x \geq 0.1$ [von Löhneysen, 1998].

Chapter 3

Exact results on the Kondo lattice model

3.1 Known exact results on the Kondo lattice model

Due to their non-trivial nature many-body Hamiltonians lack many exact results. In the following we will make a list of the known exact results of the Kondo lattice model (1.2).

- The “atomic limit” or zero-bandwidth limiting case ($\epsilon_{\vec{k}} \rightarrow T_0 \forall \vec{k}$) of the correlated Kondo lattice model [Nolting and Matlak, 1984, Nolting et al., 2001]:

“Correlated” means that there is an additional Hubbard term for the conduction electrons $U \sum_i n_{i\uparrow}^c n_{i\downarrow}^c$. There are four *temperature-independent*¹ quasi-particle levels in the following order (if U is large enough):

$$\begin{aligned}\epsilon_1 &= T_0 - \frac{1}{2}JS, \quad \epsilon_2 = T_0 + \frac{1}{2}J(S+1), \\ \epsilon_3 &= T_0 + U - \frac{1}{2}J(S+1), \quad \epsilon_4 = T_0 + U + \frac{1}{2}JS.\end{aligned}$$

The decisive point is that the spectral weights of those levels are dependent on the spin, the band filling and the temperature (via $\langle S^z \rangle$). It turns out that in any case only three of the four levels have finite

¹ignoring μ and its temperature dependence

weight. The weights are given by

$$\begin{aligned}\alpha_{1\sigma} &= \frac{1}{2S+1} [S+1 + z_\sigma \langle S^z \rangle + \Delta_{-\sigma} - (S+1) \langle n_{-\sigma}^c \rangle], \\ \alpha_{2\sigma} &= \frac{1}{2S+1} [S - z_\sigma \langle S^z \rangle - \Delta_{-\sigma} - S \langle n_{-\sigma}^c \rangle], \\ \alpha_{3\sigma} &= \frac{1}{2S+1} [S \langle n_{-\sigma}^c \rangle - \Delta_{-\sigma}], \\ \alpha_{4\sigma} &= \frac{1}{2S+1} [\Delta_{-\sigma} + (S+1) \langle n_{-\sigma}^c \rangle],\end{aligned}$$

where $\langle S^z \rangle$ is the magnetization of the localized spins, $\langle n_{-\sigma}^c \rangle$ is the average electronic occupation number at a certain site, $z_\sigma = \delta_{\sigma\uparrow} - \delta_{\sigma\downarrow}$ and $\Delta_\sigma = \langle S^\sigma c_{-\sigma}^\dagger c_\sigma \rangle + z_\sigma \langle S^z n_\sigma^c \rangle$ with $S^\sigma = \delta_{\sigma\uparrow} S^+ + \delta_{\sigma\downarrow} S^-$. We will make use of this limiting case when choosing the self-energy for the impurity (oxygen vacancy) electrons.

- The ferromagnetically saturated semiconductor [Shastry and Mattis, 1981, Allen and Edwards, 1982, Nolting et al., 1985, Nolting et al., 2001]:

In this limiting case all spins are aligned parallel in the z -direction. Except for the test electron, which is put into the conduction band, the conduction band is empty. The spin-up quasi-particle band is only rigidly shifted downwards: $\Sigma_\uparrow^c = -\frac{1}{2}JS$. The spin-down spectrum is more complicated [Nolting et al., 2001]:

$$\Sigma_\downarrow^c(E) = \frac{1}{2}JS \left(1 + \frac{JG_0(E + \mu + \frac{J}{2}S)}{1 - \frac{1}{2}JG_0(E + \mu + \frac{J}{2}S)} \right) \quad (3.1)$$

where $G_0(E) = \frac{1}{N} \sum_{\vec{k}} \frac{1}{E - \epsilon_{\vec{k}}}$ is the local free Green's function. If J is large enough the spin-down density of states consists of two parts. There is spectral weight in the energy range of the spin-up density of states: this is called the scattering part because it comes from the spin flip of the spin-down electron to a spin-up electron thereby emitting a magnon and occupying a spin-up state. Secondly, there is a narrower so-called magnetic polaron part, which represents quasiparticles (magnetic polarons) of infinite lifetimes. They are characterized by repeated emission and absorption of magnons thereby polarizing the surroundings of the “dressed” electron.

- The second-order perturbation theory for the self-energy [Mori, 1965, Mori, 1966, Bulk and Jelitto, 1988, Bulk and Jelitto, 1990,

Nolting et al., 2001, Hickel and Nolting, 2004]:

$$\Sigma_{\vec{k}\sigma}^c = -\frac{J}{2}z_\sigma \langle S^z \rangle^{\{0\}} + \frac{J^2}{4}\gamma_{\vec{k}\sigma} + \mathcal{O}(J^3) \quad (3.2)$$

$$\gamma_{\vec{k}\sigma} = -\left(\langle S^z \rangle^{\{0\}}\right)^2 G_{\vec{k}c}^{\{0\}} + \frac{1}{N^2} \sum_{\vec{q}} \langle S_{-\vec{q}}^z S_{\vec{q}}^z \rangle^{\{0\}} G_{\vec{k}+\vec{q}c}^{\{0\}} \quad (3.3)$$

$$+ \frac{1}{N^2} \sum_{\vec{q}} \left[\langle S_{-\vec{q}}^{-\sigma} S_{\vec{q}}^{\sigma} \rangle^{\{0\}} + 2z_\sigma \langle S_0^z n_{\vec{q}+\vec{k},-\sigma}^c \rangle^{\{0\}} \right] G_{\vec{k}+\vec{q}c}^{\{0\}}, \quad (3.4)$$

where $\langle \dots \rangle^{\{0\}}$ means the thermodynamic average in the interaction-free system, $S_{\vec{q}}^{(\sigma,z)}$ is the Fourier transform of $S_i^{(\sigma,z)}$, $G_{\vec{k}c}^{\{0\}} = \frac{1}{E - \epsilon_{\vec{k}}}$ is the free Green's function, and N is the number of lattice sites. Note that throughout this thesis we will leave out the \hbar from the definitions of the Green's functions and spectral densities but we will leave it elsewhere to get e.g. the correct values of the transport quantities.

- The high-energy expansions of the (conduction-electron) Green's function and the self-energy [Hickel, 2004]:

The spectral density is essentially given by the imaginary part of the (conduction-electron) Green's function $G_{\vec{k}\sigma c}^{\dagger}(E) = \langle \langle c_{\vec{k}\sigma}; c_{\vec{k}\sigma}^{\dagger} \rangle \rangle$

$$A_{\vec{k}\sigma}^{\dagger}(E) = -\frac{1}{\pi} \text{Im} G_{\vec{k}\sigma c}^{\dagger}(E) \quad (3.5)$$

The so-called spectral moments are defined by

$$M_{\vec{k}\sigma}^{(n)} = \int_{-\infty}^{+\infty} dE E^n A_{\vec{k}\sigma}^{\dagger}(E). \quad (3.6)$$

They can in principle be calculated by

$$M_{\vec{k}\sigma}^{(n)} = \langle \underbrace{[\dots [c_{\vec{k}\sigma}, \mathcal{H}], \mathcal{H}], \dots, \mathcal{H}]}_{n\text{-fold commutator}}, c_{\vec{k}\sigma}^{\dagger} \rangle_+, \quad (3.7)$$

where $[\dots, \dots]_+$ means the anticommutator. From the spectral representation of the Green's function one gets its high-energy expansion:

$$G_{\vec{k}\sigma c}^{\dagger}(E) = \sum_{n=0}^{\infty} \frac{M_{\vec{k}\sigma}^{(n)}}{E^{n+1}} \quad (3.8)$$

For the self-energy one can write

$$\Sigma_{\vec{k}\sigma}^c(E) = \sum_{m=0}^{\infty} \frac{C_{\vec{k}\sigma}^{(m)}}{E^m} \quad (3.9)$$

From the Dyson equation, $EG_{\vec{k}\sigma c}(E) = 1 + [(\epsilon_{\vec{k}} - \mu) + \Sigma_{\vec{k}\sigma}^c(E)]G_{\vec{k}\sigma c}(E)$, it follows

$$\begin{aligned} M_{\vec{k}\sigma}^{(0)} &= 1 \\ M_{\vec{k}\sigma}^{(1)} &= \epsilon_{\vec{k}} + C_{\vec{k}\sigma}^{(0)} && \Rightarrow C_{\vec{k}\sigma}^{(0)} = M_{\vec{k}\sigma}^{(1)} - \epsilon_{\vec{k}} \\ M_{\vec{k}\sigma}^{(2)} &= M_{\vec{k}\sigma}^{(1)}(C_{\vec{k}\sigma}^{(0)} + \epsilon_{\vec{k}}) + M_{\vec{k}\sigma}^{(0)}C_{\vec{k}\sigma}^{(1)} && \Rightarrow C_{\vec{k}\sigma}^{(1)} = M_{\vec{k}\sigma}^{(2)} - \left(M_{\vec{k}\sigma}^{(1)}\right)^2 \\ M_{\vec{k}\sigma}^{(3)} &= M_{\vec{k}\sigma}^{(2)}(C_{\vec{k}\sigma}^{(0)} + \epsilon_{\vec{k}}) + M_{\vec{k}\sigma}^{(1)}C_{\vec{k}\sigma}^{(1)} + M_{\vec{k}\sigma}^{(0)}C_{\vec{k}\sigma}^{(2)} && \Rightarrow C_{\vec{k}\sigma}^{(2)} = M_{\vec{k}\sigma}^{(3)} - 2M_{\vec{k}\sigma}^{(2)}M_{\vec{k}\sigma}^{(1)} \\ &&& \quad + \left(M_{\vec{k}\sigma}^{(1)}\right)^3 \end{aligned} \quad (3.10)$$

The spectral moments can be calculated and the C -coefficients are the following:

$$C_{\vec{k}\sigma}^{(0)} = \frac{J}{2} z_{\sigma} \langle S^z \rangle \quad (3.11)$$

$$C_{\vec{k}\sigma}^{(1)} = \frac{J^2}{2} \Delta_{\sigma} + \frac{J^2}{4} [S(S+1) - z_{\sigma} \langle S^z \rangle] - \frac{J^2}{4} \langle S^z \rangle^2 \quad (3.12)$$

$$\begin{aligned} C_{\vec{k}\sigma}^{(2)} &= \frac{J^2}{4} \frac{1}{N} \sum_{ii'} e^{i\vec{k}(\vec{R}_i - \vec{R}_{i'})} T_{ii'} (\langle S_i^z S_{i'}^z \rangle + \langle S_i^{-\sigma} S_{i'}^{\sigma} \rangle) - \epsilon_{\vec{k}} \frac{J^2}{4} \langle S^z \rangle^2 \\ &\quad + \frac{J^2}{4} \sum_i T_{il} \left(2z_{\sigma} \langle S_l^z c_{i-\sigma}^{\dagger} c_{l-\sigma} \rangle - \langle S_l^{\sigma} c_{i-\sigma}^{\dagger} c_{l\sigma} \rangle - \langle S_l^{-\sigma} c_{i\sigma}^{\dagger} c_{l-\sigma} \rangle \right) \\ &\quad + \frac{J^2}{2} \sum_i T_{il} \left(\langle S_l^{\sigma} c_{l-\sigma}^{\dagger} c_{i\sigma} \rangle - \langle S_l^{\sigma} c_{i-\sigma}^{\dagger} c_{l\sigma} \rangle \right) \\ &\quad - \frac{J^3}{8} S(S+1) (1 + z_{\sigma} \langle S^z \rangle - 2 \langle n_{-\sigma}^c \rangle) \\ &\quad + \frac{J^3}{8} z_{\sigma} \langle S^z \rangle (1 + z_{\sigma} \langle S^z \rangle)^2 - \frac{J^3}{2} z_{\sigma} \langle S^z \rangle \Delta_{\sigma}. \end{aligned} \quad (3.13)$$

We have used the Fourier transform of the dispersion $\epsilon_{\vec{k}}$: $T_{ii'} = \frac{1}{N} \sum_{\vec{k}} \epsilon_{\vec{k}} e^{i\vec{k}(\vec{R}_i - \vec{R}_{i'})}$. \vec{R}_l in Eq. (3.13) denotes an arbitrary site.

- The ground state of the antiferromagnetic Kondo lattice model with one conduction electron [Tsunetsugu et al., 1997]:

The ground state of the antiferromagnetic Kondo lattice model with $S = \frac{1}{2}$ and one conduction electron has the total spin quantum number $S_{\text{tot}} = \frac{1}{2}(N - 1)$ and is unique, apart from its $(2S_{\text{tot}} + 1)$ -fold spin degeneracy if the nearest-neighbor hopping-matrix element $-t$ is negative. ($-t$ is $T_{\langle ii' \rangle}$ for nearest-neighbor sites \vec{R}_i and $\vec{R}_{i'}$.)

- The ground state of the half-filled Kondo lattice model [Tsunetsugu et al., 1997]:

The ground state of the half-filled Kondo lattice model is unique and has $S_{\text{tot}} = 0$ for the antiferromagnetic KLM if the lattice is bipartite, and for the ferromagnetic Kondo lattice model if the lattice is bipartite and the number of sites is equal in both sublattices.

- The “large” Fermi volume in the antiferromagnetic Kondo lattice model [Oshikawa, 2000]:

The Fermi volume of the antiferromagnetic Kondo lattice model is “large”, i.e. contains the number of the completely localized electrons (spins), if the system is in a nonmagnetic Fermi liquid state.

To all these exact statements we add in section 3.2 the exact mapping of the periodic Anderson model on the antiferromagnetic Kondo lattice model for arbitrary coupling constant J , first, for spin $S = \frac{1}{2}$, second, for spin $S = 1$ and, finally, for arbitrary spin S . In subsection 3.2.4, based on the exact mapping of the PAM on the KLM, the large Fermi volume of a nonmagnetic Fermi liquid state of the antiferromagnetic KLM for $S = \frac{1}{2}$ is shown.

3.2 Exact mapping of the periodic Anderson model on the Kondo lattice model

3.2.1 Introductory remarks

In section 3.2.2 it is shown that the antiferromagnetic Kondo lattice model for spin $S = 1/2$ and for *any* finite coupling constant $J < 0$ can be obtained by an *exact* mapping from the periodic Anderson model in an appropriate limit, which we will call the extended Kondo limit (EKL). We thus add a rigorous statement on the Kondo lattice model to the known ones described in section 3.1. The mapping allows a direct proof of the “large” Fermi volume for a nonmagnetic Fermi-liquid state of the Kondo lattice model for $S = \frac{1}{2}$ (section 3.2.4), which can replace a far more difficult topological proof by Oshikawa [Oshikawa, 2000].

As stated before, both the periodic Anderson model and the antiferromagnetic Kondo lattice model are standard models to describe heavy fermion systems [Hewson, 1997, Fazekas, 1999, Tsunetsugu et al., 1997]. The properties of those systems originate from an interplay between rather localized f electrons and itinerant s , p or d electrons. In the (nondegenerate) periodic Anderson model (PAM) this is mimicked in a minimal way. The Hamiltonian of the nondegenerate PAM is given by

$$\mathcal{H}_{\text{PAM}} = \sum_{\vec{k}\sigma} \epsilon_{\vec{k}} n_{\vec{k}\sigma}^c + \sum_{i\sigma} \epsilon_f n_{i\sigma}^f + U \sum_i n_{i\uparrow}^f n_{i\downarrow}^f + \sum_{\vec{k}i\sigma} (V_{\vec{k}} e^{-i\vec{k}\vec{R}_i} c_{\vec{k}\sigma}^\dagger f_{i\sigma} + \text{H.c.}) . \quad (3.14)$$

$c_{\vec{k}\sigma}^{(\dagger)}$ creates/annihilates a conduction electron (s electron) with momentum \vec{k} and spin σ . $f_{i\sigma}^{(\dagger)}$ is the creation/annihilation operator for an f electron at site \vec{R}_i . $n_{\vec{k}\sigma}^c$ and $n_{i\sigma}^f$ are the respective number operators. There are nondegenerate f orbitals with energy ϵ_f , with an intraorbital Coulomb interaction U and a generally \vec{k} -dependent hybridization $V_{\vec{k}}$ of these orbitals with the states of the nondegenerate conduction band $\epsilon_{\vec{k}}$.

The Kondo lattice model is used to describe the effective physics by modeling the f electrons as localized quantum mechanical spins with an antiferromagnetic spin exchange (coupling constant $J < 0$). The KLM is given by

$$\mathcal{H}_{\text{KLM}} = \sum_{\vec{k}\sigma} \epsilon_{\vec{k}} n_{\vec{k}\sigma}^c - \sum_{\vec{k}\vec{k}'i} J_{\vec{k}'\vec{k}} e^{-i(\vec{k}'-\vec{k})\vec{R}_i} \vec{S}_i \cdot \vec{s}_{\vec{k}'\vec{k}} . \quad (3.15)$$

The first part stands for the conduction band. The second part describes the interaction between localized quantum-mechanical spins \vec{S}_i of magnitude S and the spins of the conduction electrons $\vec{s}_{\vec{k}'\vec{k}} = \frac{1}{2} \sum_{\sigma'\sigma} c_{\vec{k}'\sigma'}^\dagger \vec{\tau}_{\sigma'\sigma} c_{\vec{k}\sigma}$ (with $\vec{\tau}$ representing the Pauli matrices). $J_{\vec{k}'\vec{k}}$ are the (antiferromagnetic) coupling constants ($J_{\vec{k}'\vec{k}} < 0$).

The KLM with $S = \frac{1}{2}$ represents an effective model in the so-called Kondo regime (which is relevant for the heavy-fermion systems) of the nondegenerate PAM. There is an approximate correspondence of the two models in the Kondo regime, namely in a perturbational sense. This correspondence becomes rigorous in the Kondo limit of the PAM, which means taking the weak-coupling limit ($J \rightarrow 0$) in the KLM. The Kondo regime of the PAM is a regime favorable for the formation of local f moments. A necessary condition for this is that the energy of the singly (doubly) occupied f orbital lies below (above) the chemical potential: $\epsilon_f < 0$ ($\epsilon_f + U > 0$). The energy distance of the two levels ϵ_f and $\epsilon_f + U$ to the chemical potential

should be large compared with the hybridization so that fluctuations of the f -orbital occupancy are small. This condition is sometimes formulated in terms of the width Γ of the virtual levels of the single-impurity Anderson model [Tsunetsugu et al., 1997, Schrieffer and Wolff, 1966]:

$$\frac{\Gamma}{|\epsilon_f|}, \frac{\Gamma}{\epsilon_f + U} \ll 1, \quad (3.16)$$

where $\Gamma = \pi\rho_0 V^2$. ρ_0 is the density of states of the free conduction band at the Fermi energy. V is the average hybridization ($V^2 = \{|V_k|^2\}_{\text{av}}$). Via the Schrieffer-Wolff transformation, the Kondo regime of the PAM is approximately mapped on the weak-coupling (small- J) regime of the Kondo lattice model. Assuming a constant free conduction-electron density of states at the Fermi energy (ρ_0), the limit in which the mapping becomes exact (Kondo limit) is given by

$$\frac{V^2}{\epsilon_f}, \frac{V^2}{\epsilon_f + U} \longrightarrow 0. \quad (3.17)$$

The Kondo limit can be understood as

$$V \rightarrow 0 \quad \text{or} \quad |\epsilon_f|, \epsilon_f + U \rightarrow \infty \quad [\text{Lacroix and Cyrot, 1979}]. \quad (3.18)$$

Both corresponds to $J \rightarrow 0$ on the side of the Kondo lattice model.²

This relationship between the two models is known since long ago. In 1966 Schrieffer and Wolff [Schrieffer and Wolff, 1966] showed it for the corresponding impurity models, the single impurity Anderson model [Anderson, 1961] and the Kondo impurity model [Kondo, 1964]. In the single impurity Anderson model there is just one impurity f orbital at a certain site in the infinite lattice. In the Kondo impurity model there is just one f spin at a certain site in the lattice. Later the Schrieffer-Wolff transformation was generalized to the periodic models, the PAM and the KLM [Lacroix and Cyrot, 1979, Proetto and Lopež, 1981]. More recently Matsumoto and Ohkawa [Matsumoto and Ohkawa, 1995] claimed an equivalence between the impurity models in a special “ s - d ” limit, which we will call in the following “extended Kondo limit” and which differs from the conventional Kondo limit. Based on a dynamical mean-field theory (DMFT) argument they inferred the same equivalence to hold between the periodic

²As pointed out by S. K. Kehrein and A. Mielke [Kehrein and Mielke, 1996], if ϵ_f or $\epsilon_f + U$ lie within the conduction band (which may be the case if just taking the limit $V \rightarrow 0$), the Schrieffer-Wolff transformation is actually problematic because of energy denominators which become zero. The problem, however, does not occur in the extended Kondo limit.

models in the case of *infinite* spatial dimensions. In this section we show that via the extended Kondo limit there is a *direct* and *rigorous* mapping between the periodic models, PAM and KLM, *in any dimensions*. Hence, we establish a fundamental relation between both models. In contrast with the conventional Kondo limit, the equivalence in the extended Kondo limit holds for *any* value of the coupling constant $J < 0$ of the KLM.

With the fact of a rigorous mapping of the PAM on the KLM one has a general and direct answer to the long-standing question of the “correct” Fermi surface sum rule for the Kondo lattice model. Luttinger’s theorem states that the volume enclosed by the Fermi surface (“Fermi volume”) is (a) independent of the interaction strength if no phase transitions take place and (b) otherwise only related to the total number of electrons. Luttinger’s theorem cannot be directly applied to the Kondo lattice model since, because of the localized f -spins, it is not a purely fermionic model. It is *a priori* unclear if the localized spins do count as “electrons” in this context. With the help of the mapping a *direct* and *rigorous* answer can be given: the respective sum rule of the periodic Anderson model is mapped on the Kondo lattice model. Therefore, we are able to prove in section 3.2.4 the “large” Fermi volume for spin $S = \frac{1}{2}$, which includes the number of localized spins in the KLM, if the system is in a nonmagnetic Fermi liquid state. We thus confirm in a much simpler way the same result of a recent topological proof by Oshikawa [Oshikawa, 2000]. Via the extended Kondo limit it will be possible to get further analytical and computational results for the Kondo lattice model. Based on the mapping every result and every analytical and computational method for the PAM can be directly applied to the KLM as long as it is compatible with the extended Kondo limit.

In subsection 3.2.2 the proof will be given for an exact mapping of the nondegenerate periodic Anderson model in the extended Kondo limit on the Kondo lattice model with $S = \frac{1}{2}$. In the following subsection the proof will be extended to the $S = 1$ -KLM and after that to arbitrary value of S . In subsection 3.2.4 we prove the large Fermi volume of the $S = \frac{1}{2}$ -KLM for a nonmagnetic Fermi-liquid state. All these proofs closely follow the lines of Ref. [Sinjukow and Nolting, 2002].

3.2.2 Proof of exact mapping of the PAM in the extended Kondo limit on the KLM for $S = \frac{1}{2}$

The extended Kondo limit (EKL), Matsumoto’s and Ohkawa’s s - d limit [Matsumoto and Ohkawa, 1995], which, as we will show, leads to an *exact* mapping of the periodic Anderson model to the Kondo lattice model for

$S = \frac{1}{2}$ for arbitrary $J < 0$ in any dimensions, is given by

$$\begin{aligned} \epsilon_f &\equiv -\frac{U}{2} \\ U \rightarrow \infty, \quad V \rightarrow \infty \quad &\text{with} \quad \frac{V^2}{U} \rightarrow \text{const.} \end{aligned} \quad (3.19)$$

It clearly differs from the conventional Kondo limit where one has $V \rightarrow 0$ or $|\epsilon_f|, \epsilon_f + U \rightarrow \infty$ [Lacroix and Cyrot, 1979] [see Eq. (3.18)]. Note that in the EKL $\epsilon_f \rightarrow -\infty$ as $U \rightarrow \infty$. We assume $\epsilon_f \equiv -\frac{U}{2}$ for simplicity. It is actually only required that $-\frac{2\epsilon_f}{U} \rightarrow 1$. Our proof of an exact mapping in the EKL consists of two basic steps. First, a finite unitary Schrieffer-Wolff transformation is performed on the Hamiltonian of the PAM. Second, the consequences of the EKL on the transformed Hamiltonian are checked. We rigorously prove that the only terms which remain relevant are those of the Kondo lattice model.

The first three terms of \mathcal{H}_{PAM} (3.14) are denoted by

$$\mathcal{H}_0 = \sum_{\vec{k}\sigma} \epsilon_{\vec{k}} n_{\vec{k}\sigma}^c + \sum_{i\sigma} \epsilon_f n_{i\sigma}^f + U \sum_i n_{i\uparrow}^f n_{i\downarrow}^f, \quad (3.20)$$

the hybridization term by

$$\mathcal{H}_V = \sum_{\vec{k}i\sigma} (V_{\vec{k}} e^{-i\vec{k}\vec{R}_i} c_{\vec{k}\sigma}^\dagger f_{i\sigma} + \text{H.c.}). \quad (3.21)$$

Now we eliminate all terms which are first-order in $V_{\vec{k}}$ (i.e. we eliminate \mathcal{H}_V) by a unitary transformation

$$\bar{\mathcal{H}} = e^{\mathcal{S}} \mathcal{H}_{\text{PAM}} e^{-\mathcal{S}} \quad (3.22)$$

where the generator \mathcal{S} is anti-Hermitian $\mathcal{S}^\dagger = -\mathcal{S}$. The condition to eliminate \mathcal{H}_V is

$$[\mathcal{S}, \mathcal{H}_0] = -\mathcal{H}_V. \quad (3.23)$$

The required generator turns out to be

$$\mathcal{S} = \sum_{\vec{k}i\sigma} \left(\frac{V_{\vec{k}} e^{-i\vec{k}\vec{R}_i}}{\epsilon_{\vec{k}} - \epsilon_f - U} n_{i-\sigma}^f c_{\vec{k}\sigma}^\dagger f_{i\sigma} + \frac{V_{\vec{k}} e^{-i\vec{k}\vec{R}_i}}{\epsilon_{\vec{k}} - \epsilon_f} (1 - n_{i-\sigma}^f) c_{\vec{k}\sigma}^\dagger f_{i\sigma} \right) - \text{H.c.} \quad (3.24)$$

The unitarily transformed Hamiltonian is given by

$$\bar{\mathcal{H}} = \mathcal{H}_0 + \mathcal{H}_2 + \frac{1}{3}[\mathcal{S}, [\mathcal{S}, \mathcal{H}_V]] + \frac{1}{8}[\mathcal{S}, [\mathcal{S}, [\mathcal{S}, \mathcal{H}_V]]] + \dots, \quad (3.25)$$

with

$$\mathcal{H}_2 \equiv \frac{1}{2}[\mathcal{S}, \mathcal{H}_V] = \mathcal{H}_{\text{ex}} + \mathcal{H}_{\text{dir}} + \mathcal{H}_{\text{hop}} + \mathcal{H}_{\text{ch}}, \quad (3.26)$$

where

$$\mathcal{H}_{\text{ex}} = -\frac{1}{2} \sum_{\vec{k}\vec{k}'i} J_{\vec{k}'\vec{k}} e^{-i(\vec{k}'-\vec{k})\vec{R}_i} (S_i^{f+} c_{\vec{k}'\downarrow}^\dagger c_{\vec{k}\uparrow} + S_i^{f-} c_{\vec{k}'\uparrow}^\dagger c_{\vec{k}\downarrow} + S_i^{fz} (c_{\vec{k}'\uparrow}^\dagger c_{\vec{k}\uparrow} - c_{\vec{k}'\downarrow}^\dagger c_{\vec{k}\downarrow})) \quad (3.27)$$

$$\mathcal{H}_{\text{dir}} = -\sum_{\vec{k}\vec{k}'i\sigma} [W_{\vec{k}'\vec{k}} - \frac{1}{4}J_{\vec{k}'\vec{k}}(n_{i\uparrow}^f + n_{i\downarrow}^f)] e^{-i(\vec{k}'-\vec{k})\vec{R}_i} c_{\vec{k}'\sigma}^\dagger c_{\vec{k}\sigma} \quad (3.28)$$

$$\mathcal{H}_{\text{hop}} = \sum_{\vec{k}i\sigma} [W_{\vec{k}\vec{k}} - \frac{1}{4}J_{\vec{k}\vec{k}}(n_{i-\sigma}^f + n_{i\sigma}^f)] e^{-i\vec{k}(\vec{R}_i - \vec{R}_{i'})} f_{i'\sigma}^\dagger f_{i\sigma} \quad (3.29)$$

$$\begin{aligned} \mathcal{H}_{\text{ch}} = & -\frac{1}{2} \sum_{\vec{k}\vec{k}'i\sigma} V_{\vec{k}'} V_{\vec{k}} e^{-i(\vec{k}'+\vec{k})\vec{R}_i} [(\epsilon_{\vec{k}'} - \epsilon_f - U)^{-1} - (\epsilon_{\vec{k}} - \epsilon_f)^{-1}] * \\ & * c_{\vec{k}'-\sigma}^\dagger c_{\vec{k}\sigma}^\dagger f_{i\sigma} f_{i-\sigma} + \text{H.c.} \end{aligned} \quad (3.30)$$

with coupling constants

$$\begin{aligned} J_{\vec{k}'\vec{k}} = & -V_{\vec{k}'} V_{\vec{k}}^* [-(\epsilon_{\vec{k}} - \epsilon_f - U)^{-1} - (\epsilon_{\vec{k}'} - \epsilon_f - U)^{-1} \\ & + (\epsilon_{\vec{k}} - \epsilon_f)^{-1} + (\epsilon_{\vec{k}'} - \epsilon_f)^{-1}], \end{aligned} \quad (3.31)$$

$$W_{\vec{k}'\vec{k}} = -\frac{1}{2} V_{\vec{k}'} V_{\vec{k}}^* [(\epsilon_{\vec{k}} - \epsilon_f)^{-1} + (\epsilon_{\vec{k}'} - \epsilon_f)^{-1}]. \quad (3.32)$$

The spin operators in (3.27) are given by $\vec{S}_i^f = \frac{1}{2} \sum_{\sigma'\sigma} f_{i\sigma'}^\dagger \vec{\tau}_{\sigma'\sigma} f_{i\sigma}$.

Now the consequences of the extended Kondo limit [Eq. (3.19)] on the transformed Hamiltonian $\bar{\mathcal{H}}$ are checked. If we assume a realistic conduction band of finite width, the norm of the generator in the EKL has the asymptotics

$$\|\mathcal{S}\| \stackrel{\text{EKL}}{\propto} \frac{V}{U}. \quad (3.33)$$

With

$$\|\mathcal{H}_V\| \propto V \quad \text{and} \quad V \stackrel{\text{EKL}}{\propto} \sqrt{U} \quad (3.34)$$

it follows that all higher commutators in (3.25), starting at the order V^3/U^2 , exactly vanish in the EKL,

$$[\mathcal{S}, [\mathcal{S}, \mathcal{H}_V]] , [\mathcal{S}, [\mathcal{S}, [\mathcal{S}, \mathcal{H}_V]]] , \dots \xrightarrow{\text{EKL}} 0 , \quad (3.35)$$

and it is sufficient to consider the EKL of the remaining Hamiltonian

$$\bar{\mathcal{H}}' \equiv \mathcal{H}_0 + \mathcal{H}_2 . \quad (3.36)$$

It is important to note that one cannot proceed with the original argument given by Schrieffer and Wolff for the Kondo regime of the single-impurity Anderson model [Schrieffer and Wolff, 1966]. Their argument goes as follows. For the single-impurity Anderson model the sum over i and i' in our expression for \mathcal{H}_{hop} [Eq. (3.29)] reduces to a single term for the single f orbital. Therefore, the corresponding term for \mathcal{H}_{ch} [Eq. (3.30) without the sum over i] is in Schrieffer's and Wolff's original paper the only term which changes the number of f electrons, namely between zero and two. Hence, there the Hilbert space separates at that stage into one part of single and one part of zero and double f occupancy. The part with zero and double f occupancy becomes irrelevant at low enough temperatures or if $|\epsilon_f|, \epsilon_f + U \rightarrow \infty$.

The reason why this argumentation is no longer valid for the periodic Anderson model is that apart from \mathcal{H}_{ch} [Eq. (3.30)] also \mathcal{H}_{hop} [Eq. (3.29)] changes the number of f electrons at given sites. \mathcal{H}_{hop} connects the subspace of single f occupancy with the subspaces of zero and double occupancy. Therefore, the Hilbert space cannot be separated at this stage. To prove an effective fixing of the f -orbital occupation to one, which nevertheless does happen in the extended Kondo limit, one needs to apply a different and more formal line of argumentation.

We denote the s and f electron parts of \mathcal{H}_0 separately,

$$\mathcal{H}_0^s = \sum_{\vec{k}\sigma} \epsilon_{\vec{k}} n_{\vec{k}\sigma}^c , \quad \mathcal{H}_0^U = \sum_{i\sigma} \epsilon_f n_{i\sigma}^f + U \sum_i n_{i\uparrow}^f n_{i\downarrow}^f . \quad (3.37)$$

In the EKL the norms of the different parts of $\bar{\mathcal{H}}'$ behave as:

$$\|\mathcal{H}_0^s\| \propto \mathcal{W} = \text{const.} \quad (3.38)$$

$$\|\mathcal{H}_2\| \propto \tilde{J} \equiv \frac{V^2}{U} = \text{const.} \quad (3.39)$$

$$\|\mathcal{H}_0^U\| \propto U \xrightarrow{\text{EKL}} \infty . \quad (3.40)$$

\mathcal{W} is the width of the free conduction band. Obviously, with respect to $\bar{\mathcal{H}}'$ the EKL is equivalent to just taking the limit $U \rightarrow \infty$ (and $\epsilon_f \equiv -\frac{U}{2} \rightarrow -\infty$). V

needs not to be considered explicitly since it only appears within the ratio $V^2/U \equiv \tilde{J}$, which is a constant in the EKL.

Let us consider $\bar{\mathcal{H}}'$ and its eigenstates as functions of the three parameters \mathcal{W} , \tilde{J} and U . It is clear that the eigenstates $\{|\Psi(\mathcal{W}, \tilde{J}, U)\rangle\}$ actually only depend on the ratios \mathcal{W}/U and \tilde{J}/U since any Hamiltonian can be multiplied by any constant without changing its eigenstates. Therefore, in the EKL ($U \rightarrow \infty$) each eigenstate $|\Psi\rangle$ of $\bar{\mathcal{H}}'$ approaches an eigenstate $|\Psi^0\rangle$ of \mathcal{H}_0^U :

$$|\Psi(\mathcal{W}, \tilde{J}, U)\rangle \xrightarrow{U \rightarrow \infty} |\Psi(0, 0, U')\rangle \equiv |\Psi^0\rangle \quad (3.41)$$

with arbitrary U' . Note that the states $\{|\Psi^0\rangle\}$ that are approached in the EKL are highly non-trivial superpositions of trivial degenerate eigenstates of \mathcal{H}_0^U . Still, they can be grouped into two classes: first, states $\{|\Psi_1^0\rangle\}$ with a single f electron at each site, and second, states $\{|\Psi_2^0\rangle\}$ with admixtures of zero and double f occupation. In the EKL of the Hamiltonian $\bar{\mathcal{H}}'$ the energies of the $|\Psi_2^0\rangle$'s are higher than the energies of the $|\Psi_1^0\rangle$'s by amounts proportional to U . In the EKL ($U \rightarrow \infty$) the statistical weights of the $|\Psi_2^0\rangle$'s obviously vanish. Moreover, the creation or annihilation of s electrons, which must be taken into account with regard to s -electron Green's functions of the KLM, do not connect the $|\Psi_1^0\rangle$'s with the $|\Psi_2^0\rangle$'s. Hence, in the EKL only the states $\{|\Psi_1^0\rangle\}$ are *relevant*, and the states $|\Psi_2^0\rangle$ are *irrelevant* for our purposes, which consist in describing s -electron excitations at finite temperatures. The number of f electrons of the relevant states is effectively fixed to one at each site,

$$n_{i\uparrow}^f + n_{i\downarrow}^f \stackrel{\text{EKL}}{\equiv} 1, \quad (3.42)$$

despite the hopping terms in \mathcal{H}_{hop} and the terms which change the f occupation by two in \mathcal{H}_{ch} .

Based on this, an effective Hamiltonian $\bar{\mathcal{H}}''$ can be formulated, which describes only the relevant states of $\bar{\mathcal{H}}'$ in the EKL. Using $n_{i\uparrow}^f + n_{i\downarrow}^f \equiv 1$ or applying the corresponding projection operators $\mathcal{P}_i = n_{i\uparrow}^f + n_{i\downarrow}^f - 2n_{i\uparrow}^f n_{i\downarrow}^f$ from the right- and left-hand side, several terms of $\bar{\mathcal{H}}'$ can be neglected. Since \mathcal{H}_0^U is the only diverging term, there cannot be any finite effective interactions that are omitted this way³. \mathcal{H}_{ch} can be neglected completely. \mathcal{H}_{hop} reduces

³ A case where one has to take care of such effective interactions which remain in perturbation theory is the exactly half-filled Hubbard model in the case of $T_{ii'} \rightarrow \infty$ and $U \rightarrow \infty$ with $\frac{T_{ii'}^2}{U} = \text{const.}$. $T_{ii'}$ are the hopping integrals. $J_{ii'} = -2\frac{T_{ii'}^2}{U}$ are the exchange constants of an effective spin-spin coupling of the electrons, which, however, vanishes if only $U \rightarrow \infty$ but $T_{ii'} = \text{const.}$ Similar effective exchange interactions occur in the interplay of \mathcal{H}_{hop} [Eq. (3.29)] and H_U^0 [Eq. (3.37)] but vanish in the EKL since U is the only diverging parameter [see Eqs. (3.38)–(3.40)].

to the constant $N \sum_{\vec{k}} W_{\vec{k}\vec{k}}$, N being the number of lattice sites. The coupling constants simplify to

$$W_{\vec{k}'\vec{k}} \stackrel{\text{EKL}}{=} -\frac{2V_{\vec{k}'}V_{\vec{k}}^*}{U} \quad (3.43)$$

$$\text{and } J_{\vec{k}'\vec{k}} \stackrel{\text{EKL}}{=} -\frac{8V_{\vec{k}'}V_{\vec{k}}^*}{U}. \quad (3.44)$$

Taking (3.43) and (3.44) into account, \mathcal{H}_{dir} exactly vanishes. Neglecting the Hubbard term ($U \sum_i n_{i\uparrow}^f n_{i\downarrow}^f$) as it describes double f occupation, the effective Hamiltonian in the EKL is finally given by

$$\bar{\mathcal{H}}'' = \sum_{\vec{k}\sigma} \epsilon_{\vec{k}} n_{\vec{k}\sigma}^c + \mathcal{H}_{\text{ex}} + N\epsilon_f + N \sum_{\vec{k}} W_{\vec{k}\vec{k}}. \quad (3.45)$$

Apart from constants, $\bar{\mathcal{H}}''$ corresponds to the Kondo lattice model \mathcal{H}_{KLM} (3.15) for $S = \frac{1}{2}$. As there are no f -electron fluctuations, the spin operators \vec{S}_i in \mathcal{H}_{ex} now describe localized quantum-mechanical spins of magnitude $1/2$.

As $V/U \xrightarrow{\text{EKL}} 0$, for the generator one has $\mathcal{S} \xrightarrow{\text{EKL}} 0$. Therefore, the unitary Schrieffer-Wolff transformation reduces to an identical transformation. Thus, in terms of *relevant* states and disregarding *unimportant* constants, we have proven

$$\mathcal{H}_{\text{PAM}} \xrightarrow{\text{EKL}} \mathcal{H}_{\text{KLM}}. \quad (3.46)$$

The coupling constants of the KLM (3.15) are given by (3.44).

3.2.3 Proof of exact mapping of a degenerate PAM with spin constraint on the KLM for $S \geq 1$

In this subsection we first show that the exact mapping of the PAM on the KLM can be applied to spins $S = 1$. At the end we generalize this result further to arbitrary spin S . The proofs for $S > \frac{1}{2}$ follow closely the lines of the proof for $S = \frac{1}{2}$ in the previous subsection 3.2.2. Therefore, we will only give the essential steps of argumentation here and presuppose that the reader has gone through the proof in section 3.2.2. For the mapping on the KLM with spin $S = 1$ we need a twofold degenerate periodic Anderson model with a spin constraint. The Hamiltonian consists of three parts:

$$\mathcal{H}_{\text{dPAM}} = \mathcal{H}_0 + \mathcal{H}_V + \mathcal{H}_S \quad (3.47)$$

with

$$\mathcal{H}_0 = \sum_{\vec{k}\sigma} \epsilon_{\vec{k}} n_{\vec{k}\sigma}^c + \sum_{i\sigma} \epsilon_f (n_{1i\sigma}^f + n_{2i\sigma}^f) + U \sum_i (n_{1i\uparrow}^f n_{1i\downarrow}^f + n_{2i\uparrow}^f n_{2i\downarrow}^f), \quad (3.48)$$

$$\mathcal{H}_V = \sum_{\vec{k}i\sigma} \left[V_{\vec{k}} e^{-i\vec{k}\vec{R}_i} c_{\vec{k}\sigma}^\dagger (f_{1i\sigma} + f_{2i\sigma}) + \text{H.c.} \right] \quad (3.49)$$

$$\begin{aligned} \mathcal{H}_S &= -U_S \sum_i \vec{S}_{1i}^f \cdot \vec{S}_{2i}^f \\ &= -U_S \sum_i \left[\frac{1}{2} f_{1i\uparrow}^\dagger f_{1i\downarrow} f_{2i\downarrow}^\dagger f_{2i\uparrow} + \frac{1}{2} f_{1i\downarrow}^\dagger f_{1i\uparrow} f_{2i\uparrow}^\dagger f_{2i\downarrow} \right. \\ &\quad \left. + \frac{1}{4} \left(f_{1i\uparrow}^\dagger f_{1i\uparrow} - f_{1i\downarrow}^\dagger f_{1i\downarrow} \right) \left(f_{2i\uparrow}^\dagger f_{2i\uparrow} - f_{2i\downarrow}^\dagger f_{2i\downarrow} \right) \right] \end{aligned} \quad (3.50)$$

The Hamiltonian (3.47) contains two f orbitals at each lattice site with intra-orbital Coulomb interaction and hybridization to the conduction states. \mathcal{H}_S is the spin constraint which assures (if U_S is big enough) that at each site there is an effective spin $S = 1$ if the f orbitals are singly occupied. The proof of single occupancy of each f orbital is very similar to the proof of single f occupancy in the $S = \frac{1}{2}$ case of subsection 3.2.2. Now at the same time the spin $S = 1$ constraint has to be ensured. For this reason U_S should diverge in the extended Kondo limit. On the other hand the divergence should not disturb the argumentation which leads to the statement of single occupation of each f orbital. These conditions are fulfilled by the following extension of the extended Kondo limit [Eq. (3.19)]:

$$U_S \equiv \sqrt{U} \rightarrow \infty. \quad (3.51)$$

The new generator which fulfills the condition $[\mathcal{S}, \mathcal{H}_0] \stackrel{!}{=} -\mathcal{H}_V$ is given by

$$\begin{aligned} \mathcal{S} &= \sum_{\vec{k}i\sigma} \left\{ \frac{V_{\vec{k}} e^{-i\vec{k}\vec{R}_i}}{\epsilon_{\vec{k}} - \epsilon_f - U} \left(n_{1i-\sigma}^f c_{\vec{k}\sigma}^\dagger f_{1i\sigma} + n_{2i-\sigma}^f c_{\vec{k}\sigma}^\dagger f_{2i\sigma} \right) \right. \\ &\quad \left. + \frac{V_{\vec{k}} e^{-i\vec{k}\vec{R}_i}}{\epsilon_{\vec{k}} - \epsilon_f} \left[(1 - n_{1i-\sigma}^f) c_{\vec{k}\sigma}^\dagger f_{1i\sigma} + (1 - n_{2i-\sigma}^f) c_{\vec{k}\sigma}^\dagger f_{2i\sigma} \right] \right\} - \text{H.c.} \end{aligned} \quad (3.52)$$

The unitarily transformed Hamiltonian is

$$\bar{\mathcal{H}} = e^{\mathcal{S}} \mathcal{H}_{\text{dPAM}} e^{-\mathcal{S}} \quad (3.53)$$

$$\begin{aligned} &= \mathcal{H}_0 + \mathcal{H}_S + [\mathcal{S}, \mathcal{H}_S] + \frac{1}{2} [\mathcal{S}, \mathcal{H}_V] + \frac{1}{2} [\mathcal{S}, [\mathcal{S}, \mathcal{H}_S]] + \frac{1}{3} [\mathcal{S}, [\mathcal{S}, \mathcal{H}_V]] \\ &\quad + \frac{1}{6} [\mathcal{S}, [\mathcal{S}, [\mathcal{S}, \mathcal{H}_S]]] + \frac{1}{8} [\mathcal{S}, [\mathcal{S}, [\mathcal{S}, \mathcal{H}_V]]] + \dots \end{aligned} \quad (3.54)$$

Because of $\|\mathcal{H}_S\| \propto U_S$ and the analogs of Eqs. (3.33) and (3.34) for S and \mathcal{H}_V defined in Eqs. (3.52) and (3.49), respectively, all higher order commutators vanish in the extended Kondo limit as in the $S = \frac{1}{2}$ case:

$$[\mathcal{S}, [\mathcal{S}, \mathcal{H}_S]], [\mathcal{S}, [\mathcal{S}, \mathcal{H}_V]], [\mathcal{S}, [\mathcal{S}, [\mathcal{S}, \mathcal{H}_S]]], [\mathcal{S}, [\mathcal{S}, [\mathcal{S}, \mathcal{H}_V]]], \dots \xrightarrow{\text{EKL}} 0. \quad (3.55)$$

In the EKL it is sufficient to consider the Hamiltonian

$$\bar{\mathcal{H}}' = \mathcal{H}_0 + \mathcal{H}_S + \mathcal{H}_{fs} + \frac{1}{2}[\mathcal{S}, \mathcal{H}_V] \quad (3.56)$$

$$\text{with } \mathcal{H}_{fs} \equiv [\mathcal{S}, \mathcal{H}_S]. \quad (3.57)$$

\mathcal{H}_{fs} contains the correlated hopping of electrons from f to s orbitals and *vice versa*. If we denote the parts of the Hamiltonian and the generator which consist of electron operators of the first and the second f orbital by superscripts $f1$ and $f2$ then the second commutator of $\bar{\mathcal{H}}'$ is given by

$$\begin{aligned} \frac{1}{2}[\mathcal{S}, \mathcal{H}_V] &= \frac{1}{2}[\mathcal{S}^{f1} + \mathcal{S}^{f2}, \mathcal{H}_V^{f1} + \mathcal{H}_V^{f2}] \\ &= \mathcal{H}_2^{f1} + \mathcal{H}_2^{f2} + \mathcal{H}_{f1f2} \\ \text{with } \mathcal{H}_2^{f1} &= \frac{1}{2}[\mathcal{S}^{f1}, \mathcal{H}_V^{f1}] \\ \mathcal{H}_2^{f2} &= \frac{1}{2}[\mathcal{S}^{f2}, \mathcal{H}_V^{f2}] \\ \mathcal{H}_{f1f2} &= \frac{1}{2}[\mathcal{S}^{f1}, \mathcal{H}_V^{f2}] + \frac{1}{2}[\mathcal{S}^{f2}, \mathcal{H}_V^{f1}]. \end{aligned} \quad (3.58)$$

All the terms of \mathcal{H}_2^{f1} and \mathcal{H}_2^{f2} are defined analogously to the terms of \mathcal{H}_2 in Eqs. (3.26)–(3.30) for the first and the second f orbital, respectively. \mathcal{H}_2 in this subsection denotes the sum of \mathcal{H}_2^{f1} and \mathcal{H}_2^{f2} . \mathcal{H}_{f1f2} contains hopping terms from the first to the second f orbital and *vice versa*.

The next steps of our proof are in full analogy to the $S = \frac{1}{2}$ -case. We separate \mathcal{H}_0 into the s and f electron parts:

$$\mathcal{H}_0^s = \sum_{\vec{k}\sigma} \epsilon_{\vec{k}} n_{\vec{k}\sigma}^c, \quad \mathcal{H}_0^f = \sum_{i\sigma} \epsilon_f \left(n_{1i\sigma}^f + n_{2i\sigma}^f \right) + U \sum_i \left(n_{1i\uparrow}^f n_{1i\downarrow}^f + n_{2i\uparrow}^f n_{2i\downarrow}^f \right). \quad (3.59)$$

In the EKL the norms of the different parts of $\bar{\mathcal{H}}'$ behave as:

$$\|\mathcal{H}_0^s\| \propto \mathcal{W} = \text{const.} \quad (3.60)$$

$$\|\mathcal{H}_2\| = \|\mathcal{H}_2^{f1} + \mathcal{H}_2^{f2}\| \propto \tilde{J} \equiv \frac{V^2}{U} = \text{const.} \quad (3.61)$$

$$\|\mathcal{H}_{f_1 f_2}\| \propto \tilde{J} = \text{const.} \quad (3.62)$$

$$\|\mathcal{H}_{f_s}\| \propto \tilde{J} = \text{const.} \quad (\text{since } U_S \xrightarrow{\text{EKL}} V) \quad (3.63)$$

$$\|\mathcal{H}_S\| \propto U_S \equiv \sqrt{U} \xrightarrow{\text{EKL}} \infty \quad (3.64)$$

$$\|\mathcal{H}_0^U\| \propto U \xrightarrow{\text{EKL}} \infty. \quad (3.65)$$

The EKL can be considered as simply the limit $U \rightarrow \infty$ (and with it $\epsilon_f \equiv -\frac{U}{2} \rightarrow -\infty$ and $U_S \equiv \sqrt{U} \rightarrow \infty$). Let us look at the eigenstates of $\bar{\mathcal{H}}'$ as functions of four parameters. Then, in the EKL ($U \rightarrow \infty$) each eigenstate $|\Psi\rangle$ of $\bar{\mathcal{H}}'$ approaches an eigenstate $|\Psi^0\rangle$ of \mathcal{H}_0^U :

$$\left| \Psi(\mathcal{W}, \tilde{J}, U_S, U) \right\rangle \xrightarrow{U \rightarrow \infty} \left| \Psi(0, 0, 0, U') \right\rangle \equiv \left| \Psi^0 \right\rangle \quad (3.66)$$

with arbitrary U' . Note that the states $\{|\Psi^0\rangle\}$ that are approached in the EKL are highly non-trivial superpositions of trivial degenerate eigenstates of \mathcal{H}_0^U . Still, they can be grouped into two classes: first, states $\{|\Psi_1^0\rangle\}$ with a single f electron in each of the two orbitals at each site, and second, states $\{|\Psi_2^0\rangle\}$ with admixtures of zero and double occupation of f orbitals. With respect to the EKL of $\bar{\mathcal{H}}'$ the energies of the $|\Psi_2^0\rangle$'s are higher than the energies of the $|\Psi_1^0\rangle$'s by amounts proportional to U . In the EKL ($U \rightarrow \infty$) the statistical weights of the $|\Psi_2^0\rangle$'s obviously vanish. Moreover, the creation or annihilation of s electrons, which must be taken into account with regard to s -electron Green's functions of the KLM, do not connect the $|\Psi_1^0\rangle$'s with the $|\Psi_2^0\rangle$'s. Hence, in the EKL only the states $\{|\Psi_1^0\rangle\}$ are relevant. The number of electrons in each f orbital at each site is effectively fixed to one: $n_{li\uparrow}^f + n_{li\downarrow}^f = 1$, $l = 1, 2$.

Based on this an effective Hamiltonian $\bar{\mathcal{H}}''$ can be formulated which only describes the relevant states $|\Psi_1^0\rangle$. Several terms can be neglected after making sure that they do not leave any effective interactions (see footnote 3 on page 22). Special care has to be taken in the case of \mathcal{H}_S as its norm diverges as \sqrt{U} . But since \mathcal{H}_S [Eq. (3.50)] does not contain non-diagonal hopping terms no effective interactions should remain in the EKL. Let us first consider the different parts of $\mathcal{H}_2 = \mathcal{H}_2^{f1} + \mathcal{H}_2^{f2}$. $\mathcal{H}_{\text{ch}} = \mathcal{H}_{\text{ch}}^{f1} + \mathcal{H}_{\text{ch}}^{f2}$ can be neglected completely. $\mathcal{H}_{\text{hop}} = \mathcal{H}_{\text{hop}}^{f1} + \mathcal{H}_{\text{hop}}^{f2}$ reduces to a constant ($2N \sum_k W_{kk}$). The

coupling constants are given by

$$W_{\vec{k}'\vec{k}} \stackrel{\text{EKL}}{=} -\frac{2V_{\vec{k}'}V_{\vec{k}}^*}{U} \quad (3.67)$$

$$\text{and } J_{\vec{k}'\vec{k}} \stackrel{\text{EKL}}{=} -\frac{8V_{\vec{k}'}V_{\vec{k}}^*}{U}. \quad (3.68)$$

With this $\mathcal{H}_{\text{dir}} = \mathcal{H}_{\text{dir}}^{f1} + \mathcal{H}_{\text{dir}}^{f2}$ exactly vanishes. The only non-constant terms remaining from \mathcal{H}_2 are $\mathcal{H}_{\text{ex}}^{f1} + \mathcal{H}_{\text{ex}}^{f2}$. \mathcal{H}_{f1f2} and \mathcal{H}_{fs} can be neglected because they describe the hopping between different f orbitals and between f and s orbitals, respectively. The Hubbard term $U \sum_i (n_{1i\uparrow}^f n_{1i\downarrow}^f + n_{2i\uparrow}^f n_{2i\downarrow}^f)$ can be neglected since it describes double f occupation. The spin-constraint Hamiltonian \mathcal{H}_S forces as $U_S \rightarrow \infty$ the spins of the f electrons in different orbitals at the same sites to align parallel. Therefore, $\mathcal{H}_S \stackrel{\text{EKL}}{=} -U_S \frac{1}{4}N$, and $\mathcal{H}_{\text{ex}}^{f1} + \mathcal{H}_{\text{ex}}^{f2}$ can be replaced by

$$\mathcal{H}_{\text{ex}} = -\frac{1}{2} \sum_{\vec{k}'\vec{k}i} J_{\vec{k}'\vec{k}} e^{-i(\vec{k}'-\vec{k})\vec{R}_i} (S_i^+ c_{\vec{k}'\downarrow}^\dagger c_{\vec{k}\uparrow} + S_i^- c_{\vec{k}'\uparrow}^\dagger c_{\vec{k}\downarrow} + S_i^z (c_{\vec{k}'\uparrow}^\dagger c_{\vec{k}\uparrow} - c_{\vec{k}'\downarrow}^\dagger c_{\vec{k}\downarrow})) \quad (3.69)$$

with the spin operators standing for localized quantum-mechanical spins $S = 1$. The effective Hamiltonian in the EKL is given by

$$\bar{\mathcal{H}}'' = \sum_{\vec{k}\sigma} \epsilon_{\vec{k}} n_{\vec{k}\sigma}^c + \mathcal{H}_{\text{ex}} - U_S \frac{1}{4}N + 2N\epsilon_f + 2N \sum_{\vec{k}} W_{\vec{k}\vec{k}}. \quad (3.70)$$

Again apart from unimportant constants $\bar{\mathcal{H}}''$ corresponds to the Kondo lattice model for f spins $S = 1$.

As the generator goes to zero in the EKL ($\mathcal{S} \xrightarrow{\text{EKL}} 0$), the unitary transformation becomes an identical one, and one can state that, disregarding unimportant constants, the doubly degenerate PAM with spin constraint [Eqs. (3.47)–(3.50)] is mapped exactly on the Kondo lattice model (3.15) for $S = 1$ with the coupling constants given by Eq. (3.68).

The proof of an exact mapping of an l -fold degenerate PAM with maximum spin constraint on a $S = \frac{l}{2}$ KLM is fully analogous to the proof for $S = 1$. All the operators containing f orbitals have to be sensibly generalized to the l -fold degenerate case. The spin constraint is to guarantee maximum total spin of the f orbitals. One has to maximize the total spin squared at each site

$$\begin{aligned} (\vec{S}_{\text{tot},i}^f)^2 &= \left(\vec{S}_{1i}^f + \vec{S}_{2i}^f + \dots + \vec{S}_{li}^f \right)^2 = (\vec{S}_{1i}^f)^2 + (\vec{S}_{2i}^f)^2 + \dots + (\vec{S}_{li}^f)^2 + 2 \cdot \text{TP}_i \\ &= l \frac{3}{4} + 2 \cdot \text{TP}_i \end{aligned} \quad (3.71)$$

where TP_i is the total pairing of spin operators

$$\text{TP}_i = \left(\vec{S}_{1i}^f \vec{S}_{2i}^f + \vec{S}_{1i}^f \vec{S}_{3i}^f + \dots + \vec{S}_{1i}^f \vec{S}_{li}^f \right) + \left(\vec{S}_{2i}^f \vec{S}_{3i}^f + \dots + \vec{S}_{2i}^f \vec{S}_{li}^f \right) + \dots + \vec{S}_{l-1i}^f \vec{S}_{li}^f . \quad (3.72)$$

Maximizing the total spin squared is equivalent to maximizing the total pairing. That is why we set

$$\mathcal{H}_S = -U_S \sum_i \text{TP}_i . \quad (3.73)$$

All the other steps in the proof are equivalent to the $S = 1$ proof. Hence, we have shown that the l -fold degenerate periodic Anderson model with the spin constraint operator (3.73) is mapped on the spin $S = \frac{l}{2}$ Kondo lattice model in the extended Kondo limit (3.19) including the spin-constraint limit (3.51).

3.2.4 Proof of the large Fermi volume in the $S = \frac{1}{2}$ KLM for a nonmagnetic Fermi-liquid state

Only very recently the long-standing issue of the large Fermi volume for a nonmagnetic Fermi-liquid state of the antiferromagnetic Kondo lattice model was solved by Oshikawa by means of a nonperturbative topological proof of Luttinger's theorem [Oshikawa, 2000]. Oshikawa's result represents the first proof of the large Fermi volume for arbitrary dimensions, spins and coupling strengths after a number of special results for the $S = \frac{1}{2}$ Kondo lattice model had been achieved. There were the variational results by Shiba and Fazekas [Shiba and Fazekas, 1990], a proof for the strong-coupling limit in one dimension [Ueda et al., 1994], a proof for infinite dimensions [Matsumoto and Ohkawa, 1995], and a general proof for one dimension [Yamanaka et al., 1997]. The exact mapping of the periodic Anderson model to the Kondo lattice model in the extended Kondo limit implies immediately another general proof for $S = \frac{1}{2}$, which is more direct than the one given by Oshikawa.

For the PAM the Luttinger theorem [Luttinger and Ward, 1960] states that the Fermi volume of a nonmagnetic Fermi-liquid state is equal to the sum of s and f electrons [Martin, 1982]:

$$N_s + N_f = 2 \sum_{\vec{q}\vec{k}} \theta(\mu - \eta_{\vec{k}}^{\vec{q}}) \equiv V_F . \quad (3.74)$$

$\eta_{\vec{k}}^q$ ($q = 1, 2$) are the eigenvalues of the matrix

$$\begin{pmatrix} \epsilon_{\vec{k}} & \sqrt{N}V_{\vec{k}} \\ \sqrt{N}V_{\vec{k}}^* & \epsilon_f + \Sigma_{\vec{k}}(0) \end{pmatrix}, \quad (3.75)$$

where $\Sigma_{\vec{k}}(\omega)$ is the proper diagrammatic self-energy of the PAM. A couple of rearrangements (see Appendix A) lead to:

$$N_s + N_f = 2 \sum_{\vec{k}} \left[\theta(\mu - \epsilon_{\vec{k}}) + \theta\left(\alpha_{\vec{k}} - \frac{N|V_{\vec{k}}|^2}{(\mu - \epsilon_{\vec{k}})}\right) \right] \quad (3.76)$$

$$\text{with } \alpha_{\vec{k}} = \mu - \epsilon_f - \Sigma_{\vec{k}}(0). \quad (3.77)$$

We introduce the s -electron self-energy $\Sigma_{s,\vec{k}}$ as defined by an appropriate Dyson equation of the s -electron Green's function,

$$G_{s,\vec{k}}(\omega) = \frac{1}{\omega - \epsilon_{\vec{k}} + \mu - \Sigma_{s,\vec{k}}(\omega)}. \quad (3.78)$$

It is related to the proper self-energy $\Sigma_{\vec{k}}(\omega)$ by

$$\Sigma_{s,\vec{k}}(\omega) = \frac{N|V_{\vec{k}}|^2}{\omega - \epsilon_f + \mu - \Sigma_{\vec{k}}(\omega)} \quad (3.79)$$

$$\text{and } \Sigma_{\vec{k}}(\omega) = \omega - \epsilon_f + \mu - \frac{N|V_{\vec{k}}|^2}{\Sigma_{s,\vec{k}}(\omega)}. \quad (3.80)$$

$$\text{Therefore, } \alpha_{\vec{k}} = \frac{N|V_{\vec{k}}|^2}{\Sigma_{s,\vec{k}}(0)} \quad (3.81)$$

Eqs. (3.76) and (3.77) are analogous to the ones obtained for the special case of infinite dimensions [Matsumoto and Ohkawa, 1995]. Now the θ functions in Eq. (3.76) have to be evaluated in dependence on $\alpha_{\vec{k}}$ (see Appendix A). The result is

$$N_s + N_f = 2 \sum_{\vec{k}} \delta_{\alpha_{\vec{k}} \geq 0} + 2 \sum_{\vec{k}} \delta_{\alpha_{\vec{k}} \neq 0} \theta(\mu - \epsilon_{\vec{k}} - \Sigma_{s,\vec{k}}(0)) \quad (3.82)$$

$$\text{where } \delta_{\alpha_{\vec{k}} \geq 0} = \begin{cases} 0 & \alpha_{\vec{k}} < 0 \\ 1 & \alpha_{\vec{k}} \geq 0 \end{cases}, \quad \delta_{\alpha_{\vec{k}} \neq 0} = \begin{cases} 0 & \alpha_{\vec{k}} = 0 \\ 1 & \alpha_{\vec{k}} \neq 0 \end{cases}. \quad (3.83)$$

According to the exact mapping of the PAM to the Kondo lattice model the s -electron self-energy of the PAM becomes identical to an analogously defined s -electron self-energy of the KLM in the extended Kondo limit

$$\Sigma_{s,\vec{k}} \xrightarrow{\text{EKL}} \Sigma_{s,\vec{k}}^{\text{KLM}}. \quad (3.84)$$

Hence, Eq. (3.82) with $\Sigma_{s,\vec{k}}$ replaced by $\Sigma_{s,\vec{k}}^{\text{KLM}}$ represents the analog of the Fermi-surface sum rule for a non-magnetic Fermi-liquid state of the Kondo lattice model. The Fermi volume includes the number N_f of localized spins. This becomes clearer if a \vec{k} independent proper self-energy and hybridization are assumed, which also means that the s -electron self-energy at the Fermi energy is \vec{k} independent. As in Ref. [Matsumoto and Ohkawa, 1995] the three cases of less, equal, and more than half filling can be distinguished:

$$(\alpha < 0) \quad N_s + N_f = 2 \sum_{\vec{k}} \theta(\mu - \epsilon_{\vec{k}} - \Sigma_s(0)) \quad (3.85)$$

$$(\alpha = 0) \quad N_s + N_f = 2N \quad (3.86)$$

$$(\alpha > 0) \quad N_s + N_f = 2N + 2 \sum_{\vec{k}} \theta(\mu - \epsilon_{\vec{k}} - \Sigma_s(0)) \quad (3.87)$$

Equations (3.85)–(3.87) replace the more general Luttinger’s theorem (3.82) in the case of a \vec{k} independent proper self-energy and hybridization. It is clear that for a magnetic Fermi-liquid state the corresponding Fermi-surface sum rule of the PAM similarly maps on the Kondo lattice model.

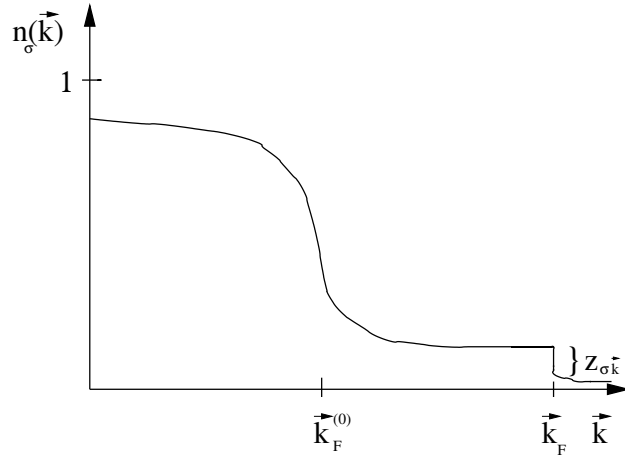


Figure 3.1: Schematic distribution of electrons n_σ in dependence on the wave vector \vec{k} for a nonmagnetic Fermi liquid state in the antiferromagnetic Kondo lattice model.

In Fig. 3.1 schematically the distribution of electrons (momentum distribution function) for a nonmagnetic Fermi liquid state in the antiferromagnetic Kondo lattice model is shown. The figure is drawn following similar pictures in Refs. [Tsunetsugu et al., 1997, Shiba and Fazekas, 1990]. The Fermi edge of the interaction free model would be $\vec{k}_F^{(0)}$. However, since the Fermi volume

3.2. EXACT MAPPING OF THE PERIODIC ANDERSON MODEL ... 31

is large as it includes the number of localized spins N_f , the discontinuity of the electron distribution occurs at a larger \vec{k}_F vector. The height of the discontinuity is the corresponding quasiparticle weight $z_{\sigma\vec{k}}$.

Chapter 4

Extension of the KLM to a realistic model describing Eu-rich EuO

The ferromagnetic Kondo lattice model is known to give a good model description of the physics of the quasiparticle conduction bands of pure EuO [Schiller, 2000]. In the one-band version it is given by¹

$$\mathcal{H}_{\text{KLM}} = \sum_{\vec{k}\sigma} \epsilon_{\vec{k}} n_{\vec{k}\sigma}^c - J \sum_i \vec{S}_i \cdot \vec{\sigma}_i^c. \quad (4.1)$$

The model shows the spin splitting into spin-up and spin-down conduction band and correspondingly the red shift of the spin-up and the blue shift of the spin-down parts of the conduction band. Since EuO is a ferromagnetic semiconductor, which does not contain conduction electrons, there must be a term accounting for the ferromagnetism of the $4f^7$ spins through an interaction between them:

$$\mathcal{H}_{ff} = - \sum_{ii'} J_{ii'} \vec{S}_i \cdot \vec{S}_{i'}. \quad (4.2)$$

The Heisenberg-like term (4.2) describes well the ferromagnetism in EuO [Wachter, 1979]. However, it is left out when considering $\langle S^z \rangle$ as an external parameter whose temperature dependence is given by a Brillouin function².

¹Note that throughout this thesis the fivefold degeneracy of the EuO $5d$ conduction band is neglected. Anyway, from band structure calculations it turns out that only the three t_{2g} bands would be relevant [Schiller, 2000]. This at most gives a factor of three e.g. to the conductivity which is not relevant when discussing orders of magnitude or which could be made up for with adjusting parameters.

²We do not use a site index in the expectation value for S_i^z since we only consider translationally invariant ferromagnetism or paramagnetism.

For pure EuO this is very well justified [Mauger et al., 1978]. We will also use a Brillouin function for the non-self-consistent calculation for Eu-rich EuO in section 6 with the Curie temperature taken from the experiment.

Now, in the Eu-rich EuO the Eu-richness is connected with oxygen vacancies [Oliver et al., 1972]. That is why Eu-rich EuO is sometimes written as EuO_{1-d} with d denoting the impurity (oxygen vacancy) concentration. These vacancies can bind two electrons which formerly stemmed from the Eu $5s^2$ and built the chemical bonding as O $2p$ orbitals in the pure material. These new impurity-electron states are modeled as orbitals with energy levels ϵ_p :

$$\mathcal{H}_{p,1} = \sum_j \epsilon_p n_{j\sigma}^p. \quad (4.3)$$

In this thesis the sum over j denotes the sum over the oxygen vacancy (impurity) sites, which are randomly distributed in EuO_{1-d} . If two electrons are at the same time at an impurity site, they should feel a Coulomb repulsion. Therefore we need a Coulomb term

$$\mathcal{H}_{p,2} = U \sum_j n_{j\uparrow}^p n_{j\downarrow}^p. \quad (4.4)$$

The next term is an exchange between the impurity electron spins and the $4f$ spins in a Kondo-like way:

$$\mathcal{H}_{pf} = -J_p \sum_j \vec{S}_j \cdot \vec{\sigma}_j^p \quad (4.5)$$

The last relevant term should consider the hybridization of the impurity states with the conduction electron states. We model this in the usual manner of a \vec{k} independent hybridization:

$$\mathcal{H}_{pc} = V \sum_{j\sigma} \left(p_{j\sigma}^\dagger c_{j\sigma} + c_{j\sigma}^\dagger p_{j\sigma} \right). \quad (4.6)$$

Our full model Hamiltonian for EuO_{1-d} is given by

$$\mathcal{H} = \mathcal{H}_{\text{KLM}} + \mathcal{H}_{p,1} + \mathcal{H}_{p,2} + \mathcal{H}_{pf} + \mathcal{H}_{pc} + (\mathcal{H}_{ff}) \quad (4.7)$$

$$\begin{aligned} &= \sum_{\vec{k}\sigma} \epsilon_{\vec{k}} n_{\vec{k}\sigma}^c - J \sum_i \vec{S}_i \cdot \vec{\sigma}_i^c \\ &+ \sum_{j\sigma} \epsilon_p n_{j\sigma}^p + U \sum_j n_{j\uparrow}^p n_{j\downarrow}^p - J_p \sum_j \vec{S}_j \cdot \vec{\sigma}_j^p \\ &+ V \sum_{j\sigma} (p_{j\sigma}^\dagger c_{j\sigma} + c_{j\sigma}^\dagger p_{j\sigma}) \left(-J_H \sum_{\langle ii' \rangle} \vec{S}_i \cdot \vec{S}_{i'} \right). \end{aligned} \quad (4.8)$$

The last term in brackets is only used for the fully self-consistent calculation in chapter 7 but not in the calculations of chapter 6 where $\langle S^z \rangle$ is taken from a Brillouin function. For reasons of simplicity the sum is only taken over nearest-neighbor sites.

For the not fully self-consistent calculation in chapter 6 we will at one point investigate the influence of a magnetic field B_0 on the transport quantities. The Brillouin function for $\langle S^z \rangle$ contains the external field but for the conduction and impurity electrons we have to model it separately. We will need additional terms

$$\mathcal{H}_{B_0}^e = -\mu_B B_0 \sum_{\vec{k}\sigma} z_\sigma n_{\vec{k}\sigma}^c - \mu_B B_0 \sum_{j\sigma} z_\sigma n_{j\sigma}^p, \quad (4.9)$$

where $\mu_B = \frac{e\hbar}{2m_e}$ is the Bohr magneton, B_0 is the magnetic field in Tesla, and $z_\sigma = \delta_{\sigma\uparrow} - \delta_{\sigma\downarrow}$. The consequence of $\mathcal{H}_{B_0}^e$ is that in all formulae $\epsilon_{\vec{k}}$ and ϵ_p have to be replaced by $\epsilon_{\vec{k}} - z_\sigma \mu_B B_0$ and $\epsilon_p - z_\sigma \mu_B B_0$, respectively.

The spin-spin exchange terms can be written in terms of Fermi operators,

$$-J \sum_i \vec{S}_i \cdot \vec{\sigma}_i^c = -\frac{J}{2} \sum_{i\sigma} (z_\sigma S_i^z n_{i\sigma}^c + S_i^{-\sigma} c_{i\sigma}^\dagger c_{i-\sigma}). \quad (4.10)$$

The analogous expression holds for \mathcal{H}_{pf} . The first part in the brackets in (4.10) is sometimes called the Ising part, and the second part the spin-flip part.

4.1 Realistic model parameters

The parameters of our model (4.8) are chosen either as close as possible to the experimental values or, if those are not available, as simple as possible or such to give the best fit to the experiment. The width of the conduction band W , which is approximately 10 eV, is taken from the absorption spectrum of Ref. [Steeneken et al., 2002] or from band structure calculations [Schiller, 2000]. For the not fully self-consistent solution in chapter 6 we will use a Brillouin function for the value of $\langle S^z \rangle$. For that solution we only need a free density of states and not a detailed electronic dispersion. We therefore assume for simplicity a semielliptical shape of the conduction band. It has the required square root dependence on energy at the lower band edge. For the fully self-consistent calculations of chapter 7 within the modified RKKY theory, we need an explicit dispersion and have chosen the tight-binding dispersion with nearest-neighbor hopping for the fcc lattice. Remember that the Eu ions in Eu-rich EuO form an fcc lattice. This dispersion also has the square

root dependence at the lower band edge, but the magnitude of the density of states at the lower band edge is by about a factor of 10 smaller than in the semielliptical case, which necessitates the adaption of our fit parameter ϵ_p .

The exchange coupling J is determined by the redshift [Wachter, 1964, Busch et al., 1964] of the spin-up conduction band, which is about 0.3 eV (half band-splitting) at low temperatures [Steeneken et al., 2002]. Theoretically it is $\frac{JS}{2}$ in the mean-field approximation, which is fulfilled to a high degree within our calculations since $\frac{JS}{W}$ is small. Therefore we have $J = 0.17$ eV for $S = \frac{7}{2}$. Within an LDA calculation as performed by Schiller [Schiller, 2000] where one considers the splitting of different features between the spin-up and spin-down density of states as mean-field like an average J value of 0.25 eV was determined. However, we are interested in the physics at the lower band edge only and therefore justify our value of 0.17 eV with the redshift alone. Moreover, it coincides with the experimental value of (0.17 ± 0.01) eV given in Ref. [Mitani and Koda, 1975].

For the terms $\mathcal{H}_{p,1}$, $\mathcal{H}_{p,2}$ and \mathcal{H}_{pf} we will use in an effective medium approach the atomic-limit selfenergy of the correlated Kondo lattice model [Nolting and Matlak, 1984]. It leads to a four-peak structure, of which only three peaks have finite weight (see section 3.1). The highest peak is at ϵ_4 . The position of ϵ_4 is a decisive parameter, since from this level the electrons will be emptied into the conduction band below the Curie temperature. According to the atomic limit, ϵ_4 will be situated at $\epsilon_p + U + \frac{J}{2}S$, which is equally determined by ϵ_p and U . Except for the fact that for the highest-resistivity samples an activation energy behavior above T_C of 0.3 eV was observed [Oliver et al., 1972, Torrance et al., 1972], the position of ϵ_4 is not known from the experiment. Fixing $U = 1$ eV leaves the parameter ϵ_p to be adjusted. This is done independently in chapters 6 ($\epsilon_p = -6.44$ eV $\Rightarrow \epsilon_4 = -5.14$ eV) and 7 ($\epsilon_p = -6.42$ eV $\Rightarrow \epsilon_4 = -5.12$ eV) to yield the best overall fit with the experimental resistivity curves. The difference in ϵ_p comes mainly from the different densities of states as described above.

The hybridization V is also not known from the experiment. Our experience within the calculations showed that it should not be too large because then it destroys the effect of the metal-insulator transition. We will give reasons for this in subsection 7.2.7. It turned out that $V = 0.01$ eV is a good value to reproduce the metal-insulator transition.

For the vacancy concentration a medium value, about which the real values vary, is about 0.1%. The variance in the experiment is not known. We assume impurity concentrations in the range between 0.01% to about 5%. To each oxygen vacancy two electrons are assigned. These are the only electrons in our model system apart from the Eu $4f$ spins.

J_H as the nearest-neighbor Heisenberg exchange constant is chosen such

that the pure Heisenberg model without the effective exchange which comes from the interaction of the conduction and the impurity electrons with the Eu spins gives the correct Curie temperature of 69.3 K for pure EuO. For this a value of $J_H = 0.734 k_B \text{ K}$ is needed. We only consider nearest-neighbor exchange for reasons of simplicity. Therefore, in our value for J_H instead of the experimental value $J_1 = 0.606 k_B \text{ K}$ we have to compensate for the missing of the next-nearest neighbor exchange of $J_2 = 0.119 k_B \text{ K}$.

Chapter 5

Current density operator and transport formulae of the model for Eu-rich EuO

In this chapter we will derive for a cubic system the current density operator j , which has to be put into the Kubo formula for the conductivity and for the other transport quantities like the thermal conductivity and the Seebeck coefficient. Using the Kubo formula means we are dealing with linear-response theory, i.e. assume that the current depends linearly on the electric field [Nolting, 2003]. This assumption is justified as long as in the experiment the conductivity (or resistivity) value is given independent on the electric field. The Kubo formula for the energy-dependent electrical-conductivity tensor in Cartesian components is given by integrals over a current-current correlation function [Kubo, 1957, Borgielet al., 2001]:

$$\sigma^{\alpha\beta}(E) = V \int_0^{(k_{\text{B}}T)^{-1}} d\lambda \int_0^{\infty} dt \langle j^{\beta}(0)j^{\alpha}(t + i\lambda\hbar) \rangle e^{\frac{i}{\hbar}(E+i0^+)t}. \quad (5.1)$$

In a cubic system only the diagonal components (e.g. $\sigma^{\alpha\alpha}$) are non-zero and are equal to each other.

We will derive an expression for the current operator j , which turns out to be the same as in the Hubbard model. We can therefore make use of the same transport formulae which have been applied for the Hubbard model by Pálsson and Kotliar in Ref. [Pálsson and Kotliar, 1998]. We would like to have an expression for the dc current operator j in a uniform electric field:

$$j = \lim_{q \rightarrow 0} \lim_{\omega \rightarrow 0} j(q, \omega) = \lim_{q \rightarrow 0} j(q) \quad (5.2)$$

For the classical quantities, current density vector \vec{j} and charge density ρ_c , we have a continuity equation:

$$\frac{\partial \rho_c}{\partial t}(\vec{r}, t) + \vec{\nabla}_{\vec{r}} \cdot \vec{j}(\vec{r}, t) = 0 \quad (5.3)$$

$$\frac{1}{(2\pi)^3} \int d^3\vec{q} \left(e^{+i\vec{q}\vec{r}} \frac{\partial \rho_c}{\partial t}(\vec{q}, t) + \vec{\nabla}_{\vec{r}} \cdot \left(\vec{j}(\vec{q}, t) \cdot e^{+i\vec{q}\vec{r}} \right) \right) = 0 \quad (5.4)$$

$$\frac{1}{(2\pi)^3} \int d^3\vec{q} \left(\frac{\partial}{\partial t} \rho_c(\vec{q}, t) + i\vec{q} \cdot \vec{j}(\vec{q}, t) \right) e^{+i\vec{q}\vec{r}} = 0 \quad (5.5)$$

Equation (5.5) has to be valid for each \vec{r} . From this it follows that the term in brackets has to be zero for each \vec{q} :

$$\frac{\partial}{\partial t} \rho_c(\vec{q}, t) + i\vec{q} \cdot \vec{j}(\vec{q}, t) = 0 \quad (5.6)$$

Equation (5.6) has to be valid also for the corresponding operators in the Heisenberg picture, for which we do not introduce a separate notation:

$$i\vec{q} \cdot \vec{j}(\vec{q}, t) = - \frac{\partial}{\partial t} \rho_c(\vec{q}, t) \quad (5.7)$$

$$= \frac{i}{\hbar} [\rho_c(\vec{q}, t), \mathcal{H}] \quad (5.8)$$

Equation (5.8) is also valid in the Schrödinger picture where the time dependences of the operators disappear. If we introduce the particle density operator $\rho = -\frac{1}{e}\rho_c$, where $e > 0$ is the elementary charge, we get:

$$i\vec{q} \cdot \vec{j}(\vec{q}) = \frac{ie}{\hbar} [\mathcal{H}, \rho(\vec{q})] \quad (5.9)$$

Equation (5.9) corresponds to Eq. (14) in Ref. [Czycholl and Leder, 1981]. In a cubic environment we can assume without loss of generality the current to flow into the x direction and the \vec{q} -vector to point into the x -direction, too.

$$j = \lim_{\vec{q} \rightarrow 0} \frac{e}{\hbar|\vec{q}|} [\mathcal{H}, \rho(\vec{q})] \quad (5.10)$$

The \vec{q} dependent charge density operator is given as the Fourier transform of the space dependent operator

$$\rho(\vec{q}) = \int d^3\vec{r} e^{-i\vec{q}\vec{r}} \rho(\vec{r}) \quad (5.11)$$

where the space dependent operator is

$$\rho(\vec{r}) = \sum_{m=1}^{N_e} \delta(\vec{r} - \hat{r}_m). \quad (5.12)$$

Hence,

$$\rho(\vec{q}) = \sum_{m=1}^{N_e} e^{-i\vec{q}\hat{r}_m}. \quad (5.13)$$

N_e is the number of electrons in the system. In second quantized form we get

$$\begin{aligned} \rho(\vec{q}) = & \sum_{ii'\sigma} \langle c_i | e^{-i\vec{q}\hat{r}} | c_{i'} \rangle c_{i\sigma}^\dagger c_{i'\sigma} + \sum_{jj'\sigma} \langle p_j | e^{-i\vec{q}\hat{r}} | p_{j'} \rangle p_{j\sigma}^\dagger p_{j'\sigma} \\ & + \sum_{ij} \left(\langle c_i | e^{-i\vec{q}\hat{r}} | p_j \rangle c_{i\sigma}^\dagger p_j + \langle p_j | e^{-i\vec{q}\hat{r}} | c_i \rangle p_{j\sigma}^\dagger c_{i\sigma} \right). \end{aligned} \quad (5.14)$$

With the consecutive approximations we follow Ref. [Czycholl and Leder, 1981]. We assume that the impurity states are rather localized. That is the reason why we introduced energy levels ϵ_p in the Hamiltonian (4.8). Therefore we apply a ‘‘small core approximation’’, assuming $e^{-i\vec{q}\hat{r}} | p_j \rangle \approx e^{-i\vec{q}\vec{R}_j} | p_j \rangle$. Hence,

$$\langle c_i | e^{-i\vec{q}\hat{r}} | p_j \rangle \approx e^{-i\vec{q}\vec{R}_j} \langle c_i | p_j \rangle = 0 \quad (5.15)$$

$$\langle p_j | e^{-i\vec{q}\hat{r}} | p_{j'} \rangle \approx e^{-i\vec{q}\vec{R}_{j'}} \delta_{jj'} \quad (5.16)$$

Since we are interested only in the $|\vec{q}| \rightarrow 0$ limit, we get for the Wannier states of the conduction electrons

$$\langle c_i | e^{-i\vec{q}\hat{r}} | c_{i'} \rangle = \int d^3\vec{r} w_c^*(\vec{r} - \vec{R}_i) e^{-i\vec{q}\vec{r}} w_c(\vec{r} - \vec{R}_{i'}) \quad (5.17)$$

$$\approx e^{-i\vec{q}(\vec{R}_i + \vec{R}_{i'})/2} \int d^3\vec{r} w_c^* \left(\vec{r} - \frac{\vec{R}_i - \vec{R}_{i'}}{2} \right) (1 - i\vec{q}\vec{r}) w_c \left(\vec{r} - \frac{\vec{R}_{i'} - \vec{R}_i}{2} \right), \quad (5.18)$$

where we have expanded the exponential function within the integral up to the first order term in q . From (5.17) to (5.18) we made the substitution $\vec{r} \rightarrow \vec{r} + (\vec{R}_i + \vec{R}_{i'})/2$. For the zeroth order term in q we have to evaluate the integral

$$I_0 = \int d^3\vec{r} w_c^*(\vec{r} - \vec{r}_1) w_c(\vec{r} - \vec{r}_2) \quad (5.19)$$

The integral is non-trivial since $\vec{r}_1 = \frac{\vec{R}_i - \vec{R}_{i'}}{2}$ and $\vec{r}_2 = \frac{\vec{R}_{i'} - \vec{R}_i}{2}$ need not be vectors from the Bravais lattice.

$$I_0 = \int d^3\vec{r} \frac{1}{N} \sum_{\vec{k}\vec{k}'} e^{i\vec{k}\vec{r}_1} \psi_{\vec{k}\sigma}^*(\vec{r}) e^{-i\vec{k}'\vec{r}_2} \psi_{\vec{k}'\sigma}(\vec{r}) \quad (5.20)$$

The $\psi_{\vec{k}\sigma}(\vec{r})$'s are the Bloch wave functions. They are orthonormal:

$$\int d^3\vec{r} \psi_{\vec{k}\sigma}^*(\vec{r}) \psi_{\vec{k}'\sigma}(\vec{r}) = \delta_{\vec{k}\vec{k}'} . \quad (5.21)$$

Hence, the integral still turns out to be simple:

$$I_0 = \frac{1}{N} \sum_{\vec{k}} e^{i\vec{k}(\vec{r}_1 - \vec{r}_2)} = \frac{1}{N} \sum_{\vec{k}} e^{i\vec{k}(\vec{R}_i - \vec{R}_{i'})} = \delta_{ii'} . \quad (5.22)$$

For the first order term in q in Eq. (5.18) we have to evaluate the following integral

$$I_1 = \int d^3\vec{r} w_c^*(\vec{r} - \vec{r}_1) \vec{r} w_c(\vec{r} + \vec{r}_1) \approx 0 , \quad (5.23)$$

As pointed out by Czycholl and Leder in Ref. [Czycholl and Leder, 1981] I_1 can be neglected if there is a fixed parity of the Wannier states. It is fulfilled if $w_c^*(\vec{r}) = w_c(-\vec{r})$. However, this is in general an approximation. With (5.22) and (5.23), (5.18) becomes

$$\langle c_i | e^{-i\vec{q}\vec{r}} | c_{i'} \rangle \approx e^{-i\vec{q}\vec{R}_i} \delta_{ii'} + O(q^2) \quad (5.24)$$

For the density operator (5.14) we now have

$$\rho(\vec{q}) = \sum_{ii'\sigma} e^{-i\vec{q}\vec{R}_i} \delta_{ii'} c_{i\sigma}^\dagger c_{i'\sigma} + \sum_{j\sigma} e^{-i\vec{q}\vec{R}_j} p_{j\sigma}^\dagger p_{j\sigma} \quad (5.25)$$

Let us evaluate

$$\sum_{\vec{k}} c_{\vec{k}-\vec{q}\sigma}^\dagger c_{\vec{k}\sigma} = \sum_{\vec{k}} \frac{1}{N} \sum_{ii'} e^{i(\vec{k}-\vec{q})\vec{R}_i} e^{-i\vec{k}\vec{R}_{i'}} c_{i\sigma}^\dagger c_{i'\sigma} \quad (5.26)$$

$$= \sum_{ii'} e^{-i\vec{q}\vec{R}_i} \delta_{ii'} c_{i\sigma}^\dagger c_{i\sigma} = \sum_i e^{-i\vec{q}\vec{R}_i} c_{i\sigma}^\dagger c_{i\sigma} . \quad (5.27)$$

Therefore,

$$\rho(\vec{q}) = \sum_{\vec{k}\sigma} c_{\vec{k}-\vec{q}\sigma}^\dagger c_{\vec{k}\sigma} + \sum_{j\sigma} e^{-i\vec{q}\vec{R}_j} p_{j\sigma}^\dagger p_{j\sigma} \quad (5.28)$$

$$= \sum_{i\sigma} e^{-i\vec{q}\vec{R}_i} c_{i\sigma}^\dagger c_{i\sigma} + \sum_{j\sigma} e^{-i\vec{q}\vec{R}_j} p_{j\sigma}^\dagger p_{j\sigma} \quad (5.29)$$

The sum over i is a sum over all lattice sites, while the sum over j is only a sum over the randomly distributed impurity sites.

The density operator now has to be put into Eq. (5.10) where the commutator with the Hamiltonian (4.8) has to be performed. The details of that calculation are given in Appendix B. The surprisingly simple result is

$$j = -\frac{e}{\hbar} \sum_{\vec{k}\sigma} \frac{\partial \epsilon_{\vec{k}}}{\partial k_x} c_{\vec{k}\sigma}^\dagger c_{\vec{k}\sigma}. \quad (5.30)$$

Equation (5.30) means that only the electrons in conduction electron states contribute to the electrical current. At first sight this looks puzzling. Why should the impurity electrons not take part in the conduction? Well, they take part but only via the conduction electron channel. Note, that this goes together with the fact that according to our Hamiltonian (4.8) the impurity electrons cannot hop themselves from one site to the other but only via the hybridization with the conduction electron channel. The hybridization, however, is an on-site hybridization. It itself does not contribute to the electrical current. If we had allowed for a non-local hybridization the situation would be different. While changing from impurity to conduction electron states the electrons would also change their sites and hence contribute to the conduction. The commutator $[\mathcal{H}_{pc}, \rho(\vec{q})]$ (B.8) would not vanish.

The current operator in Eq. (5.30) is identical to the current operator in the Hubbard model (for the Hubbard model see Refs. [Hubbard, 1963, Hubbard, 1964a, Hubbard, 1964b]). Furthermore, all the selfenergies which we will use are local. Therefore we can apply the transport formulae formulated for the Hubbard model in dynamical mean-field theory (DMFT), where the selfenergy is local, by Pálsson and Kotliar in Ref. [Pálsson and Kotliar, 1998]. These transport equations only contain the spectral density of the conduction electrons, $A_{\vec{k}\sigma}(E)$ (normalized to one and not to \hbar). All the so-called vertex corrections in a diagrammatic expansion vanish [Khurana, 1990, Möller et al., 1992, Pruschke et al., 1993]. The transport functions are:

$$A_s = \frac{\pi}{\hbar V} \frac{T}{(k_B T)^s} \sum_{\vec{k}\sigma} \int_{-\infty}^{\infty} dE [-f'(E)] E^s A_{\vec{k}\sigma}(E)^2 \left(\frac{\partial \epsilon_{\vec{k}}}{\partial k_x} \right)^2, \quad s = 0, 1, 2 \quad (5.31)$$

V is the volume, $f'(E)$ is the derivative of the Fermi function. The transport quantities electrical conductivity, thermal conductivity and the Seebeck

coefficient follow from the transport functions [Pálsson and Kotliar, 1998]:

$$\sigma = \frac{e^2}{T} A_0, \quad (5.32)$$

$$\kappa = k_B^2 \left(A_2 - \frac{A_1^2}{A_0} \right). \quad (5.33)$$

$$S_E = \frac{-k_B}{e} \frac{A_1}{A_0} \quad (5.34)$$

The transport quantities are defined as follows (see [Mahan, 1993]). An electric field \mathcal{E} causes without a temperature gradient and a gradient of the chemical potential ($\vec{\nabla}T = \vec{0}$ and $\vec{\nabla}\mu = \vec{0}$, respectively) an electrical current density j . The ratio between both is the conductivity σ :

$$j = \sigma \mathcal{E} \quad (5.35)$$

In a cubic system both the electric field and the current density show in the same direction. So, the conductivity is a scalar. The resistivity ρ is simply the inverse of the conductivity

$$\rho = \frac{1}{\sigma}. \quad (5.36)$$

It is connected to the resistance R of a material with cross section A and length l via

$$R = \rho \frac{l}{A}. \quad (5.37)$$

A temperature gradient $\vec{\nabla}T$ causes an energy current density \vec{J}_E to flow. The constant of proportionality in the case of no particle current $j = 0$ is the thermal conductivity κ :

$$\vec{J}_E = -\kappa \vec{\nabla}T. \quad (5.38)$$

Due to the second law of thermodynamics the energy flows opposite to the temperature gradient. Therefore the minus sign in Eq. (5.38) makes the thermal conductivity κ a positive quantity. Throughout this work we will concentrate on the thermal conductivity κ of the electrons. There is another contribution to the thermal conductivity from the lattice, κ_L , which has to be taken into account when calculating quantities like the figure of merit (see below).

The third transport quantity, in which we are interested in is the thermopower (thermoelectric coefficient) or Seebeck coefficient S_E . If there is

a temperature difference ΔT at the two ends of a metal without particle currents $j = 0$ and gradients of the chemical potential ($\vec{\nabla}\mu = \vec{0}$) a voltage difference ΔV is induced. The Seebeck coefficient is the ratio between both:

$$S_E = \frac{\Delta V}{\Delta T} . \quad (5.39)$$

It may be positive or negative in the case of positive or negative charge of the carriers (e.g. in ion diffusion models [Girvin, 1978]). In the case of electrons S_E is negative.

For a free electron gas and, therefore, also for a Fermi liquid the Wiedemann-Franz ratio of the thermal conductivity, the electric conductivity and the temperature,

$$\frac{\kappa}{\sigma T} , \quad (5.40)$$

assumes a certain value, which is called the Lorenz number [Ibach and Lüth, 1995]

$$L = \frac{\pi^2}{3} \left(\frac{k_B}{e} \right)^2 . \quad (5.41)$$

Whether this value is taken on by the Wiedemann-Franz ratio is an indicator of whether one is dealing with a Fermi liquid or not.

The performance of a thermoelectric material is measured with the so-called dimensionless figure of merit, which is given by [Pálsson and Kotliar, 1998]

$$Z_T T = \frac{S_E^2 \sigma T}{\kappa + \kappa_L} . \quad (5.42)$$

When converting an applied voltage into a temperature gradient, the figure of merit gives a measure of how efficiently irreversible effects of Joule heating and thermal conduction are avoided. Materials currently used in thermoelectric devices have $Z_T T$ values between 0.4 and 1.3 [Mahan et al., 1997].

Equation (5.31) can be further transformed to get rid of the cumbersome \vec{k} summation. Let us consider

$$\sum_{\vec{k}} A_{\vec{k}\sigma}(E)^2 \left(\frac{\partial \epsilon_{\vec{k}}}{\partial k_x} \right)^2 = \int_{-\infty}^{+\infty} dx A_{x\sigma}(E)^2 \sum_{\vec{k}} \left(\frac{\partial \epsilon_{\vec{k}}}{\partial k_x} \right)^2 \delta(x - \epsilon_{\vec{k}}) . \quad (5.43)$$

Equation (5.43) presupposes that the \vec{k} dependence of $A_{\vec{k}\sigma}(E)$ is only via the conduction electron dispersion $\epsilon_{\vec{k}}$ (which is fulfilled if all the selfenergies are

\vec{k} independent, i.e. local) so that

$$A_{x\sigma}(E) = A_{\vec{k}\sigma}(E)_{\epsilon_{\vec{k}} \rightarrow x} . \quad (5.44)$$

We transform the sum over \vec{k} on the r.h.s. in (5.43) in an integral and apply partial integration. We are interested in cubic lattices in the nearest-neighbor tight-binding approximation only

$$\frac{V}{(2\pi)^3} \int d^3\vec{k} \left(\frac{\partial \epsilon_{\vec{k}}}{\partial k_x} \right)^2 \delta(x - \epsilon_{\vec{k}}) \quad (5.45)$$

$$= \frac{V}{(2\pi)^3} \iiint dk_y dk_z dk_x \underbrace{\left(\frac{\partial \epsilon_{\vec{k}}}{\partial k_x} \right)}_u \cdot \underbrace{\left(\frac{\partial \epsilon_{\vec{k}}}{\partial k_x} \right)}_{v'} \delta(x - \epsilon_{\vec{k}}) \quad (5.46)$$

$$= 0 + \frac{V}{(2\pi)^3} \iiint dk_y dk_z dk_x \underbrace{\frac{\partial^2 \epsilon_{\vec{k}}}{\partial k_x^2}}_{u'} \underbrace{\theta(x - \epsilon_{\vec{k}})}_v . \quad (5.47)$$

The fact that the u - v term of the partial integration of the term (5.46) is zero in Eq. (5.47) for the cubic lattices is proven in appendix C.

We would like to make use of the fact that

$$\vec{\nabla}_{\vec{k}}^2 \epsilon_{\vec{k}} = \frac{\partial^2 \epsilon_{\vec{k}}}{\partial k_x^2} + \frac{\partial^2 \epsilon_{\vec{k}}}{\partial k_y^2} + \frac{\partial^2 \epsilon_{\vec{k}}}{\partial k_z^2} = -ca^2 \epsilon_{\vec{k}} \quad (5.48)$$

for simple cubic ($c = 1$), body-centered cubic ($c = \frac{3}{4}$) and face-centered cubic systems [$c = \frac{1}{2}$, see Eq. (E.51)] in the nearest-neighbor tight-binding approximation. (a is the lattice constant). Therefore we use instead of (5.45) a symmetrized form and get with the same steps from (5.45) to (5.47) for the y and z directions the following:

$$(5.45) = \frac{1}{3} \frac{V}{(2\pi)^3} \int d^3\vec{k} \left[\left(\frac{\partial \epsilon_{\vec{k}}}{\partial k_x} \right)^2 + \left(\frac{\partial \epsilon_{\vec{k}}}{\partial k_y} \right)^2 + \left(\frac{\partial \epsilon_{\vec{k}}}{\partial k_z} \right)^2 \right] \delta(x - \epsilon_{\vec{k}}) \quad (5.49)$$

$$= \frac{1}{3} \frac{V}{(2\pi)^3} \iiint dk_y dk_z dk_x \vec{\nabla}_{\vec{k}}^2 \epsilon_{\vec{k}} \theta(x - \epsilon_{\vec{k}}) \quad (5.50)$$

$$= -\frac{ca^2}{3} \sum_{\vec{k}} \epsilon_{\vec{k}} \theta(x - \epsilon_{\vec{k}}) = \frac{ca^2}{3} \sum_{\vec{k}}^{\epsilon_{\vec{k}} < x} \epsilon_{\vec{k}} \quad (5.51)$$

$$= -\frac{ca^2}{3} N \int_{-\infty}^x d\epsilon' \epsilon' \frac{1}{N} \sum_{\vec{k}} \delta(\epsilon' - \epsilon_{\vec{k}}) = -\frac{ca^2}{3} N \int_{-\infty}^x d\epsilon' \epsilon' \rho_0(\epsilon') \quad (5.52)$$

$$= \frac{ca^2}{3} N \hat{v}(x) \quad (5.53)$$

with the velocity function

$$\hat{v}(x) = - \int_{-\infty}^x d\epsilon' \epsilon' \rho_0(\epsilon') \quad (5.54)$$

Equations (5.31), (5.43) and (5.53) lead to the following expression for the transport functions in an fcc lattice ($c = \frac{1}{2}$)

$$A_s = \frac{\pi}{6\hbar a} \frac{T}{(k_B T)^s} \sum_{\sigma} \int_{-\infty}^{\infty} dE [-f'(E)] E^s \int_{-\infty}^{\infty} dx A_{x\sigma}(E)^2 \hat{v}(x), \quad s = 0, 1, 2 \quad (5.55)$$

with $A_{x\sigma}(E)$ and $\hat{v}(x)$ given by (5.44) and (5.54), respectively. Since the \vec{k} summation is replaced by an energy integration, (5.55) is much easier to handle than (5.31). For the electrical conductivity this means that we have derived the same formula as given in Ref. [Borgielet al., 2001] with the correct prefactor. We will use Eq. (5.55) and Eqs. (5.32) to (5.34) to calculate the transport properties in the chapters 6 and 7.

Chapter 6

Solution and results of the model with external parameter $\langle S^z \rangle$

6.1 Solution of the model with external parameter $\langle S^z \rangle$

The general concept of the solution of our model is an effective medium approach. We define the self-energies for the conduction and the impurity electrons and make independent, appropriate ansatzes for those, and include them in the equations of motion. They can then be solved for the conduction- and impurity-electron Green's functions within a coherent-potential approximation (CPA) for the impurity electrons. We use the solution with external parameter $\langle S^z \rangle$ to test our theory. It has the advantage over the fully self-consistent solution that the calculations are by far less time-consuming.

6.1.1 Self-energies

We would like to obtain the conduction-electron Green's function, from which we can get the spectral density

$$A_{\vec{k}\sigma}(E) = -\frac{1}{\pi} \text{Im} G_{\vec{k}\sigma c}(E) , \quad (6.1)$$

which is needed in the transport functions Eqs. (5.31) and (5.55). We will closely follow the lines of Ref. [Sinjukow and Nolting, 2003]. We need self-

energies, which are defined in the following way:

$$\left\langle\left\langle\left[c_{\vec{k}\sigma}^-, -J \sum_i \vec{S}_i \cdot \vec{\sigma}_i^c\right]_- ; c_{\vec{k}\sigma}^\dagger\right\rangle\right\rangle = \Sigma_{\vec{k}\sigma}^c(E) \langle\langle c_{\vec{k}\sigma}^- ; c_{\vec{k}\sigma}^\dagger \rangle\rangle, \quad (6.2)$$

$$\left\langle\left\langle\left[p_{j'\sigma}^p, U \sum_j n_{j\uparrow}^p n_{j\downarrow}^p - J \sum_j \vec{S}_j \cdot \vec{\sigma}_j^p\right]_- ; p_{j'\sigma}^\dagger\right\rangle\right\rangle = \Sigma_\sigma^{p,1}(E) \langle\langle p_{j'\sigma}^p ; p_{j'\sigma}^\dagger \rangle\rangle, \quad (6.3)$$

The brackets $\langle\langle ; \rangle\rangle$ denote the respective Green's function. The main approximation of our approach is that we assume independent self-energies for the conduction and the impurity electrons. This is correct if the hybridization V is very small. As we have stated in section 4.1 and as we will substantiate in chapter 7, V indeed has to be fairly small (of the order of 0.01 eV) in order not to destroy the insulator–metal transition. The impurity self-energy $\Sigma_\sigma^{p,1}$ is denoted with an additional superscript 1 because a second impurity self-energy will be necessary within the fully self-consistent treatment in chapter 7.

The conduction-electron self-energy is taken from an interpolating ansatz [Nolting et al., 2001] for the conduction-electron part \mathcal{H}_{KLM} of the Hamiltonian (4.8):

$$\Sigma_\sigma^c(E) = -\frac{1}{2}z_\sigma J \langle S^z \rangle + \frac{1}{4}J^2 \frac{a_\sigma G_0(E + \mu - \frac{1}{2}z_\sigma J \langle S^z \rangle)}{1 - b_\sigma G_0(E + \mu - \frac{1}{2}z_\sigma J \langle S^z \rangle)}, \quad (6.4)$$

$$a_\sigma = S(S+1) - z_\sigma \langle S^z \rangle (z_\sigma \langle S^z \rangle + 1), \quad b_\sigma = \frac{1}{2}J,$$

where $G_0(E)$ is the free conduction-electron Green's function. Ansatz (6.4) fulfills all known limiting cases for $n_c \rightarrow 0$ (atomic limit [Nolting and Matlak, 1984], second-order perturbation theory in J [Mori, 1965, Mori, 1966, Bulk and Jelitto, 1988, Bulk and Jelitto, 1990, Nolting et al., 2001], ferromagnetic saturation [Shastry and Mattis, 1981, Allen and Edwards, 1982, Nolting et al., 1985, Nolting et al., 2001, Meyer et al., 2001], and high-energy expansion up to the fourth moment [Nolting et al., 2001]) and is therefore especially appropriate in the present case of very small conduction-electron densities (with a maximum of 10^{-3} per unit cell).

For the impurity self-energy $\Sigma_\sigma^{p,1}(E)$ we take the *atomic-limit* self-energy of the correlated Kondo lattice model (impurity part of our Hamiltonian: $\mathcal{H}_{p,1}$, $\mathcal{H}_{p,2}$ and \mathcal{H}_{pf} ; note that all terms are *local*), which is given in the

appendix D. If U is large compared to J , this leads to a four-peak structure in the impurity density of states with three of the four peaks having finite weight (see section 3.1 with $T_0 = \epsilon_p$). The energetically highest peak ϵ_4 will be the most decisive one, since from this peak the impurity electrons are emptied into the conduction band. Therefore, the position of ϵ_4 with respect to the bottom of the conduction band in dependence on temperature is of crucial importance.

6.1.2 Coherent-potential approximation

The oxygen vacancies in Eu-rich EuO are randomly distributed. There are lattice sites A where there is an oxygen vacancy with one-particle energy ϵ_p and self-energy $\Sigma_\sigma^{p,1}(E)$, and there are lattice sites B where there are no impurities. Our aim is to apply a coherent-potential approximation (CPA) to the impurity distribution, which gives a CPA self-energy that is valid for all lattice sites. Originally the CPA was designed to describe a multi-component system, where each component has a one-particle energy [Velický, 1969]. The trick is to introduce one-particle levels $\epsilon_{p,B}$ also for non-impurity sites B . Furthermore, a hybridization of electrons in these levels with the conduction-electron states is included for each B site: $V \sum_\sigma (p_{B\sigma}^\dagger c_{B\sigma} + c_{B\sigma}^\dagger p_{B\sigma})$. The impurity levels $\epsilon_{p,B}$ at non-impurity sites are then forced to diverge to infinity (or to adopt practically a very high energy) to be never really occupied. The latter is the precondition to correctly describe the real situation of impurity and non-impurity sites. In the so-called configurational average the disordered “levels” $\epsilon_{p,m} - \mu + \Sigma_{m\sigma}^{p,1}(E)$, where

$$\epsilon_{p,m} = \begin{cases} \epsilon_p & m = A \\ \infty & m = B \end{cases}, \quad \Sigma_{m\sigma}^{p,1} = \begin{cases} \Sigma_\sigma^{p,1} & m = A \\ 0 & m = B \end{cases},$$

are replaced by the CPA self-energy $\Sigma_\sigma^{\text{CPA},1}(E)$ at each site. With this the CPA equation can be formulated:

$$0 = \sum_{m=A,B} c_m \frac{\epsilon_{p,m} - \mu + \Sigma_{m\sigma}^{p,1}(E) - \Sigma_\sigma^{\text{CPA},1}(E)}{1 - G_\sigma^{p,1}(E) \left(\epsilon_{p,m} - \mu + \Sigma_{m\sigma}^{p,1}(E) - \Sigma_\sigma^{\text{CPA},1}(E) \right)}, \quad (6.5)$$

with $c_A = d$ and $c_B = 1 - d$ the concentrations of the impurity and non-impurity sites, respectively. Equation (6.5) has to be solved self-consistently with respect to the CPA self-energy, which is included in the local Green’s function of the effective medium $G_\sigma^{p,1}(E)$. $G_\sigma^{p,1}(E)$ is given by Eq. (6.17). From Eq. (6.5) one can derive a recursion formula for $\Sigma_\sigma^{\text{CPA},1}$ which is fairly

stable with respect to convergence [Santos, 2004]:

$$\Sigma_{\sigma}^{\text{CPA},1} = \frac{c_A E_A [1 - G_{\sigma}^{p,1} \cdot (E_B - \Sigma_{\sigma}^{\text{CPA},1})] + c_B E_B [1 - G_{\sigma}^{p,1} \cdot (E_A - \Sigma_{\sigma}^{\text{CPA},1})]}{1 - [c_A G_{\sigma}^{p,1} \cdot (E_B - \Sigma_{\sigma}^{\text{CPA},1}) + c_B G_{\sigma}^{p,1} \cdot (E_A - \Sigma_{\sigma}^{\text{CPA},1})]}, \quad (6.6)$$

$$E_A = \epsilon_{p,A} - \mu + \Sigma_{A\sigma}^{p,1}, \quad (6.7)$$

$$E_B = \epsilon_{p,B} - \mu. \quad (6.8)$$

6.1.3 Green's functions

The equations of motion for the Green's functions $G_{\vec{k}\sigma c}(E) = \langle\langle c_{\vec{k}\sigma}^-; c_{\vec{k}\sigma}^{\dagger} \rangle\rangle$, $G_{\vec{k}\sigma}^{p,c}(E) = \langle\langle p_{\vec{k}\sigma}^-; c_{\vec{k}\sigma}^{\dagger} \rangle\rangle$, $G_{\vec{k}\sigma}^{c,p}(E) = \langle\langle c_{\vec{k}\sigma}^-; p_{\vec{k}\sigma}^{\dagger} \rangle\rangle$ and $G_{\vec{k}\sigma p}(E) = \langle\langle p_{\vec{k}\sigma}^-; p_{\vec{k}\sigma}^{\dagger} \rangle\rangle$ are the following¹:

$$EG_{\vec{k}\sigma c}(E) = 1 + [\epsilon_{\vec{k}} - \mu + \Sigma_{\sigma}^c(E)]G_{\vec{k}\sigma c}(E) + VG_{\vec{k}\sigma}^{p,c}(E) \quad (6.9)$$

$$EG_{\vec{k}\sigma}^{p,c}(E) = [\Sigma_{\sigma}^{\text{CPA},1}(E)]G_{\vec{k}\sigma}^{p,c}(E) + VG_{\vec{k}\sigma c}(E) \quad (6.10)$$

$$EG_{\vec{k}\sigma p}(E) = 1 + [\Sigma_{\sigma}^{\text{CPA},1}(E)]G_{\vec{k}\sigma p}(E) + VG_{\vec{k}\sigma}^{c,p}(E) \quad (6.11)$$

$$EG_{\vec{k}\sigma}^{c,p}(E) = [\epsilon_{\vec{k}} - \mu + \Sigma_{\sigma}^c(E)]G_{\vec{k}\sigma}^{c,p}(E) + VG_{\vec{k}\sigma p}(E) \quad (6.12)$$

For Eqs. (6.10) and (6.12) it is assumed that

$$\left\langle\left\langle \left[p_{m\sigma}, U \sum_j n_{j\uparrow}^p n_{j\downarrow}^p - J \sum_j \vec{S}_j \cdot \vec{\sigma}_j^p \right]_- ; c_{m'\sigma}^{\dagger} \right\rangle\right\rangle = \Sigma_{m\sigma}^{p,1}(E) \langle\langle p_{m\sigma}; c_{m'\sigma}^{\dagger} \rangle\rangle \quad (6.13)$$

$$\text{and } \left\langle\left\langle \left[c_{\vec{k}\sigma}^-, -J \sum_i \vec{S}_i \cdot \vec{\sigma}_i^c \right]_- ; p_{\vec{k}\sigma}^{\dagger} \right\rangle\right\rangle = \Sigma_{\sigma}^c(E) \langle\langle c_{\vec{k}\sigma}^-; p_{\vec{k}\sigma}^{\dagger} \rangle\rangle. \quad (6.14)$$

The assumptions (6.13) and (6.14) in connection with the Eqs. (6.2) and (6.3) are somewhat similar to the self-energy ‘‘trick’’ in the moment-conserving decoupling approximation for the non-diagonal terms by Nolting *et al.* [Nolting et al., 1997]. From Eqs. (6.9) to (6.12) one can get the following Green's functions:

$$G_{\vec{k}\sigma c}(E) = \frac{1}{E - (\epsilon_{\vec{k}} - \mu) - \frac{V^2}{E - \Sigma_{\sigma}^{\text{CPA},1}(E)} - \Sigma_{\sigma}^c(E)} \quad (6.15)$$

$$G_{\vec{k}\sigma p}(E) = \frac{1}{E - \Sigma_{\sigma}^{\text{CPA},1}(E) - \frac{V^2}{E - (\epsilon_{\vec{k}} - \mu) - \Sigma_{\sigma}^c(E)}} \quad (6.16)$$

¹Since we have introduced (within the CPA) p states also at non-impurity sites we can sensibly define the \vec{k} dependent operators $p_{\vec{k}\sigma}^{(\dagger)}$.

The local impurity Green's function of the effective medium is simply given by

$$G_{\sigma}^{p,1}(E) = \frac{1}{N} \sum_{\vec{k}} G_{\vec{k}\sigma p}(E) = \int_{-\infty}^{+\infty} dx \frac{\rho_0(x)}{E - \Sigma_{\sigma}^{\text{CPA},1}(E) - \frac{V^2}{E - (x - \mu) - \Sigma_{\sigma}^c(E)}} , \quad (6.17)$$

where ρ_0 is the free conduction band density of states. In this chapter it is chosen to be semielliptic².

In a calculation of $\langle S^z \rangle$ from the Brillouin function for $S = \frac{7}{2}$ one can get a T dependence of $\langle S^z \rangle$ which corresponds to the mean-field result for the pure Heisenberg model, i.e. which does not self-consistently include the influence of the conduction and impurity electrons on the f spins. That will be incorporated in the next chapter.

The self-consistency cycle here goes as follows. For a certain value of $\langle S^z \rangle$ (and therewith a corresponding temperature) and a guess of μ one can calculate $\Sigma_{\sigma}^c(E)$ [Eq. (6.4)]. With initial values for $\langle n_{\sigma}^p \rangle_A = \langle n_{\sigma}^p \rangle / d$, where $\langle \dots \rangle_A$ denotes the average at an impurity site, one can calculate $\Sigma_{\sigma}^{p,1}(E)$ [Eq. (D.1)]. With an initial guess for $\Sigma_{\sigma}^{\text{CPA},1}(E)$ one can obtain $G_{0\sigma p} = G_{\sigma}^{p,1}$ [Eq. (6.17)] and $G_{0\sigma c} = \frac{1}{N} \sum_{\vec{k}} G_{\vec{k}\sigma c}$ [Eq. (6.15)]. With Eq. (6.6) one can get a new self-energy $\Sigma_{\sigma}^{\text{CPA},1}(E)$ for the next self-consistency cycle. With the Green's functions $G_{0\sigma p} = G_{\sigma}^{p,1}$ and $G_{0\sigma c}$ one can get the electron occupation numbers $\langle n_{\sigma}^p \rangle$ and $\langle n_{\sigma}^c \rangle$ by a simple integration according to the spectral theorem:

$$\langle n_{\sigma}^{p/c} \rangle = -\frac{1}{\pi} \int_{-\infty}^{+\infty} dE f(E) G_{0\sigma(p/c)}(E) , \quad (6.18)$$

where $f(E)$ is the Fermi function. Now one can correct the position of the chemical potential μ to achieve better agreement with the total electron number in the next self-consistency cycle. With the new μ we can start a new self-consistency cycle and iterate until all quantities have converged.

The inclusion of the magnetic field terms [Eq. (4.9)] will change the one-particle energies $\epsilon_{\vec{k}}$ and ϵ_p to $\epsilon_{\vec{k}} - z_{\sigma} \mu_B B_0$ and $\epsilon_p - z_{\sigma} \mu_B B_0$, respectively, in all expressions.

²Note that in the derivation of the transport formulae we have proven Eq. (5.47) strictly speaking only for the nearest-neighbor hopping tight-binding dispersions of the cubic lattices. Hence, we assume that the derivation of the transport formulae [Eq. (5.55)] also holds in the case of a semielliptic free conduction band.

6.2 Technical details of the calculations

In this section we discuss some technical details when evaluating the above theory. One of the biggest problems concerning numerical accuracy is the value of the infinitesimally small 0^+ , which has to be added as $i0^+$ whenever the energy E appears in Green's functions and self-energies to obtain the correct retarded functions. The smaller the value of 0^+ the higher the numerical accuracy but the bigger the computing time because of a smaller energy mesh which is needed for the integrations. One has to find a good compromise between accuracy and calculating time. Along our calculations we have arrived at a numerical value for 0^+ of 0.002. As we have explained in section 4.1 the highest impurity level ϵ_4 is of decisive influence on the metal-insulator transition. It is in fact not a true level but smeared out (see insets of Fig. 6.3) due to the hybridization with the conduction band, and numerically because of the "finite 0^+ ". Due to the latter it has a Lorentzian-like shape with unphysical tails that in principle reach $+$ and $-\infty$. Above the Curie temperature T_C , when the position of the impurity "level" will be below the conduction band, the position of the chemical potential would be unphysically high if we demanded an electron number of 2 per impurity site, which theoretically we should do. However, for physical and for practical reasons we take a slightly lower impurity-electron occupation of 1.995 to get a chemical potential which does not lie in the unphysical tails of the impurity "level".

The spectral density of the conduction electrons $A_{k\sigma}^-(E)$ and, therefore, also the integral $I(E) = \int_{-\infty}^{\infty} dx A_{x\sigma}(E)^2 \hat{v}(x)$ which appears in the transport functions Eq. (5.55) have similar unphysical tails due to the "finite 0^+ ". For the electrical conductivity the integral $I(E)$ has to be multiplied by the derivative of the Fermi function $f'(E)$, which at low temperatures approaches a sharp Lorentzian at the position of the chemical potential with exponentially decreasing tails. For temperatures above T_C , when the uppermost impurity level ϵ_4 is filled and the chemical potential lies below the conduction band, the very high middle parts of the Lorentzian give a big unphysical contribution when multiplied with the unphysical lower tail of the integral $I(E)$. Therefore one has to get rid of that tail. Fortunately, the unphysical tail of $I(E)$ can be recognized quite well. There is a crossover from a fairly steep part (the physical band edge) to a rather flat part (the unphysical tail). At that crossover, which approximately appears at a value of the integral of 1×10^{-4} , one has to cut the integral (put it to zero "by hand"). This is shown in the upper left panel of Fig. 6.1. The curves are calculated for an impurity density of 0.5 % and at $T = 70$ K. The thin line is $I(E)$ with and the thick line without the unphysical tail. However, one has to take care of the

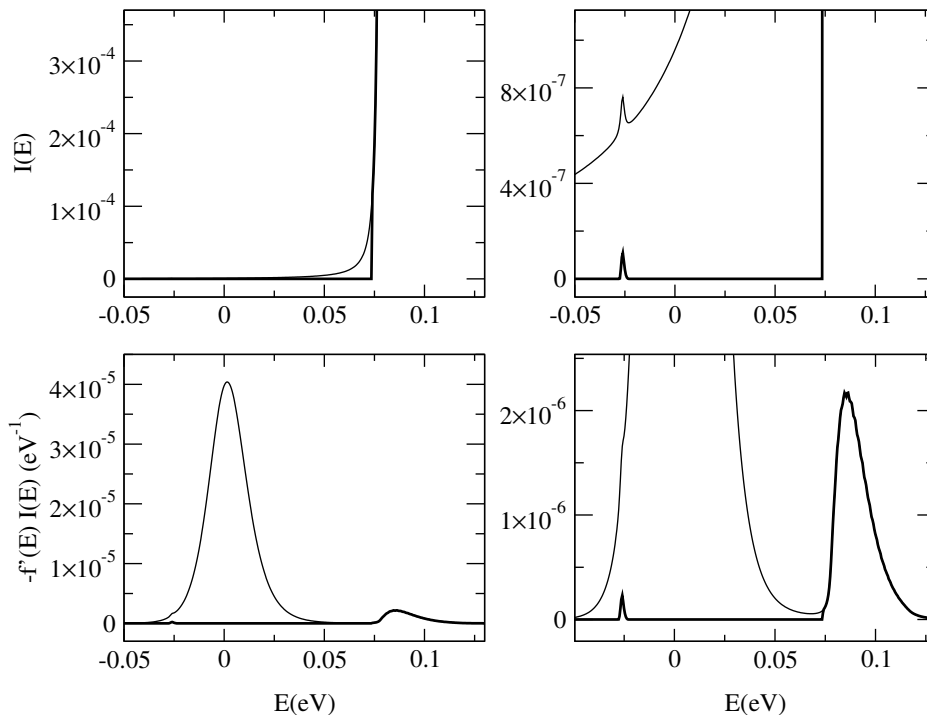


Figure 6.1: Quantities with (thick lines) and without (thin lines) tail corrections of the integral $I(E)$ as defined in the text. Upper panels: $I(E)$. Lower panels: product of $I(E)$ with the derivative of the Fermi function $f'(E)$ as it appears in the convolution for the transport functions Eq. (5.55). Right panels: the small peaks come from the hybridization of the conduction band with the impurity levels. The impurity concentration is $d = 0.5\%$, and the temperature $T = 70$ K. All the other parameters are given in section 4.1.

hybridized part of the conduction-electron spectral density at the position of the uppermost impurity level ϵ_4 which also leads to a physical contribution in the integral $I(E)$ in the shape of a peak. This peak has to be retained after subtracting the contribution of the unphysical tail. This can be seen in the right upper panel of Fig. 6.1. In the lower panels of the same figure the (negative) product of $I(E)$ with the derivative of the Fermi function $f'(E)$ can be seen, including (thin line) and excluding (thick line) the unphysical parts of $I(E)$. The exclusion of the unphysical parts obviously leads to a different but correct value for the transport coefficients A_s [Eq. (5.55)], which are basically given by integrals over $E^s[-f'(E)]I(E)$. Hence, the exclusion of the unphysical parts of $I(E)$ is an essential technical point for calculating the transport quantities correctly.

In the CPA procedure the one-particle levels $\epsilon_{p,B}$ for non-impurity sites

are set equal 10 eV (instead of theoretical ∞), which for practical calculations turns out to be high enough (with the zero of energy in the middle of the conduction band). Note that the overall spectral weight of the impurity levels ϵ_1 to ϵ_4 of $G_\sigma^{p,1}$ comes out correctly (equal to d) while the rest of the spectral weight $(1 - d)$ is concentrated at the level $\epsilon_{p,B}$, which we introduced to allow for a CPA.

6.3 Results and discussion

In this section we present results of the calculations with external parameter $\langle S^z \rangle$. Since the experimentally observed magnetization curve is very close to a theoretical Brillouin function [Mauger et al., 1978] this approach is well justified. It is one of the goals of the next chapter to show that the Brillouin function with the experimentally fixed Curie temperature is also theoretically reasonable and that the self-consistently determined Curie temperature (including the influence of the exchange of the conduction and the impurity electrons with the f spins of the Eu ions) does not differ much from the experimental one. The results of this section were published in Refs. [Sinjukow and Nolting, 2003, Sinjukow and Nolting, 2004a, Nolting et al., 2003b].

6.3.1 Fit of resistivity

First, we present a fit to experimental resistivity curves, which is meant to underline the idea that the difference in resistivity behavior of different experimental samples is due to a different content of oxygen vacancy (impurity) sites. As mentioned in section 4.1 the hybridization V has to be small to be able to reproduce the metal-insulator transition, which will be substantiated in chapter 7. Once a small value (0.01 eV) has been chosen for the hybridization, there remain two fit parameters ϵ_p (i.e. ϵ_4) and the impurity concentration d . Since ϵ_p and its possible variation with the impurity concentration d is not known from the experiment, we first chose one value for ϵ_p (-6.44 eV), which in connection with different impurity concentrations gives the best overall fit with the different experimental resistivity curves. The result is shown in Fig. 6.2. We chose three experimental curves of medium resistivity from Ref. [Oliver et al., 1972] and selected the theoretical curves with appropriate impurity concentrations d which fitted best to the experimental ones. All curves show a huge metal-insulator transition near the Curie temperature of 69 K. At low temperatures the resistivity is metallic, i.e. $\frac{d\rho}{dT} > 0$. However, the absolute values of the resistivity are quite high

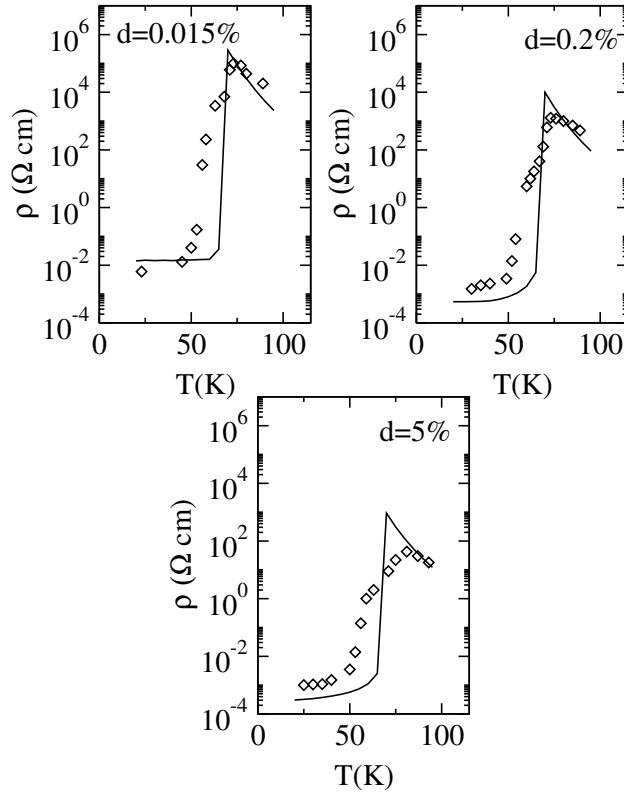


Figure 6.2: Comparison of measured (diamonds, samples 66-6, 95-BA-3 and 49-4 from Ref. [Oliver et al., 1972]) and calculated resistivity (solid lines) in dependence on temperature. The theoretical curves are calculated for three different impurity concentrations d . For the other parameters see section 4.1.

(10^{-3} – $10^{-2}\Omega\text{ cm}$) in comparison with good metals like Cu ($1.7 \times 10^{-6}\Omega\text{ cm}$). Near the Curie temperature there is a big jump in resistivity of five to seven orders of magnitude. Above T_C the resistivity is insulating, i.e. $\frac{d\rho}{dT} < 0$.

It can be seen that the theoretical curves fit quite well to the experimental ones, concerning both the height of the jump as well as the absolute values of the resistivity. We do not claim that the theoretical impurity concentrations exactly correspond to the experimental ones since we did not consider a variation of ϵ_p with the impurity concentration d . In fact, our calculations show that such a variation must be assumed to explain the resistivity behaviour of the highest-resistivity samples as it is shown in Fig. 6.4. However, the quality of the fit in Fig. 6.2 shows that the differing behavior of the medium-resistivity samples, the absolute values and height of the jump in resistivity, can be explained by differing impurity concentrations alone.

For a comparison with Steenekens calculations in Ref. [Steeneken, 2002]

see subsection 6.3.3.

6.3.2 Densities of states and mechanism of the metal-insulator transition

But how does the metal-insulator transition actually come about? The argu-

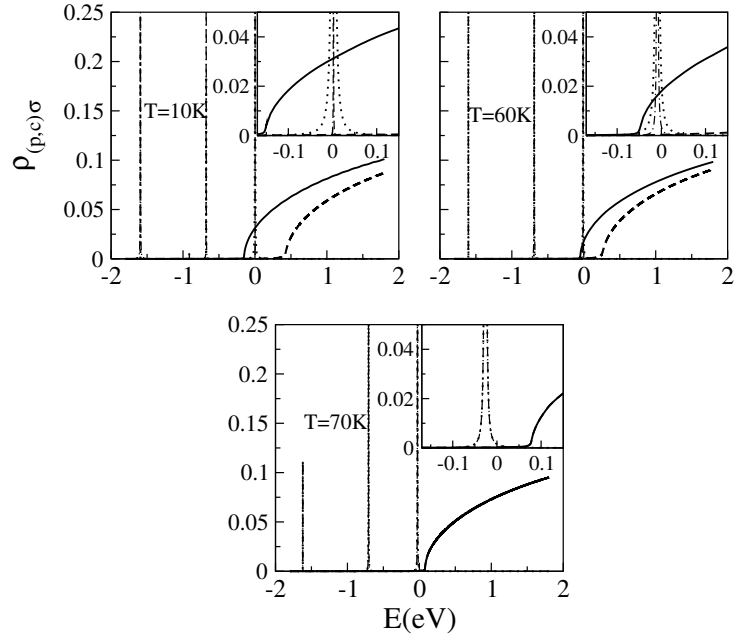


Figure 6.3: Conduction-electron densities of states ($\rho_{\uparrow}(-)$, $\rho_{\downarrow}(-)$) and impurity densities of states ($\rho_{p\uparrow}(-)$, $\rho_{p\downarrow}(-)$) for $d = 0.05\%$ and three different temperatures. For the other parameters see section 4.1. The insets show the densities of states near the Fermi level.

mentation is in principle similar to the one of the simple model by Oliver *et al.* [Oliver et al., 1970]. It can be explained best with the help of the quasi-particle densities of states as shown in Fig. 6.3 for an impurity concentration of $d = 0.05\%$. As mentioned in Sec. 6.1 and as can be seen in Fig. 6.3, there are three impurity levels (ϵ_1 , ϵ_3 and ϵ_4) with finite weight. Their positions are temperature independent on an absolute energy scale. The most important one is the uppermost level ϵ_4 . Now there are two scenarios, depending on whether the uppermost impurity level overlaps with the spin-up conduction band below a certain temperature below the Curie temperature T_C or not. The first scenario is described in this subsection, and the second in the next one.

The first scenario is shown in Fig. 6.3 and is most likely to occur in the medium-resistivity samples. Below the Curie temperature one has the spin-splitting of the conduction band due to exchange with the Eu 4*f* spins. The spin-up part of the conduction band is down-shifted (redshift) and the spin-down part up-shifted. In the first scenario the spin-up conduction band overlaps with the impurity level ϵ_4 below a certain temperature close to the Curie temperature. So the impurity electrons can at least partly empty into the conduction band. There they have almost 100 % spin polarization. The lower the temperature the lower is the (spin-up) conduction band (redshift of up to -0.3 eV near 0 K) and the higher is the overlap with the impurity level, i.e. the more electrons can empty into the conduction band. The higher the temperature the lower the overlap of the impurity level with the (spin-up) conduction band (see $T = 60$ K in Fig. 6.3), the less electrons empty into the conduction band and the higher the resistivity (metallic behavior $\frac{d\rho}{dT} > 0$). At and above the Curie temperature the uppermost impurity level is below the conduction band. Apart from the hybridized part of the conduction band at the impurity level only thermally excited electrons contribute to the electrical conduction. The Eu-rich EuO behaves like a doped semiconductor ($\frac{d\rho}{dT} < 0$).

6.3.3 Low-temperature minimum in the resistivity of high-resistivity samples

In the second scenario of the metal-insulator transition, which is more likely to apply to the high-resistivity samples, the uppermost impurity level stays at all temperatures below the (spin-up) conduction band. An interesting feature of the high-resistivity samples is a low-temperature minimum in the resistivity. Oliver *et al.* [Oliver et al., 1972] explained it by activation from additional impurities like Gd or La. However we can give a more direct explanation of this phenomenon without invoking an additional external factor. If the uppermost impurity level ϵ_4 is so low that it always stays below the conduction band even at low temperatures then the conduction is always through thermally excited electrons. If the conduction band were fixed (temperature independent) then there would be always activated behaviour, i.e. $\frac{d\rho}{dT} < 0$. However, the effect of the redshift of the spin-up conduction band with lowering the temperature is bigger than the contraction of the derivative of the Fermi function, which appears in the conductivity formula. So one has below the Curie temperature $\frac{d\rho}{dT} > 0$. Lowering the temperature further below the point at which the full redshift of the spin-up conduction band is achieved ($\langle S^z \rangle \approx S$) lowers the number of thermally excited conduc-

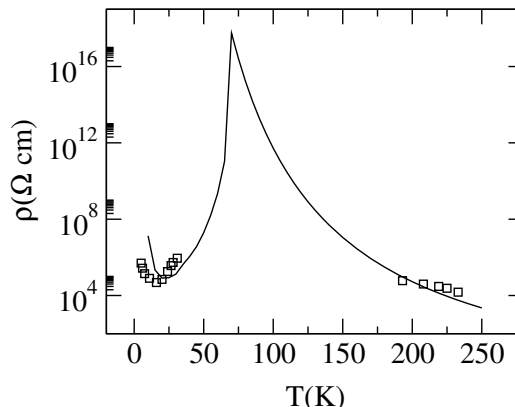


Figure 6.4: Comparison of measured (squares, sample 34-2-30 from Ref. [Oliver et al., 1972]) and calculated resistivity (solid line) for a high-resistivity sample. Impurity concentration $d = 0.01\%$, $\epsilon_p = -6.61$ eV ($\epsilon_4 = -5.31$ eV, lower band edge at -5.30 eV at $T = 0$). For the other parameters see section 4.1.

tion electrons so that the resistivity rises again: $\frac{d\rho}{dT} < 0$. Therefore we have a low-temperature minimum in the resistivity. To confirm this picture we made a fit to a high-resistivity sample with $d = 0.01\%$ and $\epsilon_p = -6.61$ eV, which means $\epsilon_4 = -5.31$ eV with the lower band edge at -5.30 eV at $T = 0$. In Fig. 6.4 we show an experimental and a calculated curve. There is a good agreement between the low-temperature minima and the high-energy tails. For the region inbetween there were no experimental points available but the run of the theoretical curve seems credible. Penney *et al.*'s “world-record” measurements of the resistivity were limited due to leakage currents to values of about $10^{11}\Omega\text{ cm}$, but interpolating their data allows values of up to $10^{16}\Omega\text{ cm}$.

In this second scenario it is in principle possible to get metallic behavior ($\frac{d\rho}{dT} > 0$) for arbitrarily low impurity concentrations in the temperature range where the redshift occurs because the redshift is faster than the smearing out of the Fermi function. This is in contradiction to the results by Leroux-Hugon [Leroux-Hugon, 1972] and Mauger [Mauger, 1983], who calculated a lower bound of the impurity concentration of about $d \approx 0.12\%$ and 0.02% for metallic behavior.

As mentioned in the introduction Steeneken's theoretical calculations of the resistivity based on his theory of a distribution of impurity levels fit fairly well for the medium-resistivity samples (in Fig. 6.2). He needs a much smaller range of impurity concentrations to get theoretical curves, which fit the lowest and the highest of the three medium-resistivity samples in Fig. 6.2.

However he fails to describe the high-resistivity samples like the one in Fig. 6.4. On the *ad hoc* assumption of additional acceptors he is able to reproduce the low-temperature minimum but not the high-temperature values of the resistivity. Either his theory on the distribution of impurity levels or the simple Drude theory fail to describe the high-resistivity samples.

6.3.4 Resistivity in a magnetic field and magnetoresistance

We can also calculate the resistivity in a magnetic field. Changes in the resistivity of up to 6 orders of magnitude were observed in the experiment [Shapira et al., 1973]. In the left panel of Fig. 6.5 the calculated resistivity

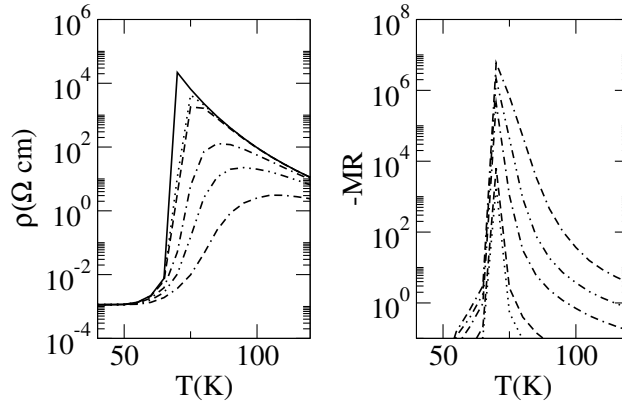


Figure 6.5: Left: Calculated resistivity for different magnetic fields B ; right: negative magnetoresistance. $B = 0\text{T}$ (—), 0.05T (\cdots), 0.1T (— —), 0.5T (— · — ·), 1T (- · · · ·), 2T (· - - ·). $d = 0.1\%$. For the other parameters see section 4.1.

is shown applying magnetic fields of up to two Tesla. What can be observed is a shift in the maximum of the resistivity to higher temperatures and at the same time a broadening of the maximum peak. Also the maximum resistivity decreases with increasing magnetic field. The curves look qualitatively similar to the ones of Fig. 3 in Ref. [Shapira et al., 1973]. They can be easily explained. The magnetic field itself causes a spin-splitting of the conduction band and a redshift of the spin-up part. Therefore the metal-insulator transition occurs at higher temperatures (maximum of resistivity at higher temperatures), and since the temperature is higher, more electrons are thermally excited into the conduction band, and the maximum is lower and smeared out.

In the right panel the negative magnetoresistance $-\text{MR} = [\rho(0) - \rho(B)]/\rho(B)$ is shown. The magnetoresistance is so big that we have normalized it by $\rho(B)$ instead of $\rho(0)$ to see the effects. If we had normalized it by $\rho(0)$, which is more common, the negative magnetoresistance above the transition temperature would be practically one, compared with a value of 0.8 for the colossal magnetoresistance (CMR) effect of the manganites like $\text{La}_{1-x}\text{Ca}_x\text{MnO}_3$ [Khomskii and Sawatzky, 1997, Coey et al., 1999]. With such big values the negative magnetoresistance according to our definition is almost only given by the ratio $\rho(0)/\rho(B)$. This ratio of the resistivities without and with a magnetic field amounts to about a maximum of six to seven orders of magnitude, which coincides with the experiment [Shapira et al., 1973].

Chapter 7

Fully self-consistent solution and results of the model

7.1 Fully self-consistent solution of the model

For the fully self-consistent solution of our model (4.8) (including \mathcal{H}_{ff}) we will rely on an adaption of the modified RKKY theory as laid out in the Refs. [Nolting et al., 1997, Santos and Nolting, 2002a, Santos and Nolting, 2002b, Kienert et al., 2003]. The single steps are given in the appendix E. We will concentrate here on the major steps only, similar to Ref. [Sinjukow and Nolting, 2004b]. The main idea of the modified RKKY theory is the mapping of the exchange terms on an effective Heisenberg model, which is then solved to give a value of $\langle S^z \rangle$. The theory has the correct RKKY behavior up to the second order in the coupling constant J but it is applicable for any coupling strength in contrast to the conventional RKKY theory. Within the modified RKKY theory reasonable results have been achieved for the Kondo lattice model [Santos and Nolting, 2002a, Santos and Nolting, 2002b, Nolting et al., 2003a]. For our model (4.8) we have to consider three types of exchange terms: the exchange of the conduction and the impurity electrons with the Eu spins and the direct exchange terms between the Eu spins. As a result the exchange integrals in the effective Heisenberg Hamiltonian consist of three parts, for the conduction electrons, for the impurity electrons, and for the original Heisenberg Hamiltonian \mathcal{H}_{ff} . As the calculations within the modified RKKY theory show (see appendix E), one arrives at an anisotropic Heisenberg Hamiltonian

$$\tilde{\mathcal{H}}'_{ff} = - \sum_{ii'} [J_{ii'}^{(1)} (S_i^+ S_{i'}^- + S_i^- S_{i'}^+) + J_{ii'}^{(2)} S_i^z S_{i'}^z] - B_{\text{eff}} \sum_i S_i^z \quad (7.1)$$

with

$$J_{ii'}^{(r)} = \begin{cases} J_{00c}^{(r)} + J_{00p}^{(r)} & i = i' \\ J_{01c}^{(r)} + J_{01p}^{(r)} + J_H^{(r)} & i, i' \text{ n.n.} \\ 0 & \text{otherwise} \end{cases} \quad (7.2)$$

$$r = 1, 2$$

$$J_H = 2J_H^{(1)} = J_H^{(2)} \quad (7.3)$$

$$B_{\text{eff}} = B_{\text{eff},c} + B_{\text{eff},p} . \quad (7.4)$$

Equations (7.1) to (7.4) correspond to Eqs. (E.62) to (E.65). We only consider on-site and nearest neighbor exchange for simplicity. Therefore, we also for the pure Heisenberg-model exchange consider only one value for the nearest neighbor exchange although in principle there is also a value for the next-nearest neighbor exchange available [Dietrich et al., 1975]. We choose the value for the nearest neighbor exchange $J_H = 0.734\text{K} * k_B \approx 6.33 \times 10^{-5} \text{eV}$ such that the correct experimental Curie temperature $T_C = 69.3 \text{K}$ comes out in the pure Heisenberg model. Now we would like to see what additional effects arise from the exchange of the conduction and the impurity electrons with the Eu spins. The eight effective exchange integrals and two effective fields have to be calculated self-consistently. They are given by integrals over Green's functions and the Fermi function $f(E)$.

$$J_{0le}^{(1)} = \frac{J^2}{8\pi} \text{Im} \int_{-\infty}^{+\infty} dE f(E) \left(G_{l\downarrow e}^{(0)}(E) G_{l\uparrow e}(E) + G_{l\uparrow e}^{(0)}(E) G_{l\downarrow e}(E) \right) , \quad (7.5)$$

$$J_{0le}^{(2)} = \frac{J^2}{4\pi} \text{Im} \int_{-\infty}^{+\infty} dE f(E) \left(G_{l\uparrow e}^{(0)}(E) G_{l\uparrow e}(E) + G_{l\downarrow e}^{(0)}(E) G_{l\downarrow e}(E) \right) , \quad (7.6)$$

$$B_{\text{eff},e} = -\frac{J}{2\pi} \text{Im} \int_{-\infty}^{+\infty} dE f(E) \left(G_{0\uparrow e}^{(0)}(E) - G_{0\downarrow e}^{(0)}(E) \right) , \quad (7.7)$$

$$l = 0, 1 \quad ; \quad e = c, p .$$

Equations (7.5), (7.6) and (7.7) for the conduction electrons ($e = c$) correspond to Eqs. (E.52), (E.44) and (E.24), respectively. As stated in the appendix E the derivations for the respective formulae for the impurity electrons are fully analogous. The Green's functions needed are the following:

$$G_{l\sigma c}^{(0)}(E) = \frac{1}{N} \sum_{\vec{k}} \frac{e^{i\vec{k}\vec{R}_l}}{E - (\epsilon_{\vec{k}} - \mu) - \frac{V^2}{E - \Sigma_{\sigma}^{\text{CPA},1}(E)}} , \quad (7.8)$$

$$G_{l\sigma c}(E) = \frac{1}{N} \sum_{\vec{k}} e^{i\vec{k}\vec{R}_l} G_{\vec{k}\sigma c}(E), \quad (7.9)$$

$$G_{\vec{k}\sigma c}(E) = \frac{1}{E - (\epsilon_{\vec{k}} - \mu) - \frac{V^2}{E - \Sigma_{\sigma}^{\text{CPA},1}(E)} - \Sigma_{\sigma}^c(E)}, \quad (7.10)$$

$$G_{l\sigma p}^{(0)}(E) = \frac{1}{N} \sum_{\vec{k}} \frac{e^{i\vec{k}\vec{R}_l}}{E - \Sigma_{\sigma}^{\text{CPA},2}(E) - \frac{V^2}{E - (\epsilon_{\vec{k}} - \mu) - \Sigma_{\sigma}^c(E)}}, \quad (7.11)$$

$$G_{l\sigma p}(E) = \frac{1}{N} \sum_{\vec{k}} \frac{e^{i\vec{k}\vec{R}_l}}{E - \Sigma_{\sigma}^{\text{CPA},1}(E) - \frac{V^2}{E - (\epsilon_{\vec{k}} - \mu) - \Sigma_{\sigma}^c(E)}}, \quad (7.12)$$

$$l = 0, 1, \quad \vec{R}_0 = \vec{0}.$$

$\Sigma_{\sigma}^{\text{CPA},2}(E)$ is a CPA self-energy, which is similarly defined as $\Sigma_{\sigma}^{\text{CPA},1}(E)$ in Eqs. (6.5) and (6.6). However, the impurity self-energy $\Sigma_{\sigma}^{p,1}$ is replaced by $\Sigma_{\sigma}^{p,2}$, and $G_{\sigma}^{p,1}(E)$ by $G_{\sigma}^{p,2}(E)$. $\Sigma_{\sigma}^{p,2}$ is defined by

$$\left\langle \left\langle \left[p_{j'\sigma}, U \sum_j n_{j\uparrow}^p n_{j\downarrow}^p \right]_- ; p_{j'\sigma}^{\dagger} \right\rangle \right\rangle = \Sigma_{\sigma}^{p,2}(E) \langle \langle p_{j'\sigma}; p_{j'\sigma}^{\dagger} \rangle \rangle. \quad (7.13)$$

We choose for $\Sigma_{\sigma}^{p,2}$ the atomic limit self-energy of the Hubbard model, which is given by (D.18). $G_{\sigma}^{p,2}(E)$ is identical to $G_{0\sigma p}^{(0)}(E)$ [Eq. (7.11) for $l = 0$]. $G_{\vec{k}\sigma c}(E)$ in Eq. (7.10) is the Green's function needed to calculate the spectral density $A_{\vec{k}\sigma}(E)$ for the transport functions in Eq. (5.55). The magnetization $\langle S^z \rangle$ still has to be determined. This is done by solving the effective Heisenberg Hamiltonian (7.1) by the Tyablikov decoupling, which is identical to the so-called random-phase approximation (RPA) [Bogoliubov and Tyablikow, 1959, Tyablikow, 1969, Nolting, 1986]. If one uses the method by Callen [Callen, 1963] one gets the following expression for the magnetization

$$\langle S_z \rangle = \frac{(1 + S + \phi)\phi^{2S+1} + (S - \phi)(1 + \phi)^{2S+1}}{(1 + \phi)^{2S+1} - \phi^{2S+1}} \quad (7.14)$$

where

$$\phi = \frac{1}{N} \sum_{\vec{k}} \frac{1}{e^{\beta E(\vec{k})} - 1} \quad (7.15)$$

and $S = \frac{7}{2}$ for the Eu spins. The magnon energies $E(\vec{k})$ are the excitation energies of the magnon Green's function $\langle\langle S^+(\vec{k}); S^-(\vec{k}) \rangle\rangle_E$ (see appendix E). They are given by

$$E(\vec{k}) = 2\langle S_z \rangle \left[J^{(2)}(0) - 2J^{(1)}(\vec{k}) \right] + J_{00}^{(2)} - 2J_{00}^{(1)} + B_{\text{eff}} \quad (7.16)$$

where

$$J^{(n)}(\vec{k}) = \frac{1}{N} \sum_{i'} J_{ii'}^{(n)} e^{i\vec{k}(\vec{R}_i - \vec{R}_{i'})}, \quad n = 1, 2. \quad (7.17)$$

We will now sketch the full self-consistency cycle to be solved. First we take a certain value for $\langle S^z \rangle$ as a guess. With that value we can calculate the Green's functions and self-energies in a sub-self-consistency cycle. This comprises Eqs. (6.4), (6.6) and the equivalent for $\Sigma_{\sigma}^{\text{CPA},2}(E)$, and Eqs. (7.8) – (7.12). The chemical potential μ is adjusted to give the correct overall electron number, which is two¹ per oxygen vacancy site. With the help of the Green's functions the effective exchange integrals and effective fields can be calculated [Eqs. (7.5) to (7.7)]. In the end a new value of $\langle S^z \rangle$ can be calculated in another sub-self-consistency cycle which consists of Eqs. (7.14) – (7.16). With the new value of $\langle S^z \rangle$ the self-consistency loop is closed.

At temperatures near the Curie temperature similar considerations about unphysical energy tails due to the numerical finiteness of the $i0^+$ are valid for the integrals in Eqs. (7.5) to (7.7). Before the convolution with the Fermi function the unphysical tails of the Green's functions have to be put to zero by hand, however properly taking care of the hybridized parts. This is absolutely essential to get correct values for the effective exchange integrals and fields especially close to T_C where the chemical potential lies below the lower band edges of the imaginary parts of the Green's functions.

7.2 Results and discussion

7.2.1 Magnetization and Curie temperature

In Figure 7.1 three different magnetization curves, ($\langle S^z \rangle$ of the Eu spins) are shown. The dotted curve is a simple Brillouin function for $S = \frac{7}{2}$ and a Curie temperature of 69.3 K. We used this curve for our non-self-consistent calculation in chapter 6 and stated that it fitted well to the experimental magnetization curve [Mauger et al., 1978]. However, we did not want

¹In the actual calculations it is a bit less than two, see Sec. 6.2.

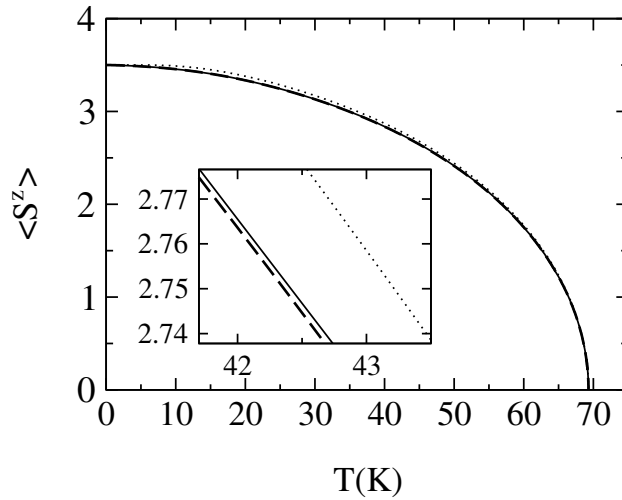


Figure 7.1: Magnetization $\langle S^z \rangle$ in dependence on temperature. The Brillouin function for $S = 7/2$ with $T_C = 69.3$ K is represented by the dotted line. The calculated curve for the pure Heisenberg model of the Eu spins with $J_H = 0.734$ K \cdot k_B to yield $T_C = 69.3$ K is given by the dashed line. The fully self-consistent $\langle S^z \rangle$ of the full model is shown by the solid line. The impurity concentration is $d = 0.1\%$. For other parameters see section 4.1. In the inset an enlarged section of the magnetization curves is shown.

to stop our considerations at this point. In particular we were interested in the actual effect of the exchange of the conduction and impurity electrons with the Eu spins. Therefore, we first introduced the pure Heisenberg model for the Bloembergen-Rowland exchange between the Eu spins with $J_H = 0.734$ K \cdot $k_B \approx 6.33 \times 10^{-5}$ eV to obtain the experimentally observed Curie temperature, too. For simplicity we consider only nearest-neighbor exchange. The resulting magnetization evaluated within the Tyablikov [Bogoliubov and Tyablikow, 1959, Tjablikow, 1969, Nolting, 1986] and Callen [Callen, 1963] approximations is the dashed line in Fig. 7.1. Second, to include the exchange of the conduction and the impurity electrons with the Eu spins we utilized the modified RKKY theory as discussed in the previous section. The result for an impurity concentration of 0.1 % is the solid line in Fig. 7.1.

It turns out that the effects are very small at the self-consistent Curie temperature, which does not differ from the non-self-consistent value within an accuracy of 1 mK. It agrees with the experimental observation of the same Curie temperature for both the Eu-rich and the pure EuO [Penney et al., 1972]. This has been used as an argument that the Eu lattice

in Eu-rich EuO is intact and that the Eu richness actually comes from an oxygen deficiency. However, this argument does not touch the question of the influence of the conduction and the impurity electrons, which is the reason why we investigated this question. For temperatures below T_C there is an enhancement of the fully self-consistent magnetization compared with the pure Heisenberg model. The exchange of the conduction and the impurity electrons with the Eu spins does lead to an additional ferromagnetic coupling between the Eu spins. However, it is an important result of our calculation that this enhancement is fairly small. Note that at least for the pure Kondo lattice model the inclusion of further exchange integrals (next-nearest neighbor, next-next-nearest neighbor exchange and so on) leads to a reduction of the magnetization because e.g. the next-nearest neighbor exchange constants are negative [Santos, 2004]. Therefore, our results represent an upper bound of the effects mentioned.

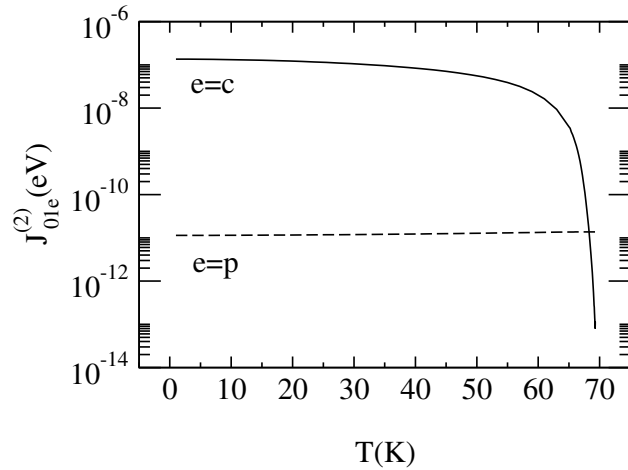


Figure 7.2: Exchange integrals $J_{01c}^{(2)}$ and $J_{01p}^{(2)}$ in dependence on temperature. The impurity concentration is $d = 0.1\%$ (same as in Fig. 7.1). For the other parameters see section 4.1.

For the same value of the magnetization there is a temperature difference of about 0.1 K in the temperature range of 30–50 K for $d = 0.1\%$ (see the inset of Fig. 7.1). At T_C this difference is reduced to a value of less than 1 mK. To understand this it is important to invoke the picture of the metal-insulator transition in Eu-rich EuO, which we discussed in section 6.3, and to look at the exchange integrals (for instance $J_{01e}^{(2)}$ with $e = c, p$, see Fig. 7.2) and at the conduction-electron (see Fig. 7.12) and the impurity-electron numbers (see Fig. 7.15). The small enhancement in the self-consistent magnetization in the range 30 – 50 K is mainly due to the value of $J_{01c}^{(2)} \approx 10^{-7} \text{eV}$ (see Fig. 7.2)

in comparison with the bare J_H value of $\approx 6 \times 10^{-5} \text{eV}$ ($J_{01p}^{(2)} \approx 10^{-11} \text{eV}$ plays no significant role). Note that the conduction electron number below

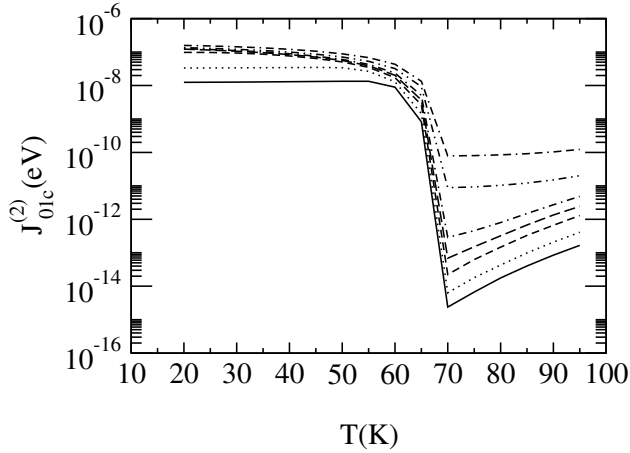


Figure 7.3: Exchange integral $J_{01c}^{(2)}$ in dependence on temperature for different impurity concentrations d (— 0.01%, \cdots 0.02%, -- 0.05%, - - 0.1%, --- 0.2%, \cdots 1%, \cdots 5%). For the other parameters see section 4.1.

T_C is at most only 5×10^{-4} for $d = 0.1\%$ (see Fig. 7.12). The exchange of the conduction electrons with the Eu spins in principle drives the Curie temperature towards a higher value. However, increasing the temperature decreases the magnetization and with it the number of conduction electrons, the exchange integrals and with it the magnetization and so on. Just below the original (non-self-consistent) T_C the bottom of the conduction band crosses the uppermost impurity level and therefore (apart from “hybridized” conduction electrons) there are only very few thermally excited conduction electrons. This is a dynamical process. The values of the magnetization, the conduction electron number and the exchange integrals (e.g. $J_{01c}^{(2)}$) take on self-consistent values. As a matter of fact just below the original (non-self-consistent) T_C there is a big jump of the conduction electron number to 10^{-10} (see Fig. 7.12) and of $J_{01c}^{(2)}$ to 10^{-13} eV. These values are so low that the theoretical self-consistent Curie temperature of Eu-rich EuO is identical within 1 mK to the original Curie-temperature of pure EuO. The exchange integral $J_{01p}^{(2)}$ of the impurity electrons is very small and almost constant over the whole temperature range so that its influence on the self-consistent Curie temperature is almost negligible. It is so small because the impurity electrons are rather immobile. It is almost temperature-independent because the impurity electron number is almost constant (0.0013 at $T = 0$ and 0.002 at T_C).

Let us take a closer look at the exchange integral $J_{01c}^{(2)}$ given by Eq. (7.6) for $l = 1$ and $e = c$. A whole bunch of curves is shown in Fig. 7.3 for different impurity concentrations. As we have mentioned the absolute values of the effective exchange integral are fairly low in comparison to the pure Heisenberg exchange with $J_H \approx 6 \times 10^{-5}$ eV. At maximum they are about 10^{-7} eV at low temperatures for impurity concentrations higher than 0.05 %. This is still enough to enhance the temperature at which the magnetization adopts the same value by 0.1 K in a temperature range of 30–50 K (for $d = 0.1$ % see above and inset of Fig. 7.1). But at the self-consistent T_C the effective exchange integrals of the conduction electrons have a big jump towards lower values ranging from 10^{-10} eV for impurity concentration $d = 5$ % to 10^{-15} eV for $d = 0.01$ %. This jump can be explained by the fact that the uppermost impurity level ϵ_4 and with it the chemical potential μ cross the lower band edge of the (spin-up) conduction band downwards. Because of the Fermi function there is a big jump downwards in the exchange integrals. This leads to the fact that the self-consistent Curie temperature is practically unchanged. In general it can be said that the lower the impurity concentration (and with it the number of “hybridized” and thermally excited conduction electrons) the lower is the effective conduction-electron exchange integral.

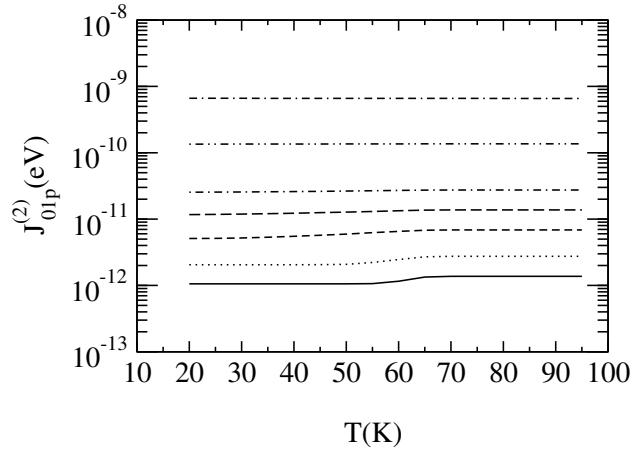


Figure 7.4: Exchange integral $J_{01p}^{(2)}$ in dependence on temperature for the same values of impurity concentrations d as in Fig. 7.3. For the other parameters see section 4.1.

The same can be said about the impurity-electron exchange integral $J_{01p}^{(2)}$. Nevertheless, the temperature dependence is different in the case of $J_{01p}^{(2)}$, which is shown in Fig. 7.4. $J_{01p}^{(2)}$ is almost temperature independent. This

is explicable by the fact that the chemical potential is almost pinned at the uppermost impurity level ϵ_4 , especially for higher impurity concentrations because the conduction band below T_C can only absorb a limited number of electrons of 0.0008 per Eu site (see upper panel of Fig. 7.12). For lower impurity concentrations this is a bit different. There the exchange integral changes slightly with increasing temperature. At temperatures below T_C $J_{01p}^{(2)}$ has a maximum value of 7×10^{-10} eV for $d = 5\%$, which is significantly lower than the value of the corresponding conduction-electron exchange integral $J_{01c}^{(2)}$. So it is the conduction electrons which have the major influence on the self-consistently determined magnetization below T_C . Above T_C the magnetization is zero but the exchange integrals of the impurity electrons are bigger than the ones of the conduction electrons (compare Figs. 7.3 and 7.4). The constancy of $J_{01p}^{(2)}$ is closely related to the constancy in the impurity electron number at higher impurity concentrations (see subsection 7.2.8).

7.2.2 Comparison of theoretical and experimental resistivity

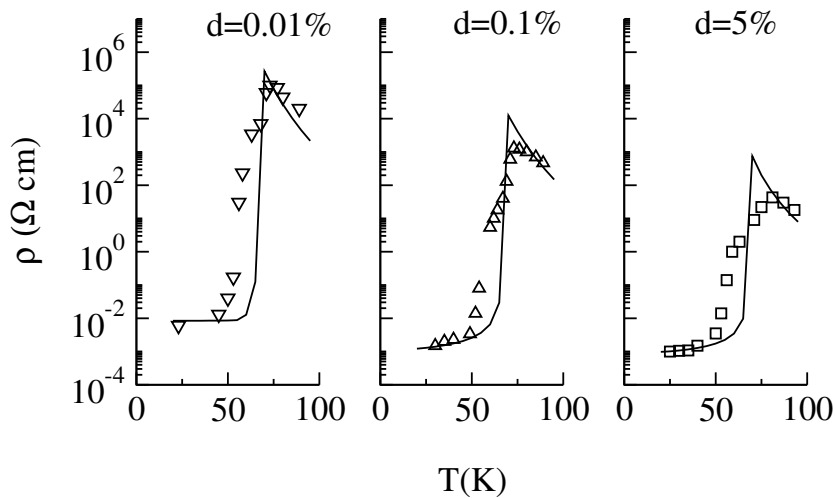


Figure 7.5: Comparison of measured (open symbols, representing from the left to the right the samples 66-6, 95-BA-3 and 49-4 from Ref. [Oliver et al., 1972]) and calculated resistivity (solid lines) in dependence on temperature. The theoretical curves are calculated for three different impurity concentrations d . For the other parameters see section 4.1.

In Fig. 7.5 a fit is shown of three theoretical to three experimental curves. The experimental curves are from medium-resistivity samples from

Ref. [Oliver et al., 1972]. They are the same as in section 6.3 in Fig. 6.2. The fit of the theoretical curves is similar to the non-selfconsistent calculations, which is not self-evident. It is true that it turns out of our calculations that the fully self-consistent magnetization ($\langle S^z \rangle$) curve differs not much from the Brioullin function. However, for technical reasons [see Eqs. (E.48) and (E.49)] we have to use a full conduction electron dispersion for the fully self-consistent calculations [we use the nearest-neighbor tight-binding dispersion for the fcc lattice (E.50)]. The free density of states, which comes out from this dispersion, also has the typical square root dependence on energy at the lower band edge but in contrast to the semielliptical density of states, which we used in the previous chapter, its height at the lower band edge is about one tenth compared to the semielliptical one. That is why the fitting parameter ϵ_p with a value of -6.42 eV in this chapter slightly differs from the value in the previous chapter (-6.44 eV). Also the theoretical value of the impurity concentration for one of the samples differs slightly (0.01% instead of 0.015%). However, the three fits in Fig. 7.5 are even better than in Fig. 6.2 probably due to a more realistic free conduction density of states.

Concerning the general properties of the fits, similar things which have been stated for the non-self-consistent calculations of section 6.3 can be repeated here. Care has to be taken when considering the fit impurity densities d too seriously, since we have not taken a possible dependence of the uppermost impurity level ϵ_4 on the impurity concentration into account. We have seen in the last chapter that such a variation has to be considered when trying to explain the low-temperature resistance minimum of the high-resistivity samples. However, it is clear from our calculations that the variation in the jump in resistivity over several orders of magnitude can in principle be explained by a variation in the impurity (oxygen vacancy) concentration without the necessity of other impurities like Gd or La.

7.2.3 Electrical resistivity and chemical potential

In Figure 7.6 a bunch of resistivity curves is shown with all parameters fixed except the impurity concentration d . It varies in the range from 0.01 to 5%. All the curves show a big jump of the resistivity of several orders of magnitude near the magnetic transition temperature. The variation of the impurity (oxygen vacancy) concentrations from high to low values results in a general increase in the resistivity in the whole temperature range and an increase in the jump of the resistivity at T_c . For low temperatures the increase in resistivity with decreasing impurity concentration is not very big down to $d = 0.05\%$. The reason for this is the fact that for the parameters chosen the down-shifted conduction band can only absorb up to about 0.0008

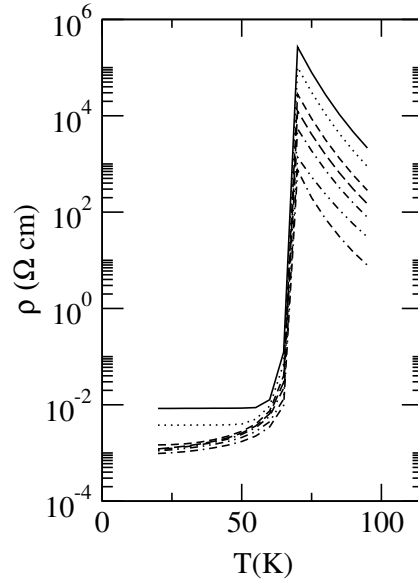


Figure 7.6: Calculated resistivity in dependence on temperature for the same values of impurity concentrations d as in Fig. 7.3. For the other parameters see section 4.1.

electrons per site (see maximum conduction electron concentration $\langle n_i^c \rangle$ in Fig. 7.12) up to the impurity level ϵ_4 , within which the chemical potential lies. The effect of a maximum conduction electron number can disappear if the position of ϵ_4 is dependent on the impurity concentration.

The behavior of the resistivity can be explained by the relative positions of the chemical potential and the lower band edge of the (spin-up) conduction band (see also subsection 6.3.2 and Fig. (6.3) therein). For temperatures well below T_C the chemical potential μ lies within the redshifted conduction band. If the impurity concentration is less than 0.05 % then at low temperatures (e.g. 20 K) the electrons from the uppermost impurity level ϵ_4 are completely emptied into the conduction band. The chemical potential lies well below the impurity level and varies with the impurity concentration d , i.e. the total electron number. This variation of μ for low temperatures (20 K) for d from 0.01 to 0.05 can be seen in Fig. 7.7. For impurity concentrations $d \geq 0.05$ the chemical potential does not vary so much any more because it lies within the impurity “level” (or band), and a maximum number of 0.0008 electrons per Eu site is emptied into the conduction band. Therefore the resistivity saturates for $d \geq 0.05$ (see above). For temperatures at and above T_C the position of the chemical potential is pinned at the upper edge of the uppermost impurity “level” (or band). The bigger the impurity concentration

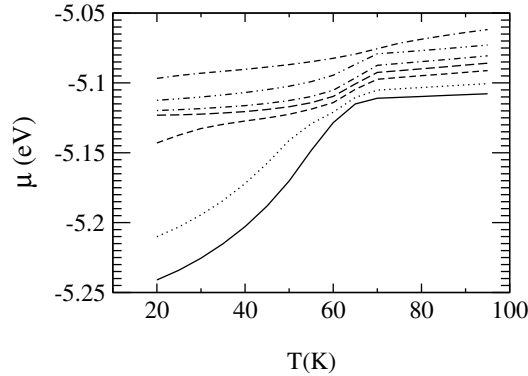


Figure 7.7: Calculated position of the chemical potential in dependence on temperature for the same values of impurity concentrations d as in Fig. 7.3. For the other parameters see section 4.1.

d the broader is the impurity “level”. The closer is therefore the chemical potential to the lower band edge of the conduction band, the bigger is the number of the thermally excited electrons and the lower is the resistivity. A relatively small variation of the position of the chemical potential has a big effect on the resistivity due to the exponential tail of the Fermi function.

7.2.4 Electronic thermal conductivity

In Fig. 7.8 a bunch of curves is shown for the electronic thermal conductivity in dependence on temperature for different impurity concentrations d . All curves show a big jump in the thermal conductivity near the Curie temperature T_C . The lower the impurity concentration the lower the absolute values of the thermal conductivity and the bigger the jump at T_C .

The physical explanation of the jump in the electronic thermal conductivity is similar to the explanation of the jump in the resistivity (see section 6.3). Also the reason for the saturation at low temperatures for high impurity concentrations is similar. At first sight the thermal conductivity looks like the inverse of the resistivity. The quantity which governs the relation between thermal and electrical conductivity is the Wiedemann-Franz ratio $\kappa/(\sigma T)$, which is considered in the next section.

Unfortunately, there are no experimental curves for the electronic thermal conductivity of Eu-rich EuO available. Moreover, it is probably very difficult to separate the electronic (κ) from the lattice contribution (κ_L) to the thermal conductivity. In the insulator the contribution from the lattice should of course dominate. For the semiconductor Germanium it varies between 1 to 15 W/(cm K) in the temperature range from 2 to 200 K [Madelung, 1981,

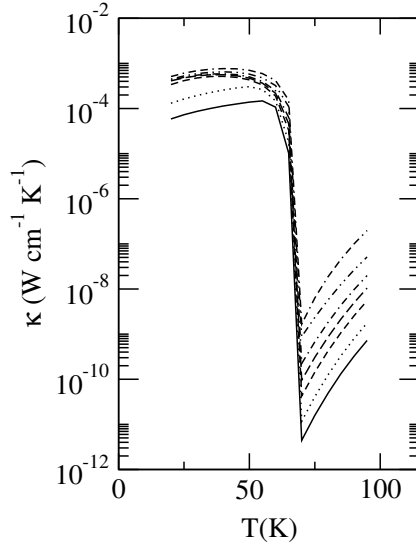


Figure 7.8: Calculated electronic thermal conductivity in dependence on temperature for the same values of impurity concentrations d as in Fig. 7.3. For the other parameters see section 4.1.

Carruthers et al., 1957].

At least for the metallic phase the Wiedemann-Franz ratio gives a good confirmation of the calculated electronic thermal conductivity, see the next section.

7.2.5 Wiedemann-Franz ratio

In Fig. 7.9 the Wiedemann-Franz ratio $\kappa/(\sigma T)$ is shown in dependence on temperature for different impurity concentrations. It is obviously almost the same for all oxygen-vacancy concentrations. For low temperatures, where Eu-rich EuO is a metal, the value of the Wiedemann-Franz ratio is very close to the Lorenz number

$$L = \frac{\pi^2}{3} \left(\frac{k_B}{e} \right)^2 = 2.45 \times 10^{-8} \text{W}\Omega\text{K}^{-2} . \quad (7.18)$$

The Lorenz number is the theoretical value of the Wiedemann-Franz ratio for a free electron gas or a Fermi liquid, respectively. The adoption of that value is called the Wiedemann-Franz law [Ibach and Lüth, 1995]. Hence our calculations confirm that at low temperatures we deal with a metal whose interacting electrons form a Fermi liquid. Above T_C the Wiedemann-Franz ratio takes on a different value of about $1.7 \times 10^{-8} \text{W}\Omega\text{K}^{-2}$ showing that in

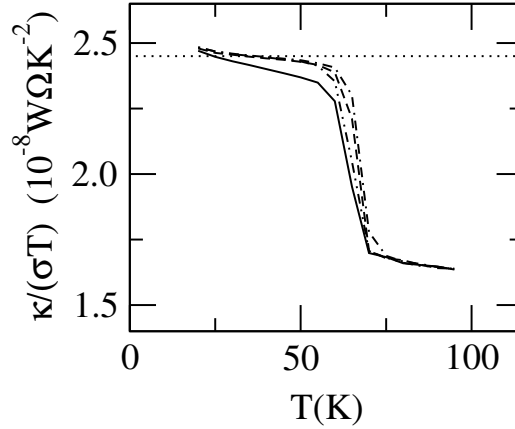


Figure 7.9: Calculated Wiedemann-Franz ratio in dependence on temperature for different impurity concentrations d (— 0.01%, - - - 0.05%, --- 0.5%, - · - 5%). For the other parameters see section 4.1. The dotted line is the theoretical Lorenz number for Fermi liquids $L = \frac{\pi^2}{3} \left(\frac{k_B}{e}\right)^2 = 2.45 \times 10^{-8} \text{ W}\Omega\text{K}^{-2}$.

the insulating phase the electrons do not form a Fermi liquid. This corresponds to what should be expected for an insulator. Hence the behavior of the Wiedemann-Franz ratio gives a good confirmation of our theory. In particular, it confirms at least for the metallic phase the calculated electronic thermal conductivity, for which there are no experimental data available.

7.2.6 Seebeck coefficient and figure of merit

In Fig. 7.10 the calculated thermopower (or Seebeck coefficient) is shown. As expected from the literature [Mahan et al., 1997] the absolute value of the thermopower is bigger in the insulating than in the metallic phase. However, the jump in thermopower at T_C is much smaller than in resistivity or thermal conductivity. It is just about one order of magnitude. Also the difference between the Seebeck coefficients for different impurity concentrations is not several orders of magnitude like in the resistivity or thermal conductivity but a factor of 1.5 for the parameters chosen. There are not many experiments on the thermopower available possibly because it is difficult to fulfill the condition that during the measurement no particle currents and no gradients of the chemical potential are allowed. There is a measurement by Samokhvalov *et al.* [curve (sample) 2 in Fig. 3 in Ref. [Samokhvalov et al., 1982]] where the thermopower reaches a maximum near T_C of only about $-160 \times 10^{-6} \text{ V/K}$. So obviously, there is a discrepancy here between theory and experiment of

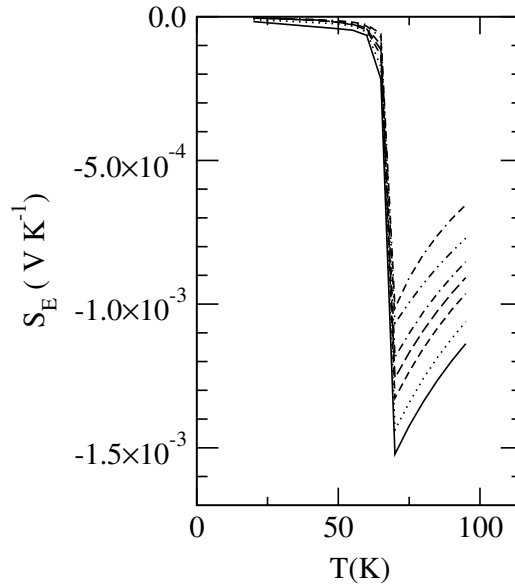


Figure 7.10: Calculated Seebeck coefficient in dependence on temperature for the same values of impurity concentrations d as in Fig. 7.3. For the other parameters see section 4.1.

one order of magnitude. However, we have already seen that there is a big variety of experimental results in the resistivity if one for instance compares the medium-resistivity samples (Fig. 6.2) with the high-resistivity samples (Fig. 6.4). The resistivity of sample 2 in Ref. [Samokhvalov et al., 1982] is with a jump in resistivity of three orders of magnitude in fact a low-resistivity sample. It is indicated by our curves that the lower the resistivity the lower the absolute value of the thermopower. A second point is, as stated, it may be difficult in the experiment to ensure the condition of no particle currents and no gradients of the chemical potential. If a particle current or a gradient of the chemical potential occur, the measured voltage difference for a given temperature difference should be smaller. This might be another reason for the small measured Seebeck coefficient.

There is a second measurement by Samokhvalov *et al.* where in Fig. 2 of Ref. [Samokhvalov et al., 1988] for sample class II a value of -1.8×10^{-3} V/K near T_C can be interpolated. This comes close to our theoretical value of -1.5×10^{-3} V/K. However, it is not clear whether the experimental curve belongs to EuO_{1-d} , $\text{Eu}_{1-x}\text{Gd}_x\text{O}$ or $\text{Eu}_{1-x}\text{Sm}_x\text{O}$. So it is ambiguous to describe that experimental result as a clear confirmation of our theory.

In Fig. 7.11 the calculated dimensionless figure of merit without the lattice

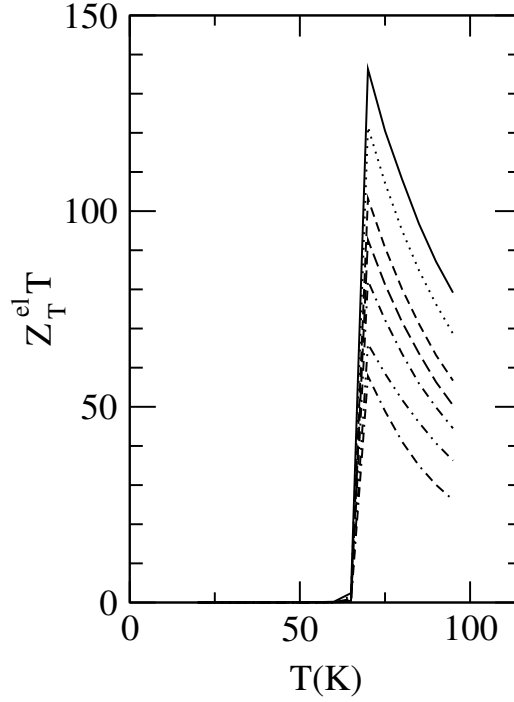


Figure 7.11: Calculated dimensionless figure of merit without the lattice contribution to the thermal conductivity. The values of the impurity concentrations d are the same as in Fig. 7.3. For the other parameters see section 4.1.

contribution of the thermal conductivity is shown, i.e. the quantity

$$Z_T^{\text{el}}T = \frac{S_E^2 \sigma T}{\kappa} \quad (7.19)$$

with κ being the pure electronic thermal conductivity. Therefore, this quantity is actually not so meaningful. It just says something about the thermoelectric efficiency if lattice effects played no role. The pure electronic efficiency is very high above the Curie temperature. However, it is not possible to switch off the phonons and the lattice effects. Without them $Z_T^{\text{el}}T$ is actually S_E^2 divided by the Wiedemann-Franz ratio $\kappa/(\sigma T)$. Since the latter is of the same order of magnitude in the whole temperature range (see Fig. 7.9), it is the Seebeck coefficient, which decisively influences the pure electronic dimensionless figure of merit. We have not found a value for the lattice thermal conductivity for Eu-rich EuO in the literature. For the purpose of an estimate the values of the semiconductor Germanium are considered, which reach values between 1 to 15 W/(cm K) in the temperature range from 2 to 200 K [Madelung, 1981, Carruthers et al., 1957]. This is much larger than

the minimum value for the electronic thermal conductivity in Fig. 7.8 of 10^{-11} W/(cm K). According to this, drastic changes of the order of 10^{-11} in the dimensionless figure of merit would occur if also the lattice contribution to the thermal conductivity were taken into account.

7.2.7 Conduction electron number and scattering time

7.2.7.1 Total conduction electron number and average scattering time

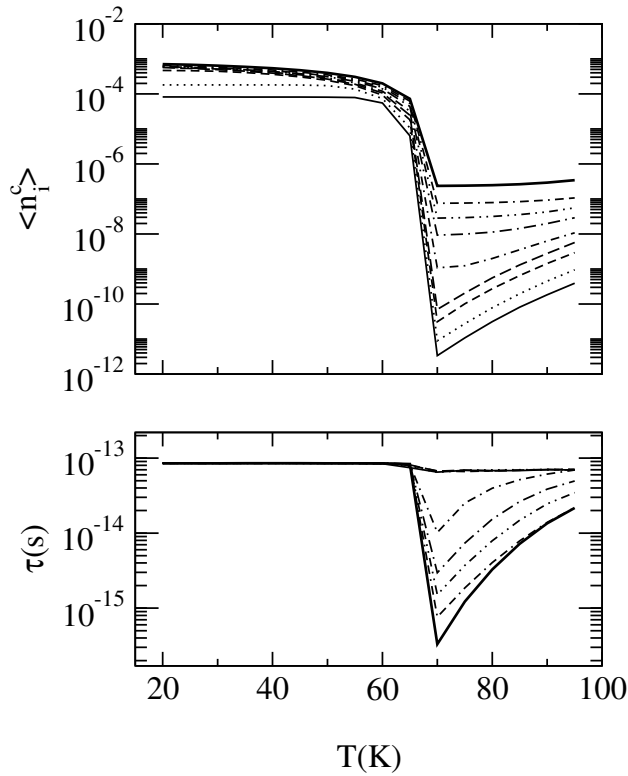


Figure 7.12: Average conduction electron number per Eu atom (upper panel) and average scattering time of the conduction electrons (lower panel) in dependence on temperature for different impurity concentrations d (— 0.01%, \cdots 0.02%, - - 0.05%, - - 0.1%, - - 0.2%, - - 0.5%, \cdots 1%, \cdots 2%, — 5%). For the other parameters see section 4.1.

Fig. 7.12 shows the average conduction electron number per Eu atom $\langle n_i^c \rangle$ and the scattering time τ in dependence on temperature. Both the electron number and the scattering time follow directly from the theory by

$\langle n_i^c \rangle = \int_{-\infty}^{+\infty} dE \left(-\frac{1}{\pi}\right) f(E) \text{Im}[G_{0\uparrow c}(E) + G_{0\downarrow c}(E)]$ and the Drude law $\sigma = n_c e \mu$, where n_c is the electron number per unit volume ($n_c = 4\langle n_i^c \rangle / a^3$) and μ the mobility ($\mu = \frac{e}{m} \tau$ with τ the scattering time).

As we mentioned earlier, the conduction electron number saturates for high impurity concentrations for a given position of the uppermost impurity level since the conduction band can only absorb electrons up to the impurity level within which the chemical potential lies. The saturation of the electron number is about 0.0008 electrons per Eu atom. Then there is a big jump of the conduction electron number at T_C since the conduction band moves upward away from the uppermost impurity level ϵ_4 . This jump amounts up to seven orders of magnitude for low impurity concentrations.

The scattering time shows an interesting behavior in dependence on the impurity concentration. For low concentrations of up to 0.1% it is almost constant in dependence on temperature at a value of 7.5×10^{-14} s. For higher concentrations it shows a jump of up to more than two orders of magnitude. This behavior corresponds to what is observed in low-resistivity materials [Oliver et al., 1972]. But the question is: What does the sudden jump in mobility result from and why does it only happen for higher impurity concentrations? The answer can be found by inspecting the conduction-electron density of states.

7.2.7.2 Conduction-electron density of states and contributions to the conduction electron number and the conductivity

Due to the hybridization there is a certain “hybridized” part of the conduction-electron density of states at the position of the uppermost impurity level, which can be seen as a small resonance in the uppermost part of Fig. 7.13. Apart from a constant factor, the negative imaginary part of the local Green’s function corresponds to the conduction-electron density of states. The resonance is small for low impurity concentrations but becomes relatively big for high oxygen vacancy concentrations. We will call the electrons filling up that “hybridized” part of the conduction-electron density of states “hybridized conduction electrons” although this term is not absolutely correct since all conduction electrons are hybridized more or less with the impurity electrons. For impurity concentrations higher than about 0.2 % and for temperatures at and above T_C the “hybridized” part contributes more conduction electrons than the “unhybridized” part of the conduction band, i.e. there are more “hybridized” than “unhybridized” conduction electrons. This is shown in the middle panel of Fig. 7.13 by the quantity $-f(E) \text{Im}G_{0\sigma c}(E)$ for $d = 5$ % at $T = 70$ K. The upper (“unhybridized”) part of the conduction band is multiplied by the high-energy tail of the Fermi function, which is

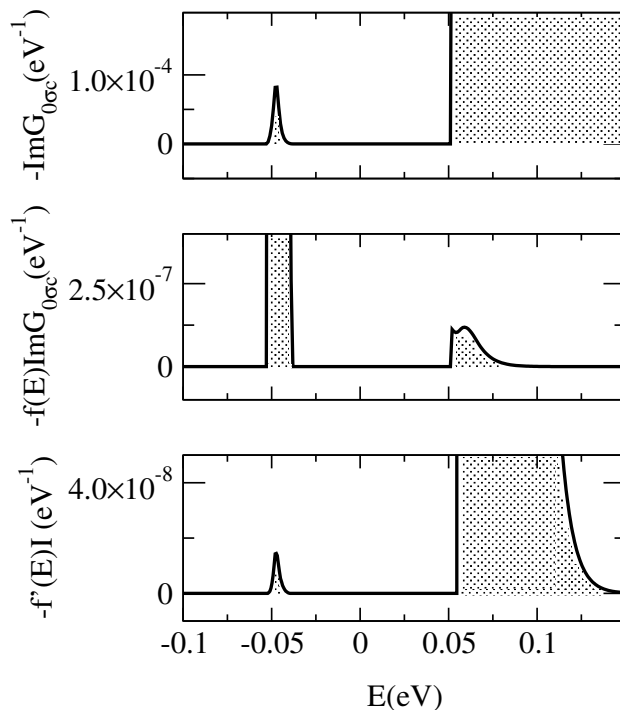


Figure 7.13: Upper panel: negative imaginary part of the on-site conduction electron Green's function. Middle panel: product of Fermi function and function of the upper panel. Lower panel: negative product of the derivative of the Fermi function and integral $I(E)$ as defined in the text. The impurity concentration is $d = 5\%$, the temperature is $T = 70$ K. For the other parameters see Sec. 4.1.

very small, whereas the “hybridized” part is multiplied by almost a factor of one. The shaded area under the curve corresponds to the number of conduction electrons which stem from the respective energy range. However, the contribution of the “hybridized” part to the conductivity is much smaller than from the “unhybridized” part, which is demonstrated by the quantity $-f'(E) \int_{-\infty}^{+\infty} \left[-\frac{1}{\pi} \text{Im}G_{\vec{k}\sigma c}(E)_{\epsilon_{\vec{k}} \rightarrow x} \right]^2 \hat{v}(x) dx = -f'(E)I(E)$ shown in the lower panel of Fig. 7.13. Here the factor is the derivative of the Fermi function, whose energy tails give the same contribution below and above zero energy. The shaded area under the curve corresponds to the contribution to the conductivity from the respective energy ranges. The inspection of the function $-f'(E)I(E)$ in Fig. 7.13 also leads to the reason why the hybridization V needs to be fairly small (as mentioned in section 4.1) to reproduce correctly the big metal-insulator transition. If the “hybridized” part of the conduction band were too big then its contribution to the conductivity would be large

even at temperatures at and above T_C and the jump in resistivity would not be as pronounced as it is with a small value of the hybridization. However, for the given hybridization and for impurity concentrations higher than 0.2 %, the “hybridized” part of the conduction-electron density of states gives relatively many electrons which contribute relatively little to the conductivity. Therefore, these “hybridized” conduction electrons have a fairly low mobility and scattering time.

It is an advantage of our theory that the resistivity is calculated by a different formula than the Drude formula $\sigma = n_c e \mu$ because we do not have to make assumptions on the mobility but we can determine the mobility after we have calculated both the resistivity and the conduction electron number. It turns out in our theory that the conductivity and the jump at T_C are not simply determined by the electron number and the jump in the electron number, respectively, but also by the mobility and the jump in the mobility at least for impurity concentrations greater than 0.2 %.

7.2.7.3 “Unhybridized” conduction electrons and specific scattering time

If one just considers the electrons from the “unhybridized” part of the conduction band, the picture changes drastically and one has an almost constant specific mobility and scattering time over the whole temperature range. In the upper part of Fig. 7.14 the conduction electron number from the upper (“unhybridized”) part of the conduction band is shown. For impurity concentrations of 5 % down to 0.2 % and for temperatures above T_C the electron number from the “unhybridized” part of the conduction band is significantly less than the overall electron number shown in Fig. 7.12. As can be seen from the lower part of Fig. 7.14 the electrons from the upper (“unhybridized”) part of the conduction band have an almost constant mobility or scattering time τ_2 over the whole temperature range. It is, however, a bit less above than it is below T_C , because of spin-disorder scattering which is more pronounced above T_C . Nevertheless, the jump in the average mobility (scattering time) shown in the lower part of Fig. 7.12 results mainly from those conduction electrons which are strongly hybridized with the impurity electrons.

7.2.8 Impurity electron number

In Fig. 7.15 we show the impurity electron number per Eu atom in dependence on temperature for the same impurity concentrations as in Fig. 7.12. *A priori* the impurity concentration corresponds to the impurity electron number, since each impurity (oxygen vacancy site) contributes two electrons

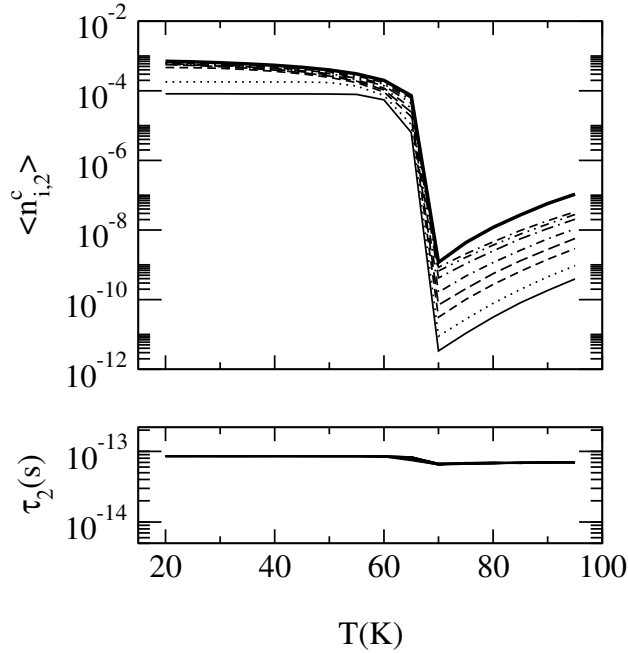


Figure 7.14: “Unhybridized” conduction electron number per Eu atom (upper panel) and specific scattering time of the “unhybridized” conduction electrons (lower panel) in dependence on temperature for the same impurity concentrations d as in Fig. 7.12. For the other parameters see section 4.1.

to the system. We have stated in subsection 6.3.2 that there are three impurity levels with finite weight out of four. The most decisive one is the uppermost level ϵ_4 because it can cross the bottom of the spin-up conduction band above a certain temperature near T_C and empty its electrons into the conduction band. Therefore, below T_C the impurity electron number per Eu atom is smaller than two times the impurity concentration. This effect is most pronounced for low impurity concentrations from 0.01 % up to about 0.05 % because then all electrons from ϵ_4 empty into the conduction band. Of course, this does not mean that there are no impurity electrons left since there are still two impurity levels below the chemical potential. As mentioned in subsections 7.2.1 and 7.2.3 the position of the uppermost impurity level ϵ_4 is such that the conduction band can absorb only a maximum 0.0008 electrons before the chemical potential is pinned to the impurity level. Therefore, the impurity electron number can be reduced at most by 0.0008 which is less and less significant as the impurity concentration is increased. That is why the impurity electron number is almost constant in dependence on the temperature for impurity concentrations higher than 0.5 %. This is closely related

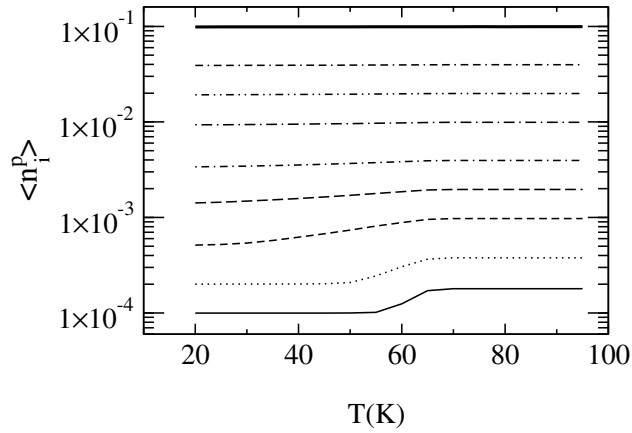


Figure 7.15: Impurity electron number per Eu atom in dependence on temperature for the same impurity concentrations d as in Fig. 7.12. For the other parameters see section 4.1.

to the fact that the effective exchange integral $J_{01p}^{(2)}$, which arises from the exchange of the impurity electrons with the Eu spins, is practically constant for high impurity concentrations d (see Fig. 7.4).

Chapter 8

Summary and outlook

We have presented a microscopic model Hamiltonian (4.8) for Eu-rich EuO and solved it with a Green's function technique. The heart of the model is the Kondo lattice model. We have added an exact statement about the KLM to the known ones, namely the rigorous mapping of the l -fold degenerate periodic Anderson model in the extended Kondo limit (with spin constraint) on the Kondo lattice model for spin $S = \frac{l}{2}$. One more or less immediate consequence which we have derived is that the antiferromagnetic spin- $\frac{1}{2}$ KLM has a large Fermi volume including the number of localized spins. Based on the exact mapping each method or result for the periodic Anderson model which is compatible with the extended Kondo limit can be translated into a method or result for the Kondo lattice model.

Since the huge metal-insulator transition is the most prominent feature of Eu-rich EuO, we were mainly interested in the theoretical modeling of the transport properties of this substance. First, we derived the current-density operator for our model. It turned out to be the same as in the Hubbard model for local selfenergies, which enabled us to use the same transport functions [Eq. (5.31)]. For those the spectral density $A_{\vec{k}\sigma}(E)$ had to be obtained. To achieve this, we used an effective medium approach. The conduction-electron selfenergy was taken from an interpolating ansatz, which fulfills all known limiting cases for $n_c \rightarrow 0$. The impurity self-energies were taken from the corresponding atomic limits. The connection between the two subsystems — conduction and impurity electrons — is given by the hybridization V . We applied a CPA to account for the random distribution of the oxygen vacancy sites.

We achieved quite good fits to experimental curves of medium resistivity already in the not fully self-consistent theory, where the magnetization of the Eu spins, $\langle S^z \rangle$, is taken as an external parameter from a Brillouin function. We do not claim that the impurity concentrations we got as fit parameters

exactly correspond to the experimental ones. It is very likely that the distribution of impurity concentrations for the medium-resistivity samples is not as big as suggested by our fits since we assumed a constant position of the uppermost impurity level independent on the impurity concentration. On the contrary it is very probable that there is a downward shift of the impurity levels with decreasing impurity concentration as we can conclude from our fit with a high-resistivity sample (Fig. 6.4). We achieved a very good fit to the high-resistivity sample with a low-temperature minimum on the assumption that the uppermost impurity level stays below the lower conduction band edge even for low temperatures, i.e. at the maximum redshift. We also calculated the resistivity in a magnetic field and the magnetoresistance. It was possible to interpret the results in a straightforward manner.

In the fully self-consistent calculations the exchange of the conduction and the impurity electrons with the Eu spins and the exchange among the Eu spins was taken into account. For this we applied a modified RKKY theory which yields for the mentioned types of exchange an effective Heisenberg model with effective, temperature- and occupation-dependent exchange integrals. The difference to the Brillouin function is noticeable. The difference to the pure Heisenberg model is minor since the conduction and impurity electron numbers are small. It turns out that the fully self-consistent Curie temperature does not differ within 1 mK from the pure Heisenberg model. This coincides with the experimental fact that the Curie temperature of pure EuO is practically the same as in the Eu-rich samples as long as no other additional impurities like Gd or La are in the material.

Within the fully self-consistent calculations various transport quantities have been determined. Very good fits to the measured resistivity have been achieved for medium-resistivity samples (Fig. 7.5). However, as in the non-self-consistent case the numbers of the theoretical impurity concentrations cannot be taken too seriously as we have not considered a possible variation of the uppermost impurity level with the impurity concentration. In any case the resistivity behavior in dependence on the impurity concentration can be explained by the relative position of the chemical potential with respect to the lower conduction band edge. Especially at temperatures above T_C when the uppermost impurity “level” or band is definitely below the lower conduction band edge then the higher the impurity concentration the broader the impurity “level” or band, the closer the chemical potential to the conduction band edge, the more electrons are excited into the conduction band and the lower the resistivity. This is the mechanism behind the different resistivities for different impurity concentrations at temperatures above T_C in a picture of constant impurity level positions, which are independent on the impurity concentration.

We have also calculated the electronic thermal conductivity for the same parameters as the electrical resistivity. It also shows a big jump of several orders of magnitude. The Wiedemann-Franz ratio between the electrical conductivity and the electronic thermal conductivity below T_C (when Eu-rich EuO is a metal) is very close to the theoretical Lorenz number for a free Fermi gas or a Fermi liquid, respectively. So we expect the conduction electrons in Eu-rich EuO to form a Fermi liquid in the metallic phase below T_C . For temperatures above T_C when the material is insulating the Wiedemann-Franz ratio deviates from the Lorenz number, showing that EuO_{1-d} can no longer be described as a Fermi liquid.

The Seebeck coefficient also shows a jump but not over several but only over about one order of magnitude. There is an experimental measurement which differs by one order of magnitude from the theoretical values [Samokhvalov et al., 1982]. There is another measurement [Samokhvalov et al., 1988] whose interpolation fits quite well to the theoretical curve but where the nature of the actual measured sample is not quite clear.

It is an advantage of our theory that the conductivity is calculated independently on the conduction electron number and the mobility. The conduction electron number can also be calculated within our theory. The mobility (or the scattering time) follows then from the Drude formula if one assumes a certain value of the effective electron mass¹. We have seen that the conduction electron number also has a jump of several orders of magnitude near the Curie temperature. However, especially for higher impurity concentrations it is not as big as the jump in conductivity. The bigger jump in conductivity is achieved by an additional jump in the average mobility or scattering time, which are lower at and above than they are below T_C . We have explained this effect by the fact that for higher impurity concentrations there are relatively many “hybridized” conduction electrons, which contribute relatively little to the conductivity and, hence, decrease the average scattering time. If one looks separately at the “non-hybridized” electrons, the specific scattering time of those stays almost constant over the whole temperature range.

Concluding one should say that an accurate experimental investigation of the dependence of the resistivity and the other transport quantities on the impurity concentration is still missing. This makes at the moment e.g. a comparison of the theoretical and experimental resistivity curves with respect to the impurity concentration impossible. Also reliable measurements, for instance photoemission, of the impurity density of states (impurity “levels” or bands) is still missing. It would be interesting to study the position

¹Usually the effective electron mass is set equal to the bare electron mass.

of the uppermost impurity level in dependence on the oxygen vacancy concentration since this is a decisive parameter as we have seen. There could be a distribution of impurity levels as suggested by Steeneken [Steeneken, 2002] but one has to state that it would be difficult to incorporate a continuum of impurity levels into our CPA scheme. Then one should try to incorporate several “uppermost” impurity levels but at least for temperatures above T_C this should make no difference since the electrons are excited into the conduction band from the true uppermost level, to which the chemical potential is pinned. Furthermore it would be nice to have some data on the electronic thermal conductivity available although it might be difficult to separate experimentally the electronic from the lattice thermal conductivity. Last but not least more measurements on the Seebeck coefficient should be performed.

How could the calculations be improved apart from the inclusion of several impurity levels ϵ_4 or from a special assumption on the dependence of one impurity level on the impurity concentration? The most obvious point would be to try to include first-principles calculations of the $5d$ conduction band of EuO. As shown by Schiller [Schiller, 2000] the interesting lowest parts of the conduction band are the three $5d_{t_{2g}}$ bands (the lower band edges of the two $5d_{e_g}$ are 4 eV higher). But apart from a factor of three we do not expect much changes e.g. in the resistivity.

In the fully self-consistent calculations one could include more than just the nearest-neighbor effective exchange interactions, on which we concentrated for reasons of simplicity. The effective exchange interaction is in fact known to be a long-range interaction. However, as the experience shows [Santos, 2004], we have probably calculated an upper bound of the fully self-consistent effect of the exchange of the conduction and the impurity electrons with the Eu spins.

Furthermore, one could think of improving the applied Green’s function method, where we have chosen an effective medium approach with independent ansatzes for the conduction-electron and impurity-electron self-energies although this might turn out to be difficult because of the high complexity of the model.

Appendix A

Calculations for the proof of the large Fermi volume

We first present the calculation which leads from Eq. (3.74) to Eq. (3.76). For this we use a representation of the Heaviside step function θ :

$$\theta(x) = -\frac{1}{\pi} \text{Im} \ln(-x - i0^+) . \quad (\text{A.1})$$

We need several transformations to achieve our aim. Equation (3.74) states

$$V_{\text{F}} = 2 \sum_{\vec{k}} \theta(\mu - \eta_{\vec{k}}^q) . \quad (\text{A.2})$$

$\eta_{\vec{k}}^q$ ($q = 1, 2$) are the eigenvalues of the matrix (3.75).

$$V_F = 2 \sum_{q\vec{k}} \left(-\frac{1}{\pi} \right) \text{Im} \ln \left(\eta_{\vec{k}}^q - \mu - i0^+ \right) \quad (\text{A.3})$$

$$= 2 \sum_{\vec{k}} \left(-\frac{1}{\pi} \right) \text{Im} \text{tr} \ln \begin{pmatrix} \epsilon_{\vec{k}} - \mu - i0^+ & \sqrt{N}V_{\vec{k}} \\ \sqrt{N}V_{\vec{k}}^* & \epsilon_f + \Sigma_{\vec{k}}(0) - \mu - i0^+ \end{pmatrix} \quad (\text{A.4})$$

$$= 2 \sum_{\vec{k}} \left(-\frac{1}{\pi} \right) \text{Im} \ln \det \underbrace{\begin{pmatrix} \epsilon_{\vec{k}} - \mu - i0^+ & \sqrt{N}V_{\vec{k}} \\ \sqrt{N}V_{\vec{k}}^* & \epsilon_f + \Sigma_{\vec{k}}(0) - \mu - i0^+ \end{pmatrix}}_{(\epsilon_{\vec{k}} - \mu - i0^+) \left(\epsilon_f + \Sigma_{\vec{k}}(0) + \frac{N|V_{\vec{k}}|^2}{\mu - \epsilon_{\vec{k}} + i0^+} - \mu - i0^+ \right)} \quad (\text{A.5})$$

$$= 2 \sum_{\vec{k}} \left(-\frac{1}{\pi} \right) \text{Im} \left[\ln (\epsilon_{\vec{k}} - \mu - i0^+) \right. \quad (\text{A.6})$$

$$\left. + \ln \left(\epsilon_f + \Sigma_{\vec{k}}(0) + \frac{N|V_{\vec{k}}|^2}{\mu - \epsilon_{\vec{k}} + i0^+} - \mu - i0^+ \right) \right] \quad (\text{A.7})$$

$$= 2 \sum_{\vec{k}} \left[\theta (\mu - \epsilon_{\vec{k}}) + \theta \left(\alpha_{\vec{k}} - \frac{N|V_{\vec{k}}|^2}{(\mu - \epsilon_{\vec{k}})} \right) \right] \quad (\text{A.8})$$

$$\text{with } \alpha_{\vec{k}} = \mu - \epsilon_f - \Sigma_{\vec{k}}(0). \quad (\text{A.9})$$

Equations (A.8) and (A.9) correspond to Eqs. (3.76) and (3.77).

Now we show how one gets from Eq. (3.76) to Eq. (3.82). We have to evaluate the r.h.s. of (A.8) for each \vec{k} point.

$$V_F = 2 \sum_{\vec{k}} V_{F,\vec{k}} \quad (\text{A.10})$$

$$V_{F,\vec{k}} = \theta (\mu - \epsilon_{\vec{k}}) + \theta \left(\alpha_{\vec{k}} - \frac{N|V_{\vec{k}}|^2}{(\mu - \epsilon_{\vec{k}})} \right) \stackrel{(3.81)}{=} \theta (\mu - \epsilon_{\vec{k}}) + \theta \left(\frac{N|V_{\vec{k}}|^2}{\Sigma_{s,\vec{k}}(0)} - \frac{N|V_{\vec{k}}|^2}{(\mu - \epsilon_{\vec{k}})} \right) \quad (\text{A.11})$$

$$= \theta (\mu - \epsilon_{\vec{k}}) + \theta \left(\frac{1}{\Sigma_{s,\vec{k}}(0)} - \frac{1}{(\mu - \epsilon_{\vec{k}})} \right) \quad (\text{A.12})$$

We evaluate the second θ function:

$$\theta_{2,\vec{k}} = \theta \left(\frac{1}{\Sigma_{s,\vec{k}}(0)} - \frac{1}{(\mu - \epsilon_{\vec{k}})} \right) \quad (\text{A.13})$$

$$= \begin{cases} 1 & \left\{ \begin{array}{l} \text{if } \mu - \epsilon_{\vec{k}} > \Sigma_{s,\vec{k}}(0) \text{ and } \text{sign}(\mu - \epsilon_{\vec{k}})\text{sign}(\Sigma_{s,\vec{k}}(0)) = 1 \\ \text{or } \mu - \epsilon_{\vec{k}} < \Sigma_{s,\vec{k}}(0) \text{ and } \text{sign}(\mu - \epsilon_{\vec{k}})\text{sign}(\Sigma_{s,\vec{k}}(0)) = -1 \end{array} \right. \\ 0 & \left\{ \begin{array}{l} \text{if } \mu - \epsilon_{\vec{k}} < \Sigma_{s,\vec{k}}(0) \text{ and } \text{sign}(\mu - \epsilon_{\vec{k}})\text{sign}(\Sigma_{s,\vec{k}}(0)) = 1 \\ \text{or } \mu - \epsilon_{\vec{k}} > \Sigma_{s,\vec{k}}(0) \text{ and } \text{sign}(\mu - \epsilon_{\vec{k}})\text{sign}(\Sigma_{s,\vec{k}}(0)) = -1 \end{array} \right. \end{cases} \quad (\text{A.14})$$

$$V_{\text{F},\vec{k}} = \theta(\mu - \epsilon_{\vec{k}}) + \theta_{2,\vec{k}} \quad (\text{A.15})$$

As one can immediately see from Eq. (A.11), for each \vec{k}

$$\text{with } \underline{\alpha_{\vec{k}} = 0} \text{ we have a contribution of } \underline{V_{\text{F},\vec{k}} = 1}. \quad (\text{A.16})$$

Now we have to distinguish $\alpha_{\vec{k}} < 0$ and $\alpha_{\vec{k}} > 0$:

$$\underline{\alpha_{\vec{k}} < 0} \Rightarrow \Sigma_{s,\vec{k}}(0) < 0 \quad (\text{A.17})$$

$$(\mu - \epsilon_{\vec{k}}) > 0 \quad (\text{A.18})$$

$$\Rightarrow \theta_{2,\vec{k}} = 0 \Rightarrow \underline{V_{\text{F},\vec{k}} = \theta(\mu - \epsilon_{\vec{k}} - \Sigma_{s,\vec{k}}(0))} = 1 \quad (\text{A.19})$$

$$(\mu - \epsilon_{\vec{k}}) < 0 \quad (\text{A.20})$$

$$\Rightarrow \theta_{2,\vec{k}} = \begin{cases} 1 & \text{if } \mu - \epsilon_{\vec{k}} > \Sigma_{s,\vec{k}}(0) \Rightarrow \underline{V_{\text{F},\vec{k}} = \theta(\mu - \epsilon_{\vec{k}} - \Sigma_{s,\vec{k}}(0))} = 1 \\ 0 & \text{if } \mu - \epsilon_{\vec{k}} < \Sigma_{s,\vec{k}}(0) \Rightarrow \underline{V_{\text{F},\vec{k}} = \theta(\mu - \epsilon_{\vec{k}} - \Sigma_{s,\vec{k}}(0))} = 0 \end{cases} \quad (\text{A.21})$$

$$\underline{\alpha_{\vec{k}} > 0} \Rightarrow \Sigma_{s,\vec{k}}(0) > 0 \quad (\text{A.22})$$

$$(\mu - \epsilon_{\vec{k}}) > 0 \quad (\text{A.23})$$

$$\Rightarrow \theta_{2,\vec{k}} = \begin{cases} 1 & \text{if } \mu - \epsilon_{\vec{k}} > \Sigma_{s,\vec{k}}(0) \Rightarrow \underline{V_{\text{F},\vec{k}} = 1 + \theta(\mu - \epsilon_{\vec{k}} - \Sigma_{s,\vec{k}}(0))} = 2 \\ 0 & \text{if } \mu - \epsilon_{\vec{k}} < \Sigma_{s,\vec{k}}(0) \Rightarrow \underline{V_{\text{F},\vec{k}} = 1 + \theta(\mu - \epsilon_{\vec{k}} - \Sigma_{s,\vec{k}}(0))} = 1 \end{cases} \quad (\text{A.24})$$

$$(\mu - \epsilon_{\vec{k}}) < 0 \quad (\text{A.25})$$

$$\Rightarrow \theta_{2,\vec{k}} = 1 \Rightarrow \underline{V_{\text{F},\vec{k}} = 1 + \theta(\mu - \epsilon_{\vec{k}} - \Sigma_{s,\vec{k}}(0))} = 1 \quad (\text{A.26})$$

With Eqs. (A.16)–(A.26) we have proven Eq. (3.82).

Appendix B

Calculation of the commutators for the current density operator

In this appendix we show how one gets from Eq. (5.10) to Eq. (5.30) with the density operator given by (5.28) or (5.29). For this we have to evaluate a couple of commutators. First we check the commutators of the conduction electron part of $\rho(\vec{q})$ with the conduction electron parts in the Hamiltonian (4.8).

$$\left[\sum_{\vec{k}\sigma} c_{\vec{k}-\vec{q}\sigma}^\dagger c_{\vec{k}\sigma}, \sum_{\vec{k}'\sigma'} \epsilon_{\vec{k}'} c_{\vec{k}'\sigma'}^\dagger c_{\vec{k}'\sigma'} \right] = \sum_{\vec{k}\sigma} (\epsilon_{\vec{k}} c_{\vec{k}-\vec{q}\sigma}^\dagger c_{\vec{k}\sigma} - \epsilon_{\vec{k}-\vec{q}} c_{\vec{k}-\vec{q}\sigma}^\dagger c_{\vec{k}\sigma}) \quad (\text{B.1})$$

Next we evaluate the commutator which comes from the Ising term of the spin-spin exchange part of the Hamiltonian.

$$\left[\sum_{i\sigma} e^{-i\vec{q}\vec{R}_i} n_{i\sigma}^c, -\frac{J}{2} \sum_{i'\sigma'} z_{\sigma'} S_{i'}^z n_{i'\sigma'} \right] = 0 \quad (\text{B.2})$$

Now we check the commutator with the spin-flip part of the spin exchange Hamiltonian, where the following terms appear:

$$\begin{aligned} \sum_{ii'\sigma\sigma'} \left[c_{i\sigma}^\dagger c_{i\sigma}, c_{i'\sigma'}^\dagger c_{i'\sigma'} \right] &= \sum_{ii'\sigma\sigma'} \left(c_{i\sigma}^\dagger \delta_{ii'} \delta_{\sigma\sigma'} c_{i-\sigma} - c_{i-\sigma}^\dagger \delta_{ii'} \delta_{\sigma,-\sigma'} c_{i\sigma} \right) \\ &= \sum_{i\sigma} c_{i\sigma}^\dagger c_{i-\sigma} + \sum_{i\sigma} c_{i-\sigma}^\dagger c_{i\sigma} = 0 \end{aligned} \quad (\text{B.3})$$

(B.2) and (B.3) mean that

$$\left[\sum_{\vec{k}\sigma} c_{\vec{k}-\vec{q}\sigma}^\dagger c_{\vec{k}\sigma}, -J \sum_i \vec{S}_i \cdot \vec{\sigma}_i^c \right] = 0 \quad (\text{B.4})$$

Next we check the commutators of the impurity electron part of $\rho(\vec{q})$ with the impurity parts of the Hamiltonian (4.8):

$$\left[\sum_{j\sigma} e^{-i\vec{q}\vec{R}_j} n_{j\sigma}^p, \sum_{j'\sigma'} \epsilon_p n_{j'\sigma'}^p \right] = 0 \quad (\text{B.5})$$

The commutator with the spin-exchange part of the Hamiltonian is calculated in full analogy to Eqs. (B.2) and (B.3), so we have

$$\left[\sum_{j\sigma} e^{-i\vec{q}\vec{R}_j} p_{j\sigma}^\dagger p_{j\sigma}, -J_p \sum_j \vec{S}_j \cdot \vec{\sigma}_j^p \right] = 0. \quad (\text{B.6})$$

Also the commutator with the Hubbard term has to be zero since number operators commute with each other:

$$\left[\sum_{j\sigma} e^{-i\vec{q}\vec{R}_j} n_{j\sigma}^p, U \sum_{j'} n_{j'\uparrow} n_{j'\downarrow} \right] = 0 \quad (\text{B.7})$$

At last we have to check the commutator of the density operator with the hybridization term \mathcal{H}_{pc} .

$$[\rho(\vec{q}), \mathcal{H}_{pc}] \quad (\text{B.8})$$

$$= \left[\sum_{i\sigma} e^{-i\vec{q}\vec{R}_i} c_{i\sigma}^\dagger c_{i\sigma}, V \sum_{j'\sigma'} (p_{j'\sigma'}^\dagger c_{j'\sigma'} + c_{j'\sigma'}^\dagger p_{j'\sigma'}) \right] \quad (\text{B.9})$$

$$+ \left[\sum_{j\sigma} e^{-i\vec{q}\vec{R}_j} p_{j\sigma}^\dagger p_{j\sigma}, V \sum_{j'\sigma'} (p_{j'\sigma'}^\dagger c_{j'\sigma'} + c_{j'\sigma'}^\dagger p_{j'\sigma'}) \right] \quad (\text{B.10})$$

$$= V \sum_{j\sigma} e^{-i\vec{q}\vec{R}_j} (-p_{j\sigma}^\dagger c_{j\sigma} + c_{j\sigma}^\dagger p_{j\sigma}) + V \sum_{j\sigma} e^{-i\vec{q}\vec{R}_j} (p_{j\sigma}^\dagger c_{j\sigma} - c_{j\sigma}^\dagger p_{j\sigma}) \quad (\text{B.11})$$

$$= 0. \quad (\text{B.12})$$

Hence

$$[\mathcal{H}, \rho(\vec{q})] = - \sum_{\vec{k}\sigma} (\epsilon_{\vec{k}} - \epsilon_{\vec{k}-\vec{q}}) c_{\vec{k}-\vec{q}\sigma}^\dagger c_{\vec{k}\sigma}. \quad (\text{B.13})$$

If we assume without loss of generality the current to flow and \vec{q} to point into the x direction, in a cubic system we get

$$j = \lim_{\vec{q} \rightarrow 0} \frac{e}{\hbar |\vec{q}|} [\mathcal{H}, \rho(\vec{q})] = - \frac{e}{\hbar} \sum_{\vec{k}\sigma} \frac{\partial \epsilon_{\vec{k}}}{\partial k_x} c_{\vec{k}\sigma}^\dagger c_{\vec{k}\sigma}. \quad (\text{B.14})$$

(B.14) corresponds to Eq. (5.30).

Appendix C

Vanishing of the u - v term in the partial integration of Eq. (5.46)

In this appendix the vanishing of the u - v term in the partial integration of Eq. (5.46) leading to Eq. (5.47) is proven for the nearest-neighbor hopping tight-binding approximation for the cubic lattices. First we show it for the s.c. lattice with the tight-binding dispersion

$$\text{s.c.: } \epsilon_{\vec{k}} = -2t[\cos(ak_x) + \cos(ak_y) + \cos(ak_z)] \quad (\text{C.1})$$

where a is the lattice constant, and $(-t)$ is the nearest-neighbor hopping matrix element $T_{\langle ii'\rangle}$. The s.c. Brillouin zone is a cube with k_x , k_y and k_z ranging from $-\frac{\pi}{a}$ to $+\frac{\pi}{a}$.

$$\text{“}u\text{-}v\text{”} = \frac{V}{(2\pi)^3} \left(- \int_{-\frac{\pi}{a}}^{+\frac{\pi}{a}} \int_{-\frac{\pi}{a}}^{+\frac{\pi}{a}} dk_y dk_z \left(\frac{\partial \epsilon_{\vec{k}}}{\partial k_x} \right) \theta(x - \epsilon_{\vec{k}}) \Big|_{k_x = -\frac{\pi}{a}} \right) \quad (\text{C.2})$$

$$= 0 \quad \text{because} \quad \frac{\partial \epsilon_{\vec{k}}}{\partial k_x} \Big|_{k_x = \pm \frac{\pi}{a}} = 0 \quad (\text{C.3})$$

q.e.d. (s.c.)

For the evaluation of the u - v term of the fcc and bcc lattices we need the

transformation of the \vec{k} vectors on a cube with vectors \vec{x} :

$$\vec{k} = 2\pi \hat{B} \cdot \vec{x} \quad (\text{C.4})$$

$$\vec{x} = \begin{pmatrix} x_1 \\ x_2 \\ x_3 \end{pmatrix} \quad (\text{C.5})$$

$$x_i = \frac{n_i}{N_i}; \quad -\frac{N_i}{2} \leq n_i \leq +\frac{N_i}{2} \quad (\text{C.6})$$

$$-\frac{1}{2} \leq x_i \leq +\frac{1}{2} \quad (\text{C.7})$$

where \hat{B} is a matrix for the corresponding lattice. For fcc it is

$$\hat{B}_{\text{fcc}} = \frac{1}{a} \begin{pmatrix} 1 & -1 & 1 \\ 1 & 1 & -1 \\ -1 & 1 & 1 \end{pmatrix}. \quad (\text{C.8})$$

For bcc it is

$$\hat{B}_{\text{bcc}} = \frac{1}{a} \begin{pmatrix} 1 & 0 & 1 \\ 1 & 1 & 0 \\ 0 & 1 & 1 \end{pmatrix}. \quad (\text{C.9})$$

N_i is the number of unit cells in real space in the i -th direction. n_i is an integer number.

With (C.4) a transformation of variables can be made for the sum or the integral of a \vec{k} -dependent function:

$$\sum_{\vec{k}} f(\vec{k}) = \frac{V}{(2\pi)^3} \int d^3\vec{k} f(\vec{k}) = N \iiint_{-\frac{1}{2}}^{+\frac{1}{2}} d^3\vec{x} f(2\pi \hat{B}\vec{x}) \quad (\text{C.10})$$

We need to evaluate

$$“u-v” = -N \int_{-\frac{1}{2}}^{+\frac{1}{2}} dx_2 dx_3 \underbrace{\left(\frac{\partial \epsilon_{\vec{k}}}{\partial k_x} \right) \Theta(x - \epsilon_{\vec{k}})}_{C} \Big|_{\vec{k}=2\pi \hat{B}\vec{x}} \Big|_{x_1=-\frac{1}{2}}^{+\frac{1}{2}}. \quad (\text{C.11})$$

In (C.11) we have to insert the dispersions for the fcc and the bcc lattices.

For the fcc lattice one has:

$$\begin{aligned} \text{fcc: } \epsilon_{\vec{k}} &= -2t \left[\cos\left(\frac{1}{2}ak_x + \frac{1}{2}ak_y\right) + \cos\left(\frac{1}{2}ak_x - \frac{1}{2}ak_y\right) \right. \\ &\quad + \cos\left(\frac{1}{2}ak_y + \frac{1}{2}ak_z\right) + \cos\left(\frac{1}{2}ak_y - \frac{1}{2}ak_z\right) \\ &\quad \left. + \cos\left(\frac{1}{2}ak_z + \frac{1}{2}ak_x\right) + \cos\left(\frac{1}{2}ak_z - \frac{1}{2}ak_x\right) \right], \end{aligned} \quad (\text{C.12})$$

$$\begin{aligned} &= -4t \left[\cos\left(\frac{1}{2}ak_x\right) \cos\left(\frac{1}{2}ak_y\right) + \cos\left(\frac{1}{2}ak_y\right) \cos\left(\frac{1}{2}ak_z\right) \right. \\ &\quad \left. + \cos\left(\frac{1}{2}ak_x\right) \cos\left(\frac{1}{2}ak_z\right) \right] \end{aligned} \quad (\text{C.13})$$

$$\begin{aligned} \epsilon_{\vec{k}} \Big|_{\vec{k}=2\pi\hat{B}\vec{x}} \Big|_{x_1=\pm\frac{1}{2}} &= -4t \left\{ \cos\left[\pi\left(\frac{1}{2} - x_2 + x_3\right)\right] \cos\left[\pi\left(\frac{1}{2} + x_2 - x_3\right)\right] \right. \\ &\quad + \cos\left[\pi\left(\frac{1}{2} + x_2 - x_3\right)\right] \cos\left[\pi\left(-\frac{1}{2} + x_2 + x_3\right)\right] \\ &\quad \left. + \cos\left[\pi\left(\frac{1}{2} - x_2 + x_3\right)\right] \cos\left[\pi\left(-\frac{1}{2} + x_2 + x_3\right)\right] \right\} \end{aligned} \quad (\text{C.14})$$

$$\begin{aligned} \left(\frac{\partial \epsilon_{\vec{k}}}{\partial k_x} \right) \Big|_{\vec{k}=2\pi\hat{B}\vec{x}} \Big|_{x_1=\pm\frac{1}{2}} &= 2ta \sin\left[\pi\left(\frac{1}{2} - x_2 + x_3\right)\right] \left\{ \cos\left[\pi\left(\frac{1}{2} + x_2 - x_3\right)\right] \right. \\ &\quad \left. + \cos\left[\pi\left(-\frac{1}{2} + x_2 + x_3\right)\right] \right\} \end{aligned} \quad (\text{C.15})$$

From Eqs. (C.14) and (C.15) it follows that C in (C.11) is zero because the terms from the upper boundary and the lower boundary exactly cancel each other and, therefore, the u - v term for the fcc lattice with dispersion (C.13) is zero (q.e.d.).

For the bcc lattice the consideration is similar. We have

$$\begin{aligned} \text{bcc: } \epsilon_{\vec{k}} &= -2t \left[\cos\left(\frac{1}{2}ak_x + \frac{1}{2}ak_y + \frac{1}{2}ak_z\right) + \cos\left(\frac{1}{2}ak_x + \frac{1}{2}ak_y - \frac{1}{2}ak_z\right) \right. \\ &\quad \left. + \cos\left(\frac{1}{2}ak_x - \frac{1}{2}ak_y + \frac{1}{2}ak_z\right) + \cos\left(\frac{1}{2}ak_x - \frac{1}{2}ak_y - \frac{1}{2}ak_z\right) \right], \end{aligned} \quad (\text{C.16})$$

$$= -8t \left[\cos\left(\frac{1}{2}ak_x\right) \cos\left(\frac{1}{2}ak_y\right) \cos\left(\frac{1}{2}ak_z\right) \right] \quad (\text{C.17})$$

$$\epsilon_{\vec{k}} \Big|_{\vec{k}=2\pi\hat{B}\vec{x}} \Big|_{x_1=\pm\frac{1}{2}} = -8t \cos\left[\pi\left(\frac{1}{2} + x_3\right)\right] \cos\left[\pi\left(\frac{1}{2} + x_2\right)\right] \cos\left[\pi(x_2 + x_3)\right] \quad (\text{C.18})$$

$$\left. \left(\frac{\partial \epsilon_{\vec{k}}}{\partial k_x} \right) \right|_{\vec{k}=2\pi\hat{B}\vec{x} \Big|_{x_1=\pm\frac{1}{2}}} = 4ta \sin\left[\pi\left(\frac{1}{2} + x_3\right)\right] \cos\left[\pi\left(\frac{1}{2} + x_2\right)\right] \cos[\pi(x_2 + x_3)] \quad (\text{C.19})$$

Again, Eqs. (C.18) and (C.19) mean that C in (C.11) is zero because the terms from the upper boundary and the lower boundary exactly cancel each other and, therefore, the u - v term for the bcc lattice with dispersion (C.17) is zero (q.e.d.).

Appendix D

Atomic limit self-energies

The atomic-limit self-energy of the correlated Kondo lattice model [$\mathcal{H}_{p,1} + \mathcal{H}_{p,2} + \mathcal{H}_{pf}$, Eqs. (4.3) to (4.5)] is given by the following expression:

$$\Sigma_{\sigma}^{p,1}(E) = \frac{\tilde{E}\tilde{J}[\Sigma_{1,1}(1 - \langle n_{-\sigma}^p \rangle_A) - \Sigma_{1,2}\Sigma_{1,3}\langle n_{-\sigma}^p \rangle_A] + \tilde{J}^2\Sigma_{1,4}\Sigma_{1,2}}{\tilde{E}\Sigma_{2,1} - \tilde{J}[\Sigma_{2,2}\langle n_{-\sigma}^p \rangle_A - (\Sigma_{2,3} + \Sigma_{2,4})(1 - \langle n_{-\sigma}^p \rangle_A)]} \quad (\text{D.1})$$

where

$$\Sigma_{1,1} = [\tilde{E}X_{-\sigma} + \tilde{J}S(S+1)] [\tilde{E} - U - \tilde{J}(1 + Y_{-\sigma})] \quad (\text{D.2})$$

$$\Sigma_{1,2} = (\tilde{E} - U)Y_{-\sigma} - \tilde{J}S(S+1) - \frac{U}{\tilde{J}} [\tilde{E} - U - \tilde{J}(1 + Y_{-\sigma})] \quad (\text{D.3})$$

$$\Sigma_{1,3} = \tilde{E} + \tilde{J}(1 + X_{-\sigma}) \quad (\text{D.4})$$

$$\Sigma_{1,4} = \tilde{E}X_{-\sigma} + \tilde{J}S(S+1) \quad (\text{D.5})$$

$$\Sigma_{2,1} = [\tilde{E} + \tilde{J}(1 + X_{-\sigma})] [\tilde{E} - U - \tilde{J}(1 + Y_{-\sigma})] \quad (\text{D.6})$$

$$\Sigma_{2,2} = [\tilde{J}S(S+1) + \tilde{E}X_{-\sigma}] [\tilde{E} - U - \tilde{J}(1 + Y_{-\sigma})] \quad (\text{D.7})$$

$$\Sigma_{2,3} = [(\tilde{E} - U)Y_{-\sigma} - \tilde{J}S(S+1)] [\tilde{E} + \tilde{J}(1 + X_{-\sigma})] \quad (\text{D.8})$$

$$\Sigma_{2,4} = -\frac{U}{\tilde{J}} [\tilde{E} + \tilde{J}(1 + X_{-\sigma})] [\tilde{E} - U - \tilde{J}(1 + Y_{-\sigma})] \quad (\text{D.9})$$

with

$$\tilde{E} = E + \mu - \epsilon_p + i0^+ \quad (\text{D.10})$$

$$\tilde{J} = -\frac{1}{2}J \quad (\text{D.11})$$

$$X_{-\sigma} = \frac{\Delta_{-\sigma} - z_{-\sigma}\langle S^z \rangle}{1 - \langle n_{-\sigma}^p \rangle_A} \quad (\text{D.12})$$

$$Y_{-\sigma} = \frac{\Delta_{-\sigma}}{\langle n_{-\sigma}^p \rangle_A} \quad (\text{D.13})$$

$$\Delta_{\sigma} = \langle S^{\sigma} p_{-\sigma}^{\dagger} p_{\sigma} \rangle_A + z_{\sigma} \langle S^z n_{\sigma}^p \rangle_A \quad (\text{D.14})$$

$$= \begin{cases} S \left(\frac{\langle n_{\text{tot}}^p \rangle_A}{2} + z_{\sigma} \langle S^z \rangle \frac{\langle n_{\text{tot}}^p \rangle_A}{2(S+1-\langle n_{\text{tot}}^p \rangle_A)} \right) & \text{if } \langle n_{\text{tot}}^p \rangle_A \leq 1, \\ \frac{2-\langle n_{\text{tot}}^p \rangle_A}{2} S + z_{\sigma} \langle S^z \rangle \frac{\langle n_{\text{tot}}^p \rangle_A (S+2)-2}{2(S+\langle n_{\text{tot}}^p \rangle_A-1)} & \text{if } \langle n_{\text{tot}}^p \rangle_A \geq 1 \end{cases} \quad (\text{D.15})$$

$$S = \frac{7}{2} \quad (\text{D.16})$$

$\langle \dots \rangle_A$ is the average at an impurity site, which is independent on the impurity site itself.

$$\langle n_{\text{tot}}^p \rangle_A = \langle n_{\uparrow}^p \rangle_A + \langle n_{\downarrow}^p \rangle_A. \quad (\text{D.17})$$

The atomic limit self-energy of the Hubbard model [Potthoff et al., 1997] is given by

$$\Sigma_{\sigma}^{p,2}(E) = U \langle n_{-\sigma}^p \rangle_A + \frac{U^2 \langle n_{-\sigma}^p \rangle_A (1 - \langle n_{-\sigma}^p \rangle_A)}{E + \mu - \epsilon_p - U(1 - \langle n_{-\sigma}^p \rangle_A)} \quad (\text{D.18})$$

Appendix E

Modified RKKY treatment

The main idea of the modified RKKY theory is to transform the Kondo-like exchange Hamiltonians of the conduction and the impurity electrons with the Eu f spins into a Heisenberg spin-spin exchange Hamiltonian of the f spins. This is achieved by the following steps which closely follow the treatment in Ref. [Nolting et al., 1997, Kienert, 2001]. First the Kondo-like exchange Hamiltonians of the conduction and the impurity electrons¹,

$$\mathcal{H}_{ef} = -\frac{J}{2N} \sum_{i\sigma\sigma'} \sum_{\vec{k}\vec{q}} e^{-i\vec{q}\vec{R}_i} (\vec{S}_i \cdot \hat{\vec{\sigma}})_{\sigma\sigma'} (c_{\vec{k}+\vec{q}\sigma}^\dagger c_{\vec{k}\sigma'} + p_{\vec{k}+\vec{q}\sigma}^\dagger p_{\vec{k}\sigma'}) \quad (\text{E.1})$$

where $\hat{\vec{\sigma}}$ is the vector of the Pauli matrices (which do not contain a factor 1/2), are averaged in the subspace of the conduction and impurity electrons:

$$\mathcal{H}'_{ff} = \langle \mathcal{H}_{ef} \rangle^{(el)} = -\frac{J}{2N} \sum_{i\sigma\sigma'} \sum_{\vec{k}\vec{q}} e^{-i\vec{q}\vec{R}_i} (\vec{S}_i \cdot \hat{\vec{\sigma}})_{\sigma\sigma'} (\langle c_{\vec{k}+\vec{q}\sigma}^\dagger c_{\vec{k}\sigma'} \rangle^{(el)} + \langle p_{\vec{k}+\vec{q}\sigma}^\dagger p_{\vec{k}\sigma'} \rangle^{(el)}) . \quad (\text{E.2})$$

$$= \mathcal{H}'_{ff}^c + \mathcal{H}'_{ff}^p \quad (\text{E.3})$$

The expectation values $\langle c_{\vec{k}+\vec{q}\sigma}^\dagger c_{\vec{k}\sigma'} \rangle^{(el)}$ and $\langle p_{\vec{k}+\vec{q}\sigma}^\dagger p_{\vec{k}\sigma'} \rangle^{(el)}$ still have operator properties in the f spin subspace and therefore do not vanish for $\vec{q} \neq 0$ and $\sigma \neq \sigma'$. We would like to obtain $\langle c_{\vec{k}+\vec{q}\sigma}^\dagger c_{\vec{k}\sigma'} \rangle^{(el)}$ and $\langle p_{\vec{k}+\vec{q}\sigma}^\dagger p_{\vec{k}\sigma'} \rangle^{(el)}$ via the spectral theorem with the help of appropriate Green's functions

$$\hat{G}_{\vec{k},\vec{k}+\vec{q}}^{c\sigma\sigma'}(E) = \langle \langle c_{\vec{k}\sigma}; c_{\vec{k}+\vec{q}\sigma'}^\dagger \rangle \rangle^{(el)} , \quad (\text{E.4})$$

$$\hat{G}_{\vec{k},\vec{k}+\vec{q}}^{p\sigma\sigma'}(E) = \langle \langle p_{\vec{k}\sigma}; p_{\vec{k}+\vec{q}\sigma'}^\dagger \rangle \rangle^{(el)} . \quad (\text{E.5})$$

¹Since within our CPA treatment (Section 6.1) we have introduced p states also at non-impurity sites we can sensibly define the \vec{k} dependent operators $p_{\vec{k}\sigma}^{(\dagger)}$.

Also the Green's functions (E.4) and (E.5) have operator character in the f subspace. Let us first consider the conduction electron part of the Hamiltonian (E.2) and the corresponding Green's functions. The equations of motion read:

$$\begin{aligned} [E - (\epsilon_{\vec{k}} - \mu)] \hat{G}_{\vec{k}, \vec{k}+\vec{q}}^{c\sigma\sigma'}(E) &= \delta_{\vec{q}, \vec{0}} \delta_{\sigma\sigma'} - \frac{J}{2N} \sum_{i\vec{k}'\sigma''} e^{-i(\vec{k}-\vec{k}')\vec{R}_i} (\vec{S}_i \cdot \hat{\sigma})_{\sigma'\sigma''} \hat{G}_{\vec{k}', \vec{k}+\vec{q}}^{c\sigma''\sigma}(E) \\ &+ V \hat{G}_{\vec{k}, \vec{k}+\vec{q}}^{pc\sigma'\sigma}(E) \end{aligned} \quad (\text{E.6})$$

where

$$\hat{G}_{\vec{k}, \vec{k}+\vec{q}}^{pc\sigma'\sigma}(E) = \langle\langle p_{\vec{k}\sigma'}; c_{\vec{k}+\vec{q}\sigma}^\dagger \rangle\rangle^{(el)} \quad (\text{E.7})$$

with

$$[E - \Sigma_{\sigma'}^{\text{CPA},1}(E)] \hat{G}_{\vec{k}, \vec{k}+\vec{q}}^{pc\sigma'\sigma}(E) = V \hat{G}_{\vec{k}, \vec{k}+\vec{q}}^{c\sigma'\sigma}(E) . \quad (\text{E.8})$$

$\Sigma_{\sigma'}^{\text{CPA},1}(E)$ is the CPA self-energy of the impurity electrons as it is known from section 6.1. Hence, the configurational averaging of the Green's function has already been done. From Eqs. (E.6) and (E.8) it follows

$$\begin{aligned} \left[E - (\epsilon_{\vec{k}} - \mu) - \frac{V^2}{E - \Sigma_{\sigma'}^{\text{CPA},1}(E)} \right] \hat{G}_{\vec{k}, \vec{k}+\vec{q}}^{c\sigma'\sigma}(E) &= \delta_{\vec{q}, \vec{0}} \delta_{\sigma\sigma'} - \\ &- \frac{J}{2N} \sum_{i\vec{k}'\sigma''} e^{-i(\vec{k}-\vec{k}')\vec{R}_i} (\vec{S}_i \cdot \hat{\sigma})_{\sigma'\sigma''} \hat{G}_{\vec{k}', \vec{k}+\vec{q}}^{c\sigma''\sigma}(E) . \end{aligned} \quad (\text{E.9})$$

For symmetry reasons we write down the equations of motion for $\hat{G}_{\vec{k}, \vec{k}+\vec{q}}^{c\sigma\sigma'}(E)$ in an alternative way, where the ‘‘second’’ operator in (E.4), $c_{\vec{k}+\vec{q}\sigma'}^\dagger$, is the ‘‘active’’ operator.

$$\begin{aligned} [E - (\epsilon_{\vec{k}+\vec{q}} - \mu)] \hat{G}_{\vec{k}, \vec{k}+\vec{q}}^{c\sigma\sigma'}(E) &= \delta_{\vec{q}, \vec{0}} \delta_{\sigma\sigma'} - \frac{J}{2N} \sum_{i\vec{k}'\sigma''} e^{-i[\vec{k}' - (\vec{k}+\vec{q})]\vec{R}_i} (\vec{S}_i \cdot \hat{\sigma})_{\sigma''\sigma} \hat{G}_{\vec{k}', \vec{k}}^{c\sigma'\sigma''}(E) \\ &+ V \hat{G}_{\vec{k}, \vec{k}+\vec{q}}^{cp\sigma'\sigma}(E) \end{aligned} \quad (\text{E.10})$$

where

$$\hat{G}_{\vec{k}, \vec{k}+\vec{q}}^{cp\sigma'\sigma}(E) = \langle\langle c_{\vec{k}\sigma'}; p_{\vec{k}+\vec{q}\sigma}^\dagger \rangle\rangle^{(el)} \quad (\text{E.11})$$

with

$$[E - \Sigma_{\sigma'}^{\text{CPA},1}(E)] \hat{G}_{\vec{k}, \vec{k}+\vec{q}}^{cp\sigma'\sigma}(E) = V \hat{G}_{\vec{k}, \vec{k}+\vec{q}}^{c\sigma'\sigma}(E) . \quad (\text{E.12})$$

Therefore,

$$\left[E - (\epsilon_{\vec{k}+\vec{q}} - \mu) - \frac{V^2}{E - \Sigma_{\sigma}^{\text{CPA},1}(E)} \right] \hat{G}_{\vec{k},\vec{k}+\vec{q}}^{c\sigma'\sigma}(E) = \delta_{\vec{q},\vec{0}} \delta_{\sigma\sigma'} - \frac{J}{2N} \sum_{i\vec{k}'\sigma''} e^{-i[\vec{k}' - (\vec{k}+\vec{q})]\vec{R}_i} (\vec{S}_i \cdot \hat{\vec{\sigma}})_{\sigma''\sigma} \hat{G}_{\vec{k},\vec{k}'}^{c\sigma'\sigma''}(E). \quad (\text{E.13})$$

If we combine the two equations of motion (E.9) and (E.13) we get:

$$\hat{G}_{\vec{k},\vec{k}+\vec{q}}^{c\sigma'\sigma} = \delta_{\sigma\sigma'} \delta_{\vec{q},\vec{0}} G_{\vec{k}\sigma'c}^{(0)} - \frac{J}{4N} \sum_{i\vec{k}'\sigma''} \left\{ e^{-i(\vec{k}-\vec{k}')\vec{R}_i} G_{\vec{k}\sigma'c}^{(0)} (\vec{S}_i \cdot \hat{\vec{\sigma}})_{\sigma'\sigma''} \hat{G}_{\vec{k}',\vec{k}+\vec{q}}^{c\sigma''\sigma} + e^{-i[\vec{k}' - (\vec{k}+\vec{q})]\vec{R}_i} G_{\vec{k}+\vec{q}\sigma c}^{(0)} (\vec{S}_i \cdot \hat{\vec{\sigma}})_{\sigma''\sigma} \hat{G}_{\vec{k},\vec{k}'}^{c\sigma'\sigma''} \right\} \quad (\text{E.14})$$

with

$$G_{\vec{k}\sigma c}^{(0)} = \frac{1}{E - (\epsilon_{\vec{k}} - \mu) - \frac{V^2}{E - \Sigma_{\sigma}^{\text{CPA},1}(E)}}. \quad (\text{E.15})$$

The crucial approximation of the modified RKKY approach is to replace in Eq. (E.14) the operator Green's functions on the r.h.s. by the simple interacting Green's functions. A replacement by the free Green's functions leads in the simple Kondo lattice model to the correct low- J (i.e. RKKY) behavior. This gives us some confidence that the renormalization by the interacting Green's functions should be a sensible approximation. Hence on the r.h.s. of Eq. (E.14) we replace

$$\hat{G}_{\vec{k}\vec{k}'}^{c\sigma\sigma'} \rightarrow \delta_{\sigma\sigma'} \delta_{\vec{k}\vec{k}'} G_{\vec{k}\sigma c}, \quad (\text{E.16})$$

where $G_{\vec{k}\sigma c}$ is given by (6.15). Applying the spectral theorem we get

$$\begin{aligned}
\langle c_{\vec{k}+\vec{q}\sigma}^\dagger c_{\vec{k}\sigma'} \rangle^{(el)} &= -\frac{1}{\pi} \text{Im} \int_{-\infty}^{+\infty} dE f(E) \hat{G}_{\vec{k}, \vec{k}+\vec{q}}^{c\sigma'\sigma}(E) \quad (\text{E.17}) \\
&= \delta_{\sigma\sigma'} \delta_{\vec{q}\vec{0}} \left(-\frac{1}{\pi} \right) \text{Im} \int_{-\infty}^{+\infty} dE f(E) G_{\vec{k}\sigma'c}^{(0)}(E) \\
&\quad - \frac{J}{4N} \sum_i \left\{ e^{i\vec{q}\vec{R}_i} \left(-\frac{1}{\pi} \right) \text{Im} \int_{-\infty}^{+\infty} dE f(E) G_{\vec{k}\sigma'c}^{(0)}(E) G_{\vec{k}+\vec{q}\sigma c}(E) (\vec{S}_i \cdot \hat{\sigma})_{\sigma'\sigma} \right. \\
&\quad \left. + e^{i\vec{q}\vec{R}_i} \left(-\frac{1}{\pi} \right) \text{Im} \int_{-\infty}^{+\infty} dE f(E) G_{\vec{k}+\vec{q}\sigma c}^{(0)}(E) G_{\vec{k}\sigma'c}(E) (\vec{S}_i \cdot \hat{\sigma})_{\sigma'\sigma} \right\} . \quad (\text{E.18})
\end{aligned}$$

Putting (E.18) into the conduction electron part of Eq. (E.2) yields

$$\mathcal{H}'_{ff}{}^c = -\frac{J}{2} \sum_{i\sigma} (\vec{S}_i \cdot \hat{\sigma})_{\sigma\sigma} \langle n_{\sigma c}^{(0)} \rangle + \frac{J^2}{8N} \sum_{ii'\sigma\sigma'} \sum_{\vec{k}\vec{q}} e^{i\vec{q}(\vec{R}_{i'} - \vec{R}_i)} (\vec{S}_i \cdot \hat{\sigma})_{\sigma\sigma'} (\vec{S}_{i'} \cdot \hat{\sigma})_{\sigma'\sigma} D_{\vec{q}}^{c\sigma\sigma'} \quad (\text{E.19})$$

with

$$\langle n_{\sigma c}^{(0)} \rangle = \frac{1}{N} \sum_{\vec{k}} \int_{-\infty}^{+\infty} \left(-\frac{1}{\pi} \right) f(E) \text{Im} G_{\vec{k}\sigma c}^{(0)}(E) dE , \quad (\text{E.20})$$

$$D_{\vec{q}}^{c\sigma\sigma'} = -\frac{1}{\pi} \text{Im} \int_{-\infty}^{+\infty} dE f(E) \frac{1}{N} \sum_{\vec{k}} A_{\vec{k}, \vec{k}+\vec{q}}^{c\sigma'\sigma}(E) , \quad (\text{E.21})$$

$$A_{\vec{k}, \vec{k}+\vec{q}}^{c\sigma'\sigma}(E) = G_{\vec{k}\sigma'c}^{(0)}(E) G_{\vec{k}+\vec{q}\sigma c}(E) + G_{\vec{k}+\vec{q}\sigma c}^{(0)}(E) G_{\vec{k}\sigma'c}(E) . \quad (\text{E.22})$$

On the r.h.s. of (E.19) we perform the spin summations:

$$-\frac{J}{2} \sum_{i\sigma} (\vec{S}_i \cdot \hat{\sigma})_{\sigma\sigma} \langle n_{\sigma c}^{(0)} \rangle = -\frac{J}{2} \sum_{i\sigma} \left(\langle n_{\uparrow c}^{(0)} \rangle - \langle n_{\downarrow c}^{(0)} \rangle \right) \vec{S}_i^z = -B_{\text{eff},c} \sum_i \vec{S}_i^z, \quad (\text{E.23})$$

$$B_{\text{eff},c} = -\frac{J}{2\pi} \text{Im} \int_{-\infty}^{+\infty} dE f(E) \left(G_{0\uparrow c}^{(0)}(E) - G_{0\downarrow c}^{(0)}(E) \right), \quad (\text{E.24})$$

$$G_{0\sigma c}^{(0)}(E) = \frac{1}{N} \sum_{\vec{k}} G_{\vec{k}\sigma c}^{(0)}, \quad (\text{E.25})$$

$$\begin{aligned} \sum_{\sigma\sigma'} (\vec{S}_i \cdot \hat{\sigma})_{\sigma\sigma'} (\vec{S}_{i'} \cdot \hat{\sigma})_{\sigma'\sigma} D_{\vec{q}}^{c\sigma\sigma'} &= D_{\vec{q}}^{c\uparrow\downarrow} S_i^- S_{i'}^+ + D_{\vec{q}}^{c\downarrow\uparrow} S_i^+ S_{i'}^- + \\ &+ \left(D_{\vec{q}}^{c\uparrow\uparrow} + D_{\vec{q}}^{c\downarrow\downarrow} \right) S_i^z S_{i'}^z. \end{aligned} \quad (\text{E.26})$$

Now we will show that $D_{\vec{q}}^{c\uparrow\downarrow} = D_{\vec{q}}^{c\downarrow\uparrow}$.

$$\sum_{\vec{k}} G_{\vec{k}+\vec{q}-\sigma c}^{(0)}(E) G_{\vec{k}\sigma c}(E) = \sum_{\vec{k}} G_{-(\vec{k}+\vec{q})-\sigma c}^{(0)}(E) G_{\vec{k}\sigma c}(E) \quad (\text{E.27})$$

$$= \sum_{\vec{k}'} G_{\vec{k}'-\sigma c}^{(0)}(E) G_{-(\vec{k}'+\vec{q})\sigma c}(E) \quad (\text{E.28})$$

$$= \sum_{\vec{k}} G_{\vec{k}-\sigma c}^{(0)}(E) G_{(\vec{k}+\vec{q})\sigma c}(E) \quad (\text{E.29})$$

The step from Eq. (E.28) to Eq. (E.29) is justified by inversion symmetry.

$$\sum_{\vec{k}} A_{\vec{k},\vec{k}+\vec{q}}^{c\uparrow\downarrow}(E) = \sum_{\vec{k}} \left[G_{\vec{k}\downarrow c}^{(0)}(E) G_{(\vec{k}+\vec{q})\uparrow c}(E) + G_{\vec{k}+\vec{q}\uparrow c}^{(0)}(E) G_{\vec{k}\downarrow c}(E) \right] \quad (\text{E.30})$$

$$= \sum_{\vec{k}} \left[G_{\vec{k}+\vec{q}\downarrow c}^{(0)}(E) G_{\vec{k}\uparrow c}(E) + G_{\vec{k}\uparrow c}^{(0)}(E) G_{(\vec{k}+\vec{q})\downarrow c}(E) \right] \quad (\text{E.31})$$

$$= \sum_{\vec{k}} A_{\vec{k},\vec{k}+\vec{q}}^{c\downarrow\uparrow}(E) \quad (\text{E.32})$$

From (E.32) and (E.21) it follows immediately that

$$D_{\vec{q}}^{c\uparrow\downarrow} = D_{\vec{q}}^{c\downarrow\uparrow}. \quad (\text{E.33})$$

With (E.23), (E.26) and (E.33) Eq. (E.19) is transformed into

$$\begin{aligned} \mathcal{H}_{ff}^c &= \frac{J^2}{8N} \sum_{ii'\vec{q}} \left\{ D_{\vec{q}}^{c\uparrow\downarrow} (S_i^- S_{i'}^+ + S_i^+ S_{i'}^-) + \sum_{\sigma} D_{\vec{q}}^{c\sigma\sigma} S_i^z S_{i'}^z \right\} e^{-i\vec{q}(\vec{R}_i - \vec{R}_{i'})} - \\ &\quad - B_{\text{eff},c} \sum_i S_i^z \end{aligned} \quad (\text{E.34})$$

$$= - \sum_{ii'} \left\{ J_{ii'c}^{(1)} (S_i^- S_{i'}^+ + S_i^+ S_{i'}^-) + J_{ii'c}^{(2)} S_i^z S_{i'}^z \right\} - B_{\text{eff},c} \sum_i S_i^z \quad (\text{E.35})$$

with the effective exchange integrals

$$J_{ii'c}^{(1,2)} = \frac{1}{N} \sum_{\vec{q}} J_{\vec{q}c}^{(1,2)} e^{-i\vec{q}(\vec{R}_i - \vec{R}_{i'})}, \quad (\text{E.36})$$

$$J_{\vec{q}c}^{(1)} = -\frac{1}{8} J^2 D_{\vec{q}}^{c\uparrow\downarrow}, \quad (\text{E.37})$$

$$J_{\vec{q}c}^{(2)} = -\frac{1}{8} J^2 \sum_{\sigma} D_{\vec{q}}^{c\sigma\sigma}. \quad (\text{E.38})$$

We now try to get a simple expression for the exchange integral $J_{ii'c}^{(2)}$ (for $J_{ii'c}^{(1)}$ the way is fully analogous). For the Fourier transformed quantity we have Eq. (E.38). For $D_{\vec{q}}^{c\sigma\sigma}$ there is Eq. (E.21). We transform

$$\sum_{\vec{k}} A_{\vec{k}, \vec{k}+\vec{q}}^{c\sigma\sigma}(E) = \sum_{\vec{k}} \left[G_{\vec{k}\sigma c}^{(0)}(E) G_{\vec{k}+\vec{q}\sigma c}(E) + G_{\vec{k}+\vec{q}\sigma c}^{(0)}(E) G_{\vec{k}\sigma c}(E) \right] \quad (\text{E.39})$$

$$= \frac{2}{N} \sum_{\vec{k}} \sum_{ii'} G_{\vec{k}\sigma c}^{(0)}(E) G_{ii'\sigma c}(E) e^{-i(\vec{q}+\vec{k})(\vec{R}_i - \vec{R}_{i'})} \quad (\text{E.40})$$

$$= 2 \sum_{ii'} e^{-i\vec{q}(\vec{R}_i - \vec{R}_{i'})} G_{ii'\sigma c}^{(0)}(E) G_{ii'\sigma c}(E) \quad (\text{E.41})$$

For the step from (E.39) to (E.40) see also (E.29). From (E.40) to (E.41) we have made use of the fact that $G_{i'\sigma c}^{(0)}(E) = G_{ii'\sigma c}^{(0)}(E)$ due to inversion symmetry. Inserting (E.21) into (E.38) considering (E.41) we get

$$J_{\vec{q}c}^{(2)} = \frac{1}{N} \sum_{ii'} \left\{ \frac{J^2}{4\pi} \sum_{\sigma} \text{Im} \int_{-\infty}^{+\infty} dE f(E) G_{ii'\sigma c}^{(0)}(E) G_{ii'\sigma c}(E) \right\} e^{-i\vec{q}(\vec{R}_i - \vec{R}_{i'})} \quad (\text{E.42})$$

$$= \frac{1}{N} \sum_{ii'} J_{ii'c}^{(2)} e^{i\vec{q}(\vec{R}_i - \vec{R}_{i'})} = \frac{1}{N} \sum_{ii'} J_{ii'c}^{(2)} e^{-i\vec{q}(\vec{R}_i - \vec{R}_{i'})} \quad (\text{E.43})$$

In Eq. (E.43) we have used $J_{ii'c}^{(2)} = J_{i'i c}^{(2)}$ due to inversion symmetry.

For simplicity we consider only on-site and nearest-neighbor exchange:

$$J_{0lc}^{(2)} = \frac{J^2}{4\pi} \text{Im} \int_{-\infty}^{+\infty} dE f(E) \left[G_{l\uparrow c}^{(0)}(E) G_{l\uparrow c}(E) + G_{l\downarrow c}^{(0)}(E) G_{l\downarrow c}(E) \right], \quad l = 0, 1, \quad (\text{E.44})$$

with

$$G_{l\sigma c}^{(0)}(E) = \frac{1}{N} \sum_{\vec{k}} e^{i\vec{k}\vec{R}_l} G_{\vec{k}\sigma c}^{(0)}(E), \quad (\text{E.45})$$

$$G_{l\sigma c}(E) = \frac{1}{N} \sum_{\vec{k}} e^{i\vec{k}\vec{R}_l} G_{\vec{k}\sigma c}(E). \quad (\text{E.46})$$

$G_{\vec{k}\sigma c}^{(0)}(E)$ is given in Eq. (E.15), and $G_{\vec{k}\sigma c}(E)$ in Eq. (6.15). $\vec{R}_0 = \vec{0}$. \vec{R}_1 is one of the nearest-neighbor vectors. All of them are equivalent for Eqs. (E.45) and (E.46). The sums over \vec{k} on the r.h.s.'s of both equations can be transformed into energy integrals with a modified density of states since the \vec{k} dependence of the Green's functions is exclusively given via the free conduction band dispersion $\epsilon_{\vec{k}}$.

$$G_{l\sigma c}^{\{(0)\}}(E) = \frac{1}{N} \sum_{\vec{k}} \int_{-\infty}^{+\infty} dx \delta(x - \epsilon_{\vec{k}}) e^{i\vec{k}\vec{R}_l} G_{\epsilon_{\vec{k}} \rightarrow x}^{\{(0)\}}(E) \quad (\text{E.47})$$

$$= \int_{-\infty}^{+\infty} dx \rho_l(x) G_x^{\{(0)\}}(E) \quad (\text{E.48})$$

with the modified densities of states

$$\rho_l(x) = \frac{1}{N} \sum_{\vec{k}} e^{i\vec{k}\vec{R}_l} \delta(x - \epsilon_{\vec{k}}), \quad l = 0, 1 \quad (\text{E.49})$$

The summation over $e^{i\vec{k}\vec{R}_l} \delta(x - \epsilon_{\vec{k}})$ requires the usage of an explicit dispersion $\epsilon_{\vec{k}}$, for which we take the tight-binding nearest-neighbor hopping dispersion for the fcc lattice, which is given by

$$\begin{aligned} \epsilon_{\vec{k}} = & -2t \left[\cos\left(\frac{1}{2}ak_x + \frac{1}{2}ak_y\right) + \cos\left(\frac{1}{2}ak_x - \frac{1}{2}ak_y\right) \right. \\ & + \cos\left(\frac{1}{2}ak_y + \frac{1}{2}ak_z\right) + \cos\left(\frac{1}{2}ak_y - \frac{1}{2}ak_z\right) \\ & \left. + \cos\left(\frac{1}{2}ak_z + \frac{1}{2}ak_x\right) + \cos\left(\frac{1}{2}ak_z - \frac{1}{2}ak_x\right) \right]. \quad (\text{E.50}) \end{aligned}$$

$-t$ is the nearest-neighbor hopping parameter, a is the lattice constant of EuO. From (E.50) it is easily seen that for an fcc lattice we have [see Eq. (5.48)]

$$\vec{\nabla}_{\vec{k}}^2 \epsilon_{\vec{k}} = -\frac{1}{2} a^2 \epsilon_{\vec{k}} \quad (\text{E.51})$$

For $J_{0lc}^{(1)}$ we get in full analogy to $J_{0lc}^{(2)}$:

$$J_{0lc}^{(1)} = \frac{J^2}{8\pi} \text{Im} \int_{-\infty}^{+\infty} dE f(E) \left[G_{l\downarrow c}^{(0)}(E) G_{l\uparrow c}(E) + G_{l\uparrow c}^{(0)}(E) G_{l\downarrow c}(E) \right], \quad l = 0, 1. \quad (\text{E.52})$$

Now the same procedure has to be gone through with the impurity electrons. Formulating the equivalent to Eq. (E.6) we get

$$\begin{aligned} [E - \Sigma_{\sigma}^{\text{CPA},2}(E)] \hat{G}_{\vec{k},\vec{k}+\vec{q}}^{p\sigma\sigma'}(E) &= \delta_{\vec{q},\vec{0}} \delta_{\sigma\sigma'} - \frac{J}{2N} \sum_{i\vec{k}'\sigma''} e^{-i(\vec{k}-\vec{k}')\vec{R}_i} (\vec{S}_i \cdot \hat{\sigma})_{\sigma'\sigma''} \hat{G}_{\vec{k}',\vec{k}+\vec{q}}^{p\sigma''\sigma}(E) \\ &+ V \hat{G}_{\vec{k},\vec{k}+\vec{q}}^{cp\sigma'\sigma}(E) \end{aligned} \quad (\text{E.53})$$

where $\Sigma_{\sigma}^{\text{CPA},2}(E)$ is the CPA self-energy similarly defined to $\Sigma_{\sigma}^{\text{CPA},1}(E)$ but with the impurity self-energy $\Sigma_{\sigma}^{p,1}$ replaced by $\Sigma_{\sigma}^{p,2}$, which is defined by

$$\left\langle \left\langle \left[p_{j'\sigma}, U \sum_j n_{j\uparrow}^p n_{j\downarrow}^p \right]_- ; p_{j'\sigma}^{\dagger} \right\rangle \right\rangle = \Sigma_{\sigma}^{p,2}(E) \langle \langle p_{j'\sigma}; p_{j'\sigma}^{\dagger} \rangle \rangle. \quad (\text{E.54})$$

We choose for $\Sigma_{\sigma}^{p,2}$ the atomic limit self-energy of the Hubbard model, which is given by (D.18). For the impurity electrons Eq. (E.8) is replaced by

$$[E - (\epsilon_{\vec{k}} - \mu) - \Sigma_{\sigma}^c(E)] \hat{G}_{\vec{k},\vec{k}+\vec{q}}^{cp\sigma'\sigma}(E) = V \hat{G}_{\vec{k},\vec{k}+\vec{q}}^{p\sigma'\sigma}(E). \quad (\text{E.55})$$

Combining Eqs. (E.53) and (E.55) yields

$$\begin{aligned} \left[E - \Sigma_{\sigma}^{\text{CPA},2}(E) - \frac{V^2}{E - (\epsilon_{\vec{k}} - \mu) - \Sigma_{\sigma}^c(E)} \right] \hat{G}_{\vec{k},\vec{k}+\vec{q}}^{p\sigma\sigma'}(E) \\ = \delta_{\vec{q},\vec{0}} \delta_{\sigma\sigma'} - \frac{J}{2N} \sum_{i\vec{k}'\sigma''} e^{-i(\vec{k}-\vec{k}')\vec{R}_i} (\vec{S}_i \cdot \hat{\sigma})_{\sigma'\sigma''} \hat{G}_{\vec{k}',\vec{k}+\vec{q}}^{p\sigma''\sigma}(E). \end{aligned} \quad (\text{E.56})$$

The equivalents to Eqs. (E.10), (E.12) and (E.13) are

$$[E - \Sigma_{\sigma}^{\text{CPA},2}(E)] \hat{G}_{\vec{k}, \vec{k}+\vec{q}}^{p\sigma\sigma'}(E) = \delta_{\vec{q}, \vec{0}} \delta_{\sigma\sigma'} - \frac{J}{2N} \sum_{i\vec{k}'\sigma''} e^{-i(\vec{k}-\vec{k}')\vec{R}_i} (\vec{S}_i \cdot \hat{\vec{\sigma}})_{\sigma'\sigma''} \hat{G}_{\vec{k}, \vec{k}'}^{p\sigma''\sigma}(E) + V \hat{G}_{\vec{k}, \vec{k}+\vec{q}}^{pc\sigma'\sigma}(E), \quad (\text{E.57})$$

$$[E - (\epsilon_{\vec{k}+\vec{q}} - \mu) - \Sigma_{\sigma}^c(E)] \hat{G}_{\vec{k}, \vec{k}+\vec{q}}^{pc\sigma'\sigma}(E) = V \hat{G}_{\vec{k}, \vec{k}+\vec{q}}^{p\sigma'\sigma}(E), \quad (\text{E.58})$$

$$\left[E - \Sigma_{\sigma}^{\text{CPA},2}(E) - \frac{V^2}{E - (\epsilon_{\vec{k}+\vec{q}} - \mu) - \Sigma_{\sigma}^c(E)} \right] \hat{G}_{\vec{k}, \vec{k}+\vec{q}}^{p\sigma\sigma'}(E) = \delta_{\vec{q}, \vec{0}} \delta_{\sigma\sigma'} - \frac{J}{2N} \sum_{i\vec{k}'\sigma''} e^{-i(\vec{k}-\vec{k}')\vec{R}_i} (\vec{S}_i \cdot \hat{\vec{\sigma}})_{\sigma'\sigma''} \hat{G}_{\vec{k}, \vec{k}'}^{p\sigma''\sigma}(E). \quad (\text{E.59})$$

Combining Eqs. (E.56) and (E.59) we get the equivalent of Eq. (E.14):

$$\hat{G}_{\vec{k}, \vec{k}+\vec{q}}^{p\sigma'\sigma} = \delta_{\sigma\sigma'} \delta_{\vec{q}, \vec{0}} G_{\vec{k}\sigma p}^{(0)} - \frac{J}{4N} \sum_{i\vec{k}'\sigma''} \left\{ e^{-i(\vec{k}-\vec{k}')\vec{R}_i} G_{\vec{k}\sigma' p}^{(0)} (\vec{S}_i \cdot \hat{\vec{\sigma}})_{\sigma'\sigma''} \hat{G}_{\vec{k}, \vec{k}'}^{p\sigma''\sigma} + e^{-i[\vec{k}' - (\vec{k}+\vec{q})]\vec{R}_i} G_{\vec{k}+\vec{q}\sigma p}^{(0)} (\vec{S}_i \cdot \hat{\vec{\sigma}})_{\sigma''\sigma} \hat{G}_{\vec{k}, \vec{k}'}^{p\sigma'\sigma''} \right\} \quad (\text{E.60})$$

with

$$G_{\vec{k}\sigma p}^{(0)} = \frac{1}{E - \Sigma_{\sigma}^{\text{CPA},2} - \frac{V^2}{E - (\epsilon_{\vec{k}} - \mu) - \Sigma_{\sigma}^c(E)}}. \quad (\text{E.61})$$

All the other Eqs. from (E.16) to (E.52) are transformed simply by replacing the index c for the conduction electrons by the index p for the impurity electrons and by replacing the corresponding operators and Green's functions.

As our model we have now got an anisotropic Heisenberg Hamiltonian:

$$\tilde{\mathcal{H}}'_{ff} = - \sum_{ii'} \left[J_{ii'}^{(1)} (S_i^+ S_{i'}^- + S_i^- S_{i'}^+) + J_{ii'}^{(2)} S_i^z S_{i'}^z \right] - B_{\text{eff}} \sum_i S_i^z \quad (\text{E.62})$$

with

$$J_{ii'}^{(r)} = \begin{cases} J_{00c}^{(r)} + J_{00p}^{(r)} & i = i' \\ J_{01c}^{(r)} + J_{01p}^{(r)} + J_H^{(r)} & i, i' \text{ n.n.} \\ 0 & \text{otherwise} \end{cases} \quad (\text{E.63})$$

$$r = 1, 2$$

$$J_H = 2J_H^{(1)} = J_H^{(2)} \quad (\text{E.64})$$

$$B_{\text{eff}} = B_{\text{eff},c} + B_{\text{eff},p}. \quad (\text{E.65})$$

For simplicity we only consider on-site and nearest-neighbor exchange. To solve the model (E.62) we will use the Tyablikov decoupling (or random-phase approximation) [Bogoliubov and Tyablikow, 1959, Tyablikow, 1969, Nolting, 1986]. The magnetization can be obtained by the method by Callen [Callen, 1963]:

$$\langle S_z \rangle = \frac{(1 + S + \phi)\phi^{2S+1} + (S - \phi)(1 + \phi)^{2S+1}}{(1 + \phi)^{2S+1} - \phi^{2S+1}} \quad (\text{E.66})$$

with

$$\phi = \frac{1}{N} \sum_{\vec{k}} \frac{1}{e^{\beta E(\vec{k})} - 1} \quad (\text{E.67})$$

where the magnon energies $E(\vec{k})$ are the excitation energies of the magnon Green's function $\langle\langle S^+(\vec{k}); S^-(\vec{k}) \rangle\rangle_E$. They themselves depend on $\langle S^z \rangle$. Therefore Eqs. (E.66) and (E.67) have to be solved self-consistently. We will calculate the magnon energies now in the Tyablikov approximation. With the Fourier transformation of the spin-operators

$$S^\alpha(\vec{k}) = \sum_i S_i^\alpha e^{-i\vec{k}\vec{R}_i} \quad (\alpha = x, y, z, +, -) \quad (\text{E.68})$$

and the commutation relations

$$\left[S^+(\vec{k}_1), S^-(\vec{k}_2) \right]_- = 2S^z(\vec{k}_1 + \vec{k}_2), \quad (\text{E.69})$$

$$\left[S^z(\vec{k}_1), S^\pm(\vec{k}_2) \right]_- = \pm S^\pm(\vec{k}_1 + \vec{k}_2) \quad (\text{E.70})$$

and with the Fourier transforms of the exchange integrals one gets the following Hamiltonian:

$$\begin{aligned} \tilde{\mathcal{H}}'_{ff} = -\frac{1}{N} \sum_{\vec{q}} \left\{ J_{\vec{q}}^{(1)} [S^+(\vec{q})S^-(\vec{q}) + S^-(\vec{q})S^+(\vec{q})] + J_{\vec{q}}^{(2)} S^z(\vec{q})S^z(-\vec{q}) \right\} \\ - B_{\text{eff}} S^z(\vec{0}). \end{aligned} \quad (\text{E.71})$$

The equation of motion for the magnon Green's function reads

$$E \langle\langle S^+(\vec{k}); S^-(\vec{k}) \rangle\rangle_E = \underbrace{\langle\langle [S^+(\vec{k}), S^-(\vec{k})]_- \rangle\rangle}_E + \langle\langle [S^+(\vec{k}), \tilde{\mathcal{H}}'_{ff}]_-; S^-(\vec{k}) \rangle\rangle, \quad (\text{E.72})$$

$$\langle 2S^z(\vec{0}) \rangle$$

$$\begin{aligned}
[S^+(\vec{k}), \tilde{\mathcal{H}}'_{ff}]_- = & -\frac{1}{N} \sum_{\vec{q}} \left\{ J_{\vec{q}}^{(1)} \left[2S^+(\vec{q})S^z(\vec{k}-\vec{q}) + 2S^+(-\vec{q})S^z(\vec{k}+\vec{q}) + 2S^+(\vec{k}) \right] \right. \\
& + J_{\vec{q}}^{(2)} \left[-S^+(\vec{k}+\vec{q})S^z(-\vec{q}) - S^+(\vec{k}-\vec{q})S^z(\vec{q}) - S^+(\vec{k}) \right] \\
& \left. + B_{\text{eff}} S^+(\vec{k}) \right\} \quad (\text{E.73})
\end{aligned}$$

The Tyablikov decoupling means

$$\langle\langle S^\pm(\vec{k}_1)S^z(\vec{k}_2); S^\mp(\vec{k}_3) \rangle\rangle \rightarrow \langle S^z(\vec{k}_2) \rangle \langle\langle S^\pm(\vec{k}_1); S^\mp(\vec{k}_3) \rangle\rangle. \quad (\text{E.74})$$

With the Tyablikov decoupling we get the following equation of motion

$$\begin{aligned}
E \langle\langle S^+(\vec{k}); S^-(\vec{k}) \rangle\rangle = & 2 \langle S^z(\vec{0}) \rangle - \frac{1}{N} \sum_{\vec{q}} \left\{ 2J_{\vec{q}}^{(1)} \left(\langle S^z(\vec{k}-\vec{q}) \rangle \langle\langle S^+(\vec{q}); S^-(\vec{k}) \rangle\rangle \right. \right. \\
& + \langle S^z(\vec{k}+\vec{q}) \rangle \langle\langle S^+(-\vec{q}); S^-(\vec{k}) \rangle\rangle + \langle\langle S^+(\vec{k}); S^-(\vec{k}) \rangle\rangle \Big) \\
& + J_{\vec{q}}^{(2)} \left(-\langle S^z(-\vec{q}) \rangle \langle\langle S^+(\vec{k}+\vec{q}); S^-(\vec{k}) \rangle\rangle \right. \\
& \left. \left. - \langle S^z(\vec{q}) \rangle \langle\langle S^+(\vec{k}-\vec{q}); S^-(\vec{k}) \rangle\rangle - \langle\langle S^+(\vec{k}); S^-(\vec{k}) \rangle\rangle \right) \right\} \\
& + B_{\text{eff}} \langle\langle S^+(\vec{k}); S^-(\vec{k}) \rangle\rangle. \quad (\text{E.75})
\end{aligned}$$

Using

$$\langle S^z(\vec{k}-\vec{q}) \rangle = \sum_i e^{-i(\vec{k}-\vec{q})\vec{R}_i} \langle S_i^z \rangle = \langle S^z \rangle \sum_i e^{-i(\vec{k}-\vec{q})\vec{R}_i} = \langle S^z \rangle N \delta_{\vec{k}\vec{q}} \quad (\text{E.76})$$

and

$$J_{\vec{q}}^{(1)} = J_{-\vec{q}}^{(1)} \quad (\text{E.77})$$

due to inversion symmetry, Eq. (E.75) is transformed into

$$\begin{aligned}
E \langle\langle S^+(\vec{k}); S^-(\vec{k}) \rangle\rangle = & 2N \langle S^z \rangle + \left(-4 \langle S^z \rangle J_{\vec{k}}^{(1)} - 2J_{00}^{(1)} + 2 \langle S^z \rangle J_{\vec{0}}^{(2)} + J_{00}^{(2)} + B_{\text{eff}} \right) * \\
& * \langle\langle S^+(\vec{k}); S^-(\vec{k}) \rangle\rangle. \quad (\text{E.78})
\end{aligned}$$

The magnon Green's function has the following structure

$$\langle\langle S^+(\vec{k}); S^-(\vec{k}) \rangle\rangle = \frac{2N \langle S^z \rangle}{E - E(\vec{k})}. \quad (\text{E.79})$$

For the magnon energies, which have to be inserted into (E.67), we have

$$E(\vec{k}) = -4 \langle S^z \rangle J_{\vec{k}}^{(1)} - 2J_{00}^{(1)} + 2 \langle S^z \rangle J_{\vec{0}}^{(2)} + J_{00}^{(2)} + B_{\text{eff}}. \quad (\text{E.80})$$

Bibliography

- [Allen and Edwards, 1982] Allen, S. R. and Edwards, D. M. (1982). *J. Phys. C*, 15:2151.
- [Anderson, 1961] Anderson, P. W. (1961). *Phys. Rev.*, 124:41.
- [Bloembergen and Rowland, 1955] Bloembergen, N. and Rowland, T. J. (1955). *Phys. Rev.*, 97:1679.
- [Bogoliubov and Tyablikow, 1959] Bogoliubov, N. N. and Tyablikow, S. V. (1959). *Dokl. Akad. Nauk USSR*, 126:53.
- [Borgielet al., 2001] Borgieł, W., Herrmann, T., Nolting, W., and Kosimow, R. (2001). *Acta Phys. Pol. B*, 32:383.
- [Brauer, 1953] Brauer, G. (1953). *Angew. Chem.*, 65:261.
- [Bulk and Jelitto, 1988] Bulk, G. and Jelitto, R. J. (1988). *Phys. Lett. A*, 133:231.
- [Bulk and Jelitto, 1990] Bulk, G. and Jelitto, R. J. (1990). *Phys. Rev. B*, 41:413.
- [Busch et al., 1964] Busch, G., Junod, J., and Wachter, P. (1964). *Phys. Lett.*, 12:11.
- [Callen, 1963] Callen, H. B. (1963). *Phys. Rev.*, 130:890.
- [Carruthers et al., 1957] Carruthers, J. A., Geballe, T. H., Rosenberg, H. M., and Ziman, J. M. (1957). *Proc. Roy. Soc. A*, 238:502.
- [Coey et al., 1999] Coey, J. M. D., Viret, M., and von Molnar, S. (1999). *Adv. Phys.*, 48:167.
- [Czycholl and Leder, 1981] Czycholl, G. and Leder, H. J. (1981). *Z. Phys. B*, 44:59.

- [Dagotto et al., 1998] Dagotto, E., Yunoki, S., Malvezzi, A. L., Moreo, A., Hu, J., Capponi, S., Poilblanc, D., and Furukawa, N. (1998). *Phys. Rev. B*, 58:6414.
- [Dietl et al., 2001a] Dietl, T., König, J., and MacDonald, A. H. (2001a). *Phys. Rev. B*, 64:241201(R).
- [Dietl et al., 2001b] Dietl, T., Ohno, H., and Matsukura, F. (2001b). *Phys. Rev. B*, 63:195205.
- [Dietrich et al., 1975] Dietrich, O. W., A. J. Henderson, J., and Meyer, H. (1975). *Phys. Rev. B*, 12:2844.
- [Fazekas, 1999] Fazekas, P. (1999). *Lecture Notes on Electron Correlation and Magnetism*. World Scientific, Singapore.
- [Furukawa, 1994] Furukawa, N. (1994). *J. Phys. Soc. Japan*, 63:3214.
- [Girvin, 1978] Girvin, S. M. (1978). *J. Solid State Chem.*, 25:65.
- [Hewson, 1997] Hewson, A. C. (1997). *The Kondo Problem to Heavy Fermions*. Cambridge University Press, Cambridge.
- [Hickel, 2004] Hickel, T. (2004). private communications.
- [Hickel and Nolting, 2004] Hickel, T. and Nolting, W. (2004). *Phys. Rev. B*, 69:085110.
- [Hubbard, 1963] Hubbard, J. (1963). *Proc. R. Soc. Lond., A Math. Phys. Sci.*, 276:238.
- [Hubbard, 1964a] Hubbard, J. (1964a). *Proc. R. Soc. Lond., A Math. Phys. Sci.*, 277:237.
- [Hubbard, 1964b] Hubbard, J. (1964b). *Proc. R. Soc. Lond., A Math. Phys. Sci.*, 281:401.
- [Ibach and Lüth, 1995] Ibach, H. and Lüth, H. (1995). *Festkörperphysik*. Springer-Verlag Berlin Heidelberg, 4 edition.
- [Jin et al., 1994] Jin, S., Tiefel, T. H., Mc Cormack, M., Fastnacht, R. A., Ramesh, R., and Chen, L. H. (1994). *Science*, 264:413.
- [Kasuya, 1956] Kasuya, T. (1956). *Prog. Theor. Phys.*, 16:45.

- [Kehrein and Mielke, 1996] Kehrein, S. K. and Mielke, A. (1996). *Ann. Phys.*, 252:1.
- [Khomskii and Sawatzky, 1997] Khomskii, D. I. and Sawatzky, G. A. (1997). *Solid State Commun.*, 102:87.
- [Khurana, 1990] Khurana, A. (1990). *Phys. Rev. Lett.*, 64:1990.
- [Kienert, 2001] Kienert, J. (2001). Diploma thesis.
- [Kienert et al., 2003] Kienert, J., Santos, C., and Nolting, W. (2003). *phys. stat. sol. (b)*, 236:515.
- [Kondo, 1964] Kondo, J. (1964). *Prog. Theor. Phys*, 32:37.
- [König et al., 2001] König, J., Jungwirth, T., and MacDonald, A. H. (2001). *Phys. Rev. B*, 64:184423.
- [Kubo, 1957] Kubo, R. (1957). *J. Phys. Soc. Japan*, 12:570.
- [Kuneš et al., 2004] Kuneš, J., Ku, W., and Pickett, W. E. (2004). cond-mat/0406229.
- [Lacroix and Cyrot, 1979] Lacroix, C. and Cyrot, M. (1979). *Phys. Rev. B*, 20:1969.
- [Laks and da Silva, 1976] Laks, B. and da Silva, C. E. T. G. (1976). *Phys. Rev. Lett.*, 36:1204.
- [Lee and Liu, 1983] Lee, V.-C. and Liu, L. (1983). *Solid State Commun.*, 48:795.
- [Lee and Liu, 1984] Lee, V.-C. and Liu, L. (1984). *Phys. Rev. B*, 30:2026.
- [Leroux-Hugon, 1972] Leroux-Hugon, P. (1972). *Phys. Rev. Lett.*, 29:939.
- [Liu, 1980] Liu, L. (1980). *Solid State Commun.*, 35:187.
- [Liu, 1983] Liu, L. (1983). *Solid State Commun.*, 46:83.
- [Luttinger and Ward, 1960] Luttinger, J. M. and Ward, J. C. (1960). *Phys. Rev.*, 118:1417.
- [Madelung, 1981] Madelung, O. (1981). *Introduction to Solid-State Theory*. Springer-Verlag, New York, Berlin, Heidelberg, 2 edition.

- [Mahan et al., 1997] Mahan, G., Sales, B., and Sharp, J. (1997). *Phys. Today*, 50(3):42.
- [Mahan, 1993] Mahan, G. D. (1993). *Many-Particle Physics*. Plenum Press, New York, 2 edition.
- [Martin, 1982] Martin, R. M. (1982). *Phys. Rev. Lett.*, 48:362.
- [Matsukura et al., 1998] Matsukura, F., Ohno, H., Shen, A., and Sugawara, Y. (1998). *Phys. Rev. B*, 57:R2037.
- [Matsumoto and Ohkawa, 1995] Matsumoto, N. and Ohkawa, F. J. (1995). *Phys. Rev. B*, 51:4110.
- [Matthias et al., 1961] Matthias, B. T., Bozorth, R. M., and Vleck, J. H. V. (1961). *Phys. Rev. Lett.*, 7:160.
- [Mauger, 1983] Mauger, A. (1983). *Phys. Rev. B*, 27:2308.
- [Mauger and Godart, 1986] Mauger, A. and Godart, C. (1986). *Phys. Rep.*, 141:51.
- [Mauger et al., 1978] Mauger, A., Godart, C., Escorne, M., Achard, J. C., and Desfours, J. P. (1978). *J. Phys. (Paris)*, 39:1125.
- [Meyer et al., 2001] Meyer, D., Santos, C., and Nolting, W. (2001). *J. Phys.: Condens. Matter*, 13:2531.
- [Millis et al., 1996] Millis, A. J., Müller, R., and Shraiman, B. I. (1996). *Phys. Rev. B*, 54:5405.
- [Mitani and Koda, 1975] Mitani, T. and Koda, T. (1975). *Phys. Rev. B*, 12:2311.
- [Möller et al., 1992] Möller, G., Ruckenstein, A. E., and Schmitt-Rink, S. (1992). *Phys. Rev. B*, 46:7427.
- [Mori, 1965] Mori, H. (1965). *Prog. Theor. Phys.*, 33:432.
- [Mori, 1966] Mori, H. (1966). *Prog. Theor. Phys.*, 34:399.
- [Nolting, 1986] Nolting, W. (1986). *Quantentheorie des Magnetismus*, volume 2. Teubner, Stuttgart.
- [Nolting, 2003] Nolting, W. (2003). *Grundkurs Theoretische Physik*, volume 7. Springer, Berlin.

- [Nolting et al., 1987a] Nolting, W., Borgiel, W., and Borstel, G. (1987a). *Phys. Rev. B*, 35:7025.
- [Nolting et al., 1987b] Nolting, W., Borstel, G., and Borgiel, W. (1987b). *Phys. Rev. B*, 35:7015.
- [Nolting et al., 1985] Nolting, W., Dubil, U., and Matlak, M. (1985). *J. Phys. C*, 18:3687.
- [Nolting and Matlak, 1984] Nolting, W. and Matlak, M. (1984). *phys. stat. sol. (b)*, 123:155.
- [Nolting et al., 2003a] Nolting, W., Müller, W., and Santos, C. (2003a). *J. Phys. A*, 36:9275.
- [Nolting et al., 2003b] Nolting, W., Müller, W., Santos, C., and Sinjukow, P. (2003b). Local moment systems: magnetism and correlations. In *AIP Conference Proceedings*, volume 695, page 196.
- [Nolting et al., 2001] Nolting, W., Reddy, G. G., Ramakanth, A., and Meyer, D. (2001). *Phys. Rev. B*, 64:155109.
- [Nolting et al., 1997] Nolting, W., Rex, S., and Jaya, S. M. (1997). *J. Phys.: Condens. Matter*, 9:1301.
- [Okimoto et al., 1995] Okimoto, Y., Katsufuji, T., Ishikawa, T., A. Urushibara, Arima, T., and Tokura, Y. (1995). *Phys. Rev. Lett.*, 75:109.
- [Oliver et al., 1972] Oliver, M. R., Dimmock, J. O., McWhorter, A. L., and Reed, T. B. (1972). *Phys. Rev. B*, 5:1078.
- [Oliver et al., 1970] Oliver, M. R., Kafalas, J. A., Dimmock, J. O., and Reed, T. B. (1970). *Phys. Rev. Lett.*, 24:1064.
- [Oshikawa, 2000] Oshikawa, M. (2000). *Phys. Rev. Lett.*, 84:3370.
- [Pálsson and Kotliar, 1998] Pálsson, G. and Kotliar, G. (1998). *Phys. Rev. Lett.*, 80:4775.
- [Passell et al., 1976] Passell, L., Dietrich, O. W., and Als-Nielsen, J. (1976). *Phys. Rev. B*, 14:4897.
- [Penney et al., 1972] Penney, T., Shafer, M. W., and Torrance, J. B. (1972). *Phys. Rev. B*, 5:3669.

- [Pickett and Singh, 1996] Pickett, W. E. and Singh, D. J. (1996). *Phys. Rev. B*, 53:1146.
- [Potthoff et al., 1997] Potthoff, M., Wegner, T., and Nolting, W. (1997). *Phys. Rev. B*, 55:16132.
- [Proetto and Lopeź, 1981] Proetto, C. and Lopeź, A. (1981). *Phys. Rev. B*, 24:3031.
- [Pruschke et al., 1993] Pruschke, T., Cox, D. L., and Jarrell, M. (1993). *Phys. Rev. B*, 47:3553.
- [Ramirez, 1997] Ramirez, A. P. (1997). *J. Phys.: Condens. Matter*, 9:8171.
- [Rudermann and Kittel, 1954] Rudermann, M. A. and Kittel, C. (1954). *Phys. Rev.*, 96:99.
- [Samokhvalov et al., 1982] Samokhvalov, A. A., Gizhevskii, B. A., Simonova, M. I., Chebotaev, N. M., and Fal'kovskaya, L. D. (1982). *Sov. Phys. Solid State*, 24:1103.
- [Samokhvalov et al., 1988] Samokhvalov, A. A., Viglin, N. A., Gizhevskii, B. A., Arbuzova, T. I., and Chebotaev, N. M. (1988). *phys. stat. sol. (b)*, 148:361.
- [Santos, 2004] Santos, C. (2004). private communications.
- [Santos and Nolting, 2002a] Santos, C. and Nolting, W. (2002a). *Phys. Rev. B*, 65:144419.
- [Santos and Nolting, 2002b] Santos, C. and Nolting, W. (2002b). *Phys. Rev. B*, 66:019901(E).
- [Sanvito et al., 2001] Sanvito, S., Ordejón, P., and Hill, N. A. (2001). *Phys. Rev. B*, 63:165206.
- [Satpathy et al., 1996] Satpathy, S., Popovic, Z. S., and Vukajlovic, F. R. (1996). *Phys. Rev. Lett.*, 76:960.
- [Schiller, 2000] Schiller, R. (2000). PhD thesis, Humboldt-Universität zu Berlin.
- [Schoenes and Wachter, 1974] Schoenes, J. and Wachter, P. (1974). *Phys. Rev. B*, 9:3097.

- [Schrieffer and Wolff, 1966] Schrieffer, J. R. and Wolff, P. A. (1966). *Phys. Rev.*, 149:491.
- [Shapira et al., 1973] Shapira, Y., Foner, S., and Reed, T. B. (1973). *Phys. Rev. B*, 8:2299.
- [Shastry and Mattis, 1981] Shastry, B. S. and Mattis, D. C. (1981). *Phys. Rev. B*, 24:5340.
- [Shiba and Fazekas, 1990] Shiba, H. and Fazekas, P. (1990). *Prog. Theor. Phys. Suppl.*, 101:403.
- [Singh and Pickett, 1998] Singh, D. J. and Pickett, W. E. (1998). *Phys. Rev. B*, 57:88.
- [Sinjukow and Nolting, 2002] Sinjukow, P. and Nolting, W. (2002). *Phys. Rev. B*, 65:212303.
- [Sinjukow and Nolting, 2003] Sinjukow, P. and Nolting, W. (2003). *Phys. Rev. B*, 68:125107.
- [Sinjukow and Nolting, 2004a] Sinjukow, P. and Nolting, W. (2004a). *J. Magn. Magn. Mat.*, 272-276:e303.
- [Sinjukow and Nolting, 2004b] Sinjukow, P. and Nolting, W. (2004b). *Phys. Rev. B*, 69:214432.
- [Spalek et al., 1977] Spalek, J., Lubecka, M., and Węgrzyn, A. (1977). *phys. stat. sol. (b)*, 82:107.
- [Steeneken, 2002] Steeneken, P. G. (2002). PhD thesis, Rijksuniversiteit Groningen.
- [Steeneken et al., 2002] Steeneken, P. G., Tjeng, L. H., Elfimov, I., Sawatzky, G. A., Ghiringhelli, G., Brookes, N. B., and Huang, D.-J. (2002). *Phys. Rev. Lett.*, 88:047201.
- [Tjablikow, 1969] Tjablikow, S. W. (1969). *Quantentheoretische Methoden des Magnetismus*. Teubner, Stuttgart.
- [Torrance et al., 1972] Torrance, J. B., Shafer, M. W., and McGuire, T. R. (1972). *Phys. Rev. Lett.*, 29:1168.
- [Tsubokawa, 1960] Tsubokawa, I. (1960). *J. Phys. Soc. Japan*, 15:1664.

- [Tsunetsugu et al., 1997] Tsunetsugu, H., Sigrist, M., and Ueda, K. (1997). *Rev. Mod. Phys.*, 69:809.
- [Ueda et al., 1994] Ueda, K., Nishino, T., and Tsunetsugu, H. (1994). *Phys. Rev. B*, 50:612.
- [Velický, 1969] Velický, V. (1969). *Phys. Rev.*, 184:614.
- [von Löhneysen, 1998] von Löhneysen, H. (1998). in *Magnetism and Electronic Correlations in Local Moment Systems: Rare Earth Elements and Compounds*, edited by M. Donath, P. Dowben and W. Nolting. World Scientific, Singapore.
- [Wachter, 1964] Wachter, P. (1964). *Helv. Phys. Acta*, 37:637.
- [Wachter, 1979] Wachter, P. (1979). *Handbook on the Physics and Chemistry of Rare Earths*, volume 2, page 507. K. A. Gschneidner and L. Eyring, Elsevier, Amsterdam.
- [Yamanaka et al., 1997] Yamanaka, M., Oshikawa, M., and Affleck, I. (1997). *Phys. Rev. Lett.*, 79:1110.
- [Yosida, 1957] Yosida, K. (1957). *Phys. Rev.*, 106:893.
- [Zener, 1951] Zener, C. (1951). *Phys. Rev.*, 82:403.

Lebenslauf

Persönliche Daten

Name: Peter Sinjukow
Geburtstag: 4. August 1974
Geburtsort: Karl-Marx-Stadt
Nationalität: deutsch

Ausbildung

| | |
|-----------------|--|
| 06/1993 | Abitur in der Spezialklasse für Mathematik und Physik am Carl-Friedrich-Gauss Gymnasium in Chemnitz (Note: 1.0) |
| 10/1994-09/1996 | Grundstudium Physik an der Humboldt-Universität zu Berlin |
| 10/1996-09/1997 | Auslandsstudium am King's College London |
| 10/1997-09/1998 | Fortsetzung mit dem Hauptstudium an der Humboldt-Universität zu Berlin |
| 12/1998-12/1999 | Diplomarbeit an der Humboldt-Universität zu Berlin zum Thema "Quasiteilchen im ferromagnetischen Kondo-Gitter-Modell", betreut von Prof. Dr. W. Nolting (AG Festkörpertheorie) |
| 12/1999 | Physik-Diplom (Note: 1.0) |
| seit 03/2000 | Doktorand an der Humboldt-Universität zu Berlin, betreut von Prof. Dr. W. Nolting (AG Festkörpertheorie) |
| seit 04/2000 | mehrere Semester Übungsleiter am Institut für Physik der Humboldt-Universität zu Berlin |

Berlin, den 17.08.2004

Veröffentlichungen

- P. Sinjukow and W. Nolting, “Exact mapping of periodic Anderson model to Kondo lattice model”, *Phys. Rev. B* **65**, 212303 (2002).
- P. Sinjukow and W. Nolting, “Local Density of States in the Antiferromagnetic and Ferromagnetic Kondo Models”, *phys. stat. sol. (b)* **233**, 536 (2002).
- P. Sinjukow and W. Nolting, “Metal-insulator transition in EuO”, *Phys. Rev. B* **68**, 125107 (2003).
- W. Nolting, W. Müller, C. Santos, and P. Sinjukow, “Local moment systems: magnetism and correlations”, in *AIP Conference Proceedings* (2003), vol. 695, p. 196.
- P. Sinjukow and W. Nolting, “Fully self-consistent determination of transport properties in Eu-rich EuO”, *Phys. Rev. B* **69**, 214432 (2004).
- P. Sinjukow and W. Nolting, “Resistivity in Eu-rich EuO”, *J. Magn. Mater.* **272-276**, e303 (2004)

Danksagung

Mein herzlicher Dank gilt allen, die mich bei der Anfertigung meiner Doktorarbeit unterstützt haben.

An erster Stelle möchte ich mich natürlich bei meinem Doktorvater und Betreuer Prof. Dr. W. Nolting bedanken für den Vorschlag des interessanten und ergiebigen Themas der theoretischen Beschreibung des gewaltigen Metall-Isolator-Übergangs im Eu-reichen EuO. Er schenkte mir während der Arbeit stets seine Zeit und Aufmerksamkeit. Ausserdem ermöglichte er es mir, an zahlreichen Konferenzen und Workshops z.T. im Ausland teilzunehmen.

Weiterhin bedanke ich mich bei Dr. Michael Potthoff für die interessanten Diskussionen zum grossen Fermi-Volumen im Kondo-Gitter-Modell. Ich bedanke mich bei Wolf Müller, Carlos Santos und Tilmann Hickel, die mir mit Rat und Tat bei auftretenden Computer-Problemen zur Seite standen.

Mein Dank gilt Sören Henning und Stefan Hilbert, mit denen ich am Anfang, und Tilmann Hickel, mit dem ich bis zum Ende auf angenehme Art ein Arbeitszimmer teilte. Ich bedanke mich bei Stephan Schwieger, Jochen Kienert, Anand Sharma, John Hennig und Randy Mathes, mit denen ich wissenschaftliche und nicht-wissenschaftliche Diskussionen führte.

Ein ganz besonderer Dank richtet sich an Frau M. Götsch, die sich um die technischen und organisatorischen Details meiner Arbeit in der AG "Festkörpertheorie" gekümmert hat.

Nicht zuletzt möchte ich mich bei meinem Bruder Igor Ullmann, meiner Mutter Dr. T. Sinjukowa und meinen FreundInnen für den moralischen Beistand während meiner gesamten Arbeit bedanken.

Selbständigkeitserklärung

Hiermit erkläre ich, die vorliegende Arbeit selbständig ohne unerlaubte Hilfe verfasst und nur die angegebene Literatur und die angegebenen Hilfsmittel verwendet zu haben.

Berlin, den 17.08.2004